REPORT DOCUMENTATION PAGE

Form Approved
OMB No. 0704-0188

1. AGENCY USE ONLY *(Leave blank)*	2. REPORT DATE	3. REPORT TYPE AND DATES COVERED
	10 Sep 95	

4. TITLE AND SUBTITLE
Tropical Cyclone Intensity Relationships

5. FUNDING NUMBERS

6. AUTHOR(S)
Gary B. Kubat

7. PERFORMING ORGANIZATION NAME(S) AND ADDRESS(ES)
AFIT Students Attending:

Colorado State University

8. PERFORMING ORGANIZATION REPORT NUMBER
95-104

9. SPONSORING/MONITORING AGENCY NAME(S) AND ADDRESS(ES)
DEPARTMENT OF THE AIR FORCE
AFIT/CI
2950 P STREET, BLDG 125
WRIGHT-PATTERSON AFB OH 45433-7765

10. SPONSORING/MONITORING AGENCY REPORT NUMBER

11. SUPPLEMENTARY NOTES

12a. DISTRIBUTION/AVAILABILITY STATEMENT
Approved for Public Release IAW AFR 190-1
Distribution Unlimited
BRIAN D. GAUTHIER, MSgt, USAF
Chief of Administration

12b. DISTRIBUTION CODE

13. ABSTRACT *(Maximum 200 words)*

19951017 152

14. SUBJECT TERMS	15. NUMBER OF PAGES 86
	16. PRICE CODE

17. SECURITY CLASSIFICATION OF REPORT	18. SECURITY CLASSIFICATION OF THIS PAGE	19. SECURITY CLASSIFICATION OF ABSTRACT	20. LIMITATION OF ABSTRACT

THESIS

TROPICAL CYCLONE INTENSITY RELATIONSHIPS

Submitted by

Gary B. Kubat

Department of Atmospheric Science

In partial fulfillment of the requirements

for the degree of Master of Science

Colorado State University

Fort Collins, Colorado

Summer, 1995

ABSTRACT OF THESIS

TROPICAL CYCLONE INTENSITY RELATIONSHIPS

This paper provides a summary description of relationships between tropical cyclone (TC) intensity and sea surface temperatures (SST) wherein intensity is characterized in terms of both minimum central sea level pressure (MSLP) and maximum tangential wind velocity (V_{Tmax}). SSTs are represented as monthly mean climatological values on a one degree(lat x lon) grid spacing. Observational data for hurricanes and typhoons are from the Gray and Shea (1976) data summary and from the U.S. Navy Typhoon Analysis (TYAN) data set. Gridded upper-air data from the Climate Analysis Center are used to describe climatological upper air features.

A highly variable range of TC intensity values is observed for each value of SST. These differences are largely due to several factors including variations in the inner-core structure of individual TCs, latitude, season and environmental influences. Knowledge of these variable relationships helps to explain much of the observed deviation from the standard Maximum Potential Intensity (MPI) forecast relationships which are currently in use; the latter rely primarily on SST. An historical review of how MPI forecasts have been made is presented, as well as the likely route for further improvements of MPI forecasts. Variations of the commonly accepted pressure-wind relationship are analyzed and their practical limitations in operational meteorology are discussed. Extensive graphical and statistical information on intensity versus SST for different oceanic basins, latitude, and season is included in the appendices.

Gary B. Kubat
Department of Atmospheric Science
Colorado State University
Fort Collins, Colorado 80523
Summer, 1995

ACKNOWLEDGEMENTS

Above and beyond all else I must thank my wife Catherine Anne and my daughter Katrina Marie for accepting my absence during the past few months and tolerating my absentmindedness while I was home. This research could not have been done without their support. The encouragement and guidance of Professor William M. Gray has been invaluable, and Dr. Gray has literally changed my operational latitude: upon arrival at CSU I was a mid-latitude type of forecaster, but I am now comfortable with "low f" and "weather systems that move in the wrong direction". Considering my upcoming assignment to the Joint Typhoon Warning Center (JTWC) this is a good thing!

Numerous discussions with office mates John Knaff, Pat Fitzpatrick and Chris Landsea brought forth many great ideas, and prevented many mistakes before I could make them. Their assistance with programming has been invaluable as has that of Bill Thorson who also helped extensively in manipulating and plotting information from the data sets involved. Thanks also go to Barbara Brumit, Bill Thorson and John Sheaffer for ensuring this report met a timely and accurate completion. Typing, grammar and graphics are not my strong points, and their assistance in these matters is highly appreciated. This work was supported by the Air Force Institute of Technology (AFIT) Civilian Institution program, and I thank the Air Force for providing this opportunity to further my knowledge as an active duty officer.

TABLE OF CONTENTS

LIST OF FIGURES

LIST OF TABLES

LIST OF SYMBOLS AND ACRONYMS

CAC = Climate Analysis Center, NOAA/NWS/NMC.

COADS = Comprehensive Ocean-Atmosphere Data Set.

EPI = Empirical Potential Intensity; similar to MPI.

IMSL = International Mathematics and Statistics Library. A set of FORTRAN subroutines available for use at Colorado State University.

Inner-Core = The region of a TC extending from the center of the eye to 1° radius.

JTWC = Joint Typhoon Warning Center (U.S. Air Force and Navy), based on Guam.

MPI = Maximum Potential Intensity. A theoretical upper intensity limit for a tropical cyclone, based on SST.

MSLP = Mean Sea Level Pressure. Used in this document it primarily refers to minimum central pressure of a tropical cyclone.

NMC = National Meteorological Center.

NCAR = National Center for Atmospheric Research.

NOAA = National Oceanic and Atmospheric Administration.

NWS = National Weather Service.

OCS = Outer-Core Strength. An area-weighted average tangential wind speed within the outer-core region calculated relative to the cyclone's motion.

OMLT = Ocean Mixed Layer Temperature

Outer-Core = The region of a TC extending from 1° to 2.5° radius.

RH = Relative Humidity.

RMW = Radius of Maximum Wind.

SST = Sea Surface Temperature.

TC = Tropical Cyclone. Hurricanes and typhoons in this text are generically labelled TC.

TYAN = U.S. Navy Typhoon Analysis best track data set.

UCAR = University Corporation for Atmospheric Research.

V_T = Tangential Velocity.

V_{Tmax} = Maximum Tangential Velocity.

Chapter 1

INTRODUCTION: MAXIMUM POTENTIAL INTENSITY (MPI) SCHEMES

Tropical cyclone (TC) forecasters have long attempted to assess the maximum possible intensity which TCs might attain for a given set of tropical atmospheric and ocean surface conditions; this conceptual intensity value has become known as the Maximum Potential Intensity (MPI). MPI is a very useful concept as it has implications for strategic life and property saving activities including re-routing of shipping traffic and evacuation of threatened land areas. In recent decades several somewhat distinct methods for estimating MPI have been put forth. In this chapter four such methods, termed the "potential temperature", "Carnot cycle", "pure thermodynamic" and "buoyant energy" methods are reviewed.

1.1 Potential Temperature Approach to MPI

In general, tropical storms are fueled by the release of latent heat of condensation. This simple fact is the basis of one of the earliest views of MPI. Miller (1958) noted that there are two primary factors limiting the amount of latent heat energy that can be released by tropical convection: 1) the initial equivalent potential temperature of the near surface parcels, and 2) the "prevailing lapse rate within the free atmosphere". Moist adiabatic ascent occurs over a very wide area with minimal entrainment of dry or cool air into the storm center from outside the system. The enormous amount of latent heat released during parcel ascent is partially converted into kinetic energy (radial and tangential winds) and also warms the core region leading to deep surface pressure falls (Miller, 1958). Whereas Miller had a very good understanding of how TCs function, little progress had been made

towards the application of these physical interpretations in quantitative assessments of storm dynamics. Regarding maximum potential storm intensity, Miller developed a view of the constraints on intensity which involves the mean virtual temperature. Assuming hydrostatic balance, the "minimum possible pressure at the surface is dependent upon the maximum possible mean virtual temperature that can exist within the column extending from sea level to the top of the hurricane vortex (Miller, 1958).

Thus, Miller proposed that MPI is dependent upon: 1) SST; 2) relative humidity at the surface; 3) environmental lapse rates, and 4) potential temperature and height of the air which is forced to subside into the eye. From these associations Miller developed the well-known "Miller curve" of SST versus pressure (Fig. 1.1) which has been referenced for many years. Actual observational data of TC intensities versus SST values from the Atlantic and Pacific ocean basins are shown in Figs. 1.2 and 1.3. These data indicate that the general features of Miller's curve are qualitatively correct, although underforecasts of the intensity peaks are evident. Thus, the theory that TC intensity is closely regulated entirely by potential temperature does not appear to adequately explain the lowest observed surface pressure. Since 1958 a few researchers have attempted better representations of MPI based on SST, but there remains room for further improvement.

1.2 Carnot Cycle Approach to MPI

Another perspective on MPI has been termed the "Carnot cycle" approach. Emanuel (1986, 1989) proposed that TCs can be viewed as very large heat engines that can be described in terms of the Carnot cycle. Nicholas Leonard Sadi Carnot (1796-1832) was a captain in the Luxembourg Corps of Engineers who essentially founded the science of thermodynamics as well as developing the basic equations governing what is now called the Carnot cycle (Wallace and Hobbs, 1977). The Carnot cycle makes use of the Second Law of Thermodynamics as it describes the fractional amount of heat energy which can be converted into physical work.

In simple terms, the Carnot model describes the process of converting heat into work. When a certain amount of energy (or heat, Q1) is put into a system during isothermal

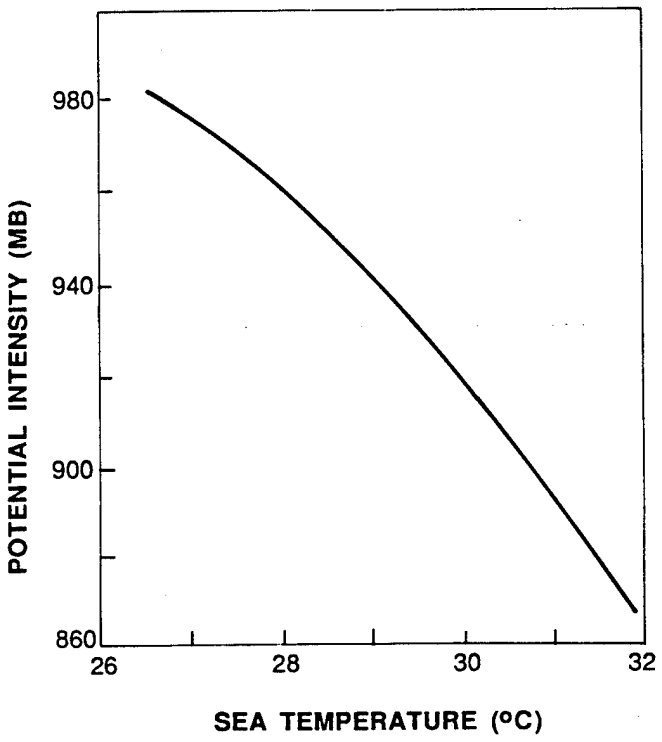

Figure 1.1: The relationship between SST and the potential intensity of tropical cyclones expressed as sea level pressure (from Miller, 1958).

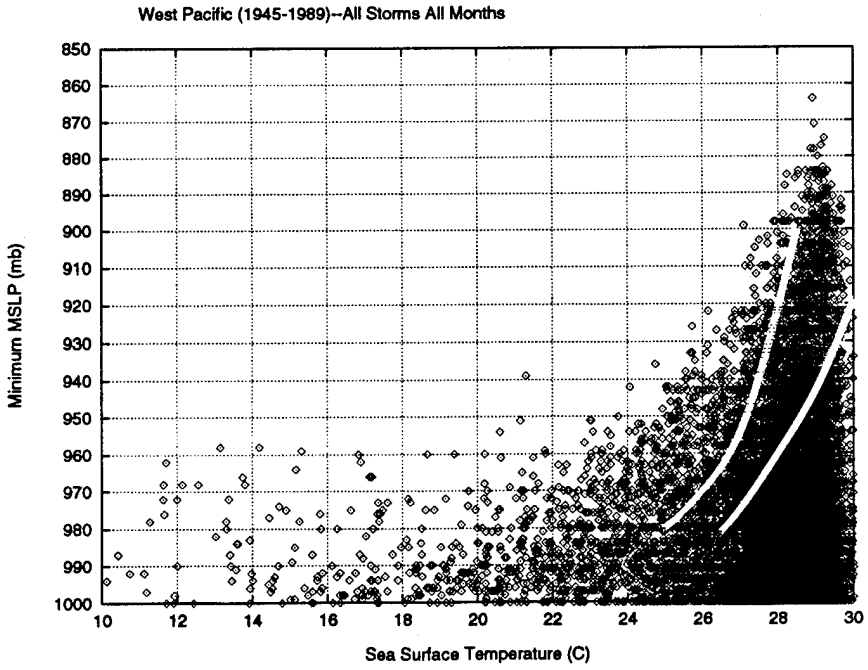

Figure 1.2: Observed intensities (MSLP) for the Northwest Pacific basin with the Miller (1958) and Merrill (1985) curves superimposed. Merrill's Empirical Intensity (EPI) curve and Miller's theoretical curve were determined from Atlantic basin data, and this shows how inappropriate it is to use such curves outside of their basin or origin.

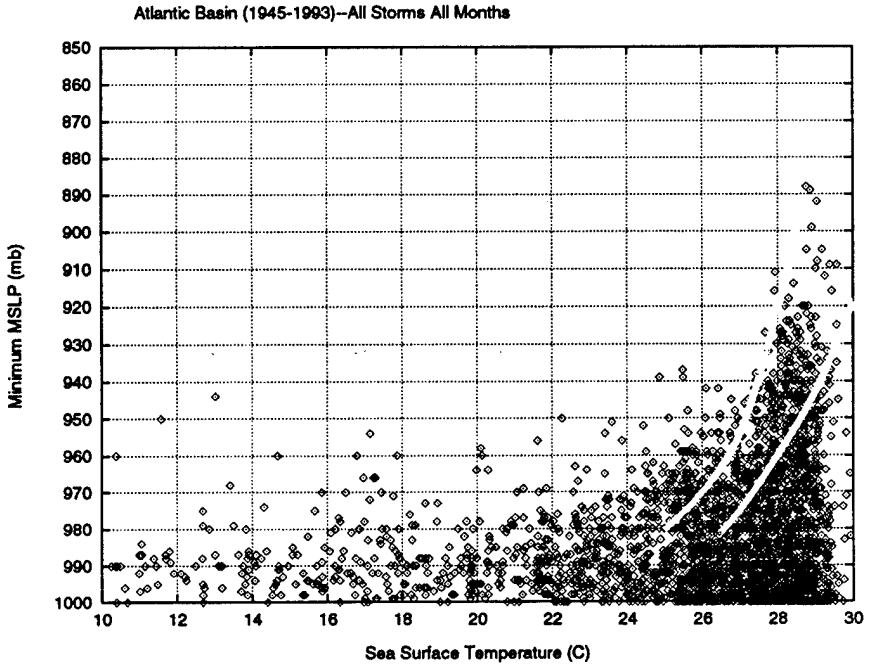

Figure 1.3: Observed intensities (MSLP) for the Atlantic basin with the Miller (1958) and Merrill (1985) curves superimposed. Note the underestimation of MPI by each MPI curve.

expansion and another amount of energy (or heat, Q2) is released by the system during isothermal compression, an optimal amount of work equal to Q1-Q2 can be performed. This concept is illustrated schematically in Fig. 1.4. Emanuel (1987) expanded this concept as it applies to the MPI of TCs. When a given amount of energy is released into the TC from the (warm) ocean surface, this heat enables the TC to do work (eg., become intense or maintain intensity) as the heat leaves the TC at a temperature colder in the outflow region.

The conceptual model used by Emanuel is shown in Figure 1.5. Air parcels enter the TC at radius r_o with constant temperature T_B. During passage over the warm ocean surface along the trajectory the air parcels gain sensible and latent heat ΔQ_1 as described by Eq. 1.1. These parcels then ascend adiabatically along constant entropy surfaces and flow radially outward, experiencing radiative cooling. Air then briefly experiences isothermal compression to balance radiative cooling (Eq. 1.2). Finally, air sinks dry adiabatically to its initial location, completing the cycle. The total heating ΔQ, is merely the sum of a gain and a loss term, as described by Eq. 1.3. It is this net heating which fuels

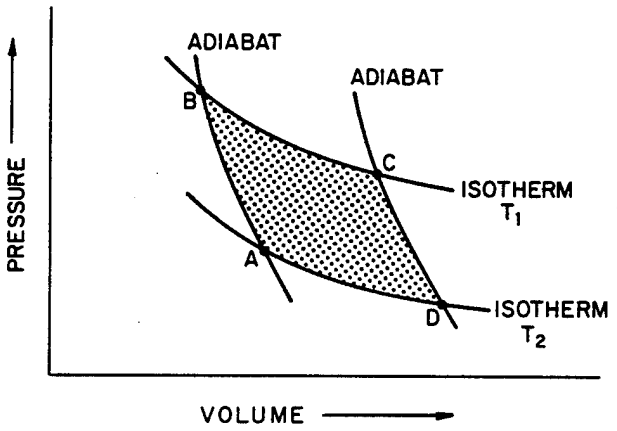

Figure 1.4: Representation of the Carnot cycle (from Wallace and Hobbs, 1977).

the sum of a gain and a loss term, as described by Eq. 1.3. It is this net heating which fuels the storm and maintains it against frictional dissipation. The balance between heating and energy loss can be written as Eq. 1.4. The work in the planetary boundary layer (W_{PBL}) is essentially frictional loss and the outflow work (W_O) in the upper troposphere is proportional to the required change in kinetic energy required to restore the angular momentum of the outflow back to the environmental value. Further manipulation of these work terms allows the explicit description of pressure values associated with specified environmental conditions and surface relative humidity.

$$\Delta Q_1 = \int_{\theta_{ea}}^{\theta_e} C_p T_B d ln\theta_e = C_p T_B ln\frac{\theta_e}{\theta_{ea}} , \tag{1.1}$$

$$\Delta Q_2 = \int_{\theta_{ea}}^{\theta_e} C_p T_{out} d ln\theta_e = -C_p \bar{T}_{out} ln\frac{\theta_e}{\theta_{ea}} , \tag{1.2}$$

$$\Delta Q = \Delta Q_1 + \Delta Q_2 = C_p T_B \varepsilon ln\frac{\theta_e}{\theta_{ea}} , \tag{1.3}$$

$$\Delta Q = W_{PBL} + W_0 , \tag{1.4}$$

$$\varepsilon \equiv \frac{T_B - \bar{T}_{out}}{T_B} \tag{1.5}$$

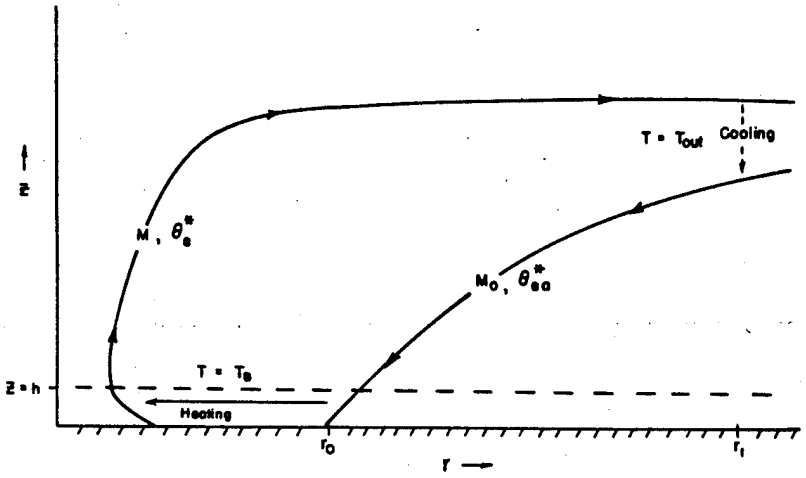

Figure 1.5: Conceptual illustration of the tropical cyclone as a Carnot heat engine (from Emanuel, 1986). Parcels enter the system near the surface at some radius r_0 and gain energy from the ocean surface while traveling radially inward. They then rise along constant entropy surfaces and travel radially outward at high altitude. While travelling outward the parcels cool radiatively to space, returning to a lower entropy surface to repeat the cycle.

One of the main problems with the Carnot cycle approach becomes apparent when examining the thermodynamic efficiency (Eq. 5) of the system. To achieve efficiency values (ε) high enough to reach the required heating ΔQ (see Eq. 1.3) needed for tropical cyclones to exist, the difference $T_B - \bar{T}_{out}$ must be very large. The inflow temperature T_B is essentially limited by the SST, and therefore the outflow temperature $\bar{T}_{out}$ must be very cold. The cold outflow temperatures required (on the order of –100°C and lower) are not in very close agreement with observations of tropical cyclones (Holland, 1995). Neglected by this approach is the conditional instability that may have already existed in the environment. Emanuel (1989) accounts for this by postulating that conditional instability roughly balances the frictional dissipation within the cumulus clouds comprising the TC and therefore does not affect MPI.

Another significant problem can be seen in sensitivity studies of the Carnot cycle approach (Holland, 1995). It has been shown that a two percent change in relative humidity values produces a change in TC intensity equal to that of a one degree Centigrade change in SST. Relative humidity values in and around TCs can vary widely, yet the actual intensities don't vary as much as would be predicted by this heat engine approach. Therefore

the Carnot model approach using only SST and outflow temperatures does not appear to be an accurate way to infer MPI.

Probably the most interesting result of Emanuel's application of the Carnot model to MPI concerns the possibility for the development of "hypercanes" as illustrated in Fig. 1.6 (Emanuel, 1991). The Carnot cycle implies that MPI is determined by the storm radius and the upper level outflow temperature (where all environmental parameters are equal). Because of these assumptions the model predicts a runaway deepening mode whereby storms intensify logarithmically with decreasing outflow temperatures and increasing SST (Emanuel, 1991). Thus, TCs far deeper than those currently observed are inferred to be possible. In Fig. 1.6, the region to the upper right of the 700 mb contour is the "hypercane" region, where the amount of mechanical energy produced by the Carnot heat engine is too large to be balanced by surface frictional dissipation. In this region, MPI is hypothesized to accelerate the 0 mb, although internal turbulence may limit this process (Emanuel, 1988).

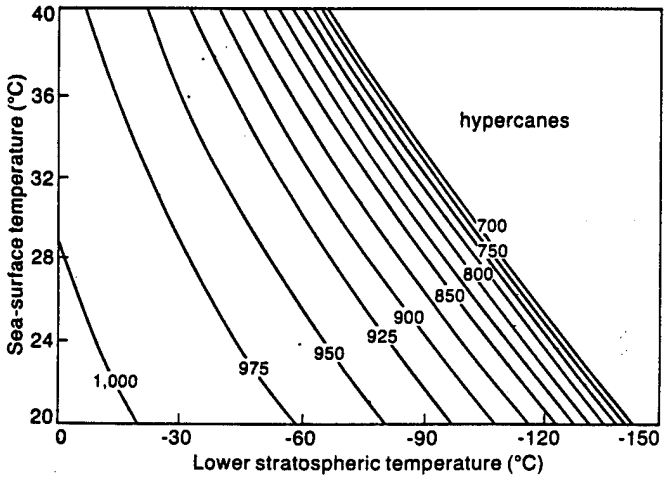

Figure 1.6: "The minimum sustainable central pressure (in millibars) as a function of sea surface temperature (T_s) and mean outflow temperature ($\bar{T}_o$), assuming an ambient surface pressure of 1015 millibar and an ambient near-surface relative humidity (RH) of 75%" (from Emanuel, 1991).

1.3 Pure Thermodynamic Approach to MPI

Another approach to MPI which has recently been developed by Holland (1995) will be termed the pure thermodynamic approach. By assuming that internal processes and dynamics provide no constraint on TC intensity, MPI can be estimated by analyzing the available thermodynamic energy present in the surrounding ocean-atmosphere environment.

The basis for this approach has been known for quite some time. Given an assumption of hydrostatic balance, warming a column of air by latent heating in a convective plume will result in a decrease in surface pressure. Riehl (1954) and Malkus and Riehl (1960) discussed this in some detail. Initially the process can yield only about 30 mb of surface pressure drop for typical tropical ocean conditions. However, after the first intensification cycle occurs and surface pressure falls, additional moist enthalpy is extracted from the ocean surface assuming the surface flux can balance adiabatic cooling such that the surface temperature remains the same, and the process repeats itself. This increase in θ_e is a result of maintaining the surface temperature at a lower pressure. For each cycle, there is a diminished return of pressure drop and a steady state condition is eventually reached. Thus, unlike the Carnot model approach, "hypercanes" are not physically achievable. Various authors have described this cyclic process, most notably Gray (1979; 1995a,b). This is the primary source of surface pressure falls in TCs with roughly three fourths of the surface pressure intensification results from this redistribution of moist enthalpy (Malkus and Riehl, 1960).

In addition to the moist enthalpy redistribution process, Holland includes subsidence within the eye in his thermodynamic approach to determining MPI in a manner similar to Miller (1958) (see section 1.1 on the potential temperature approach). Once an eye has formed within a TC, subsidence warming of the inner eye region results in further decrease of surface pressure (Miller, 1958; Holland, 1995). This subsidence warming induced pressure fall then feeds back into the moist enthalpy redistribution process, leading to further pressure fall.

The process used to determine MPI by Holland is quite simple to visualize (Fig. 1.7). Air parcels flow into the TC and establish a steady state balance of moisture and temperature with the ocean surface before ascending in the eye wall region (note the independence of air parcel origin). Given a profile of the ambient atmosphere expressed in terms of surface pressure and moisture/temperature with height, surface pressure drop due to the combined moist enthalpy redistribution and eye subsidence process can be calculated by iteration.

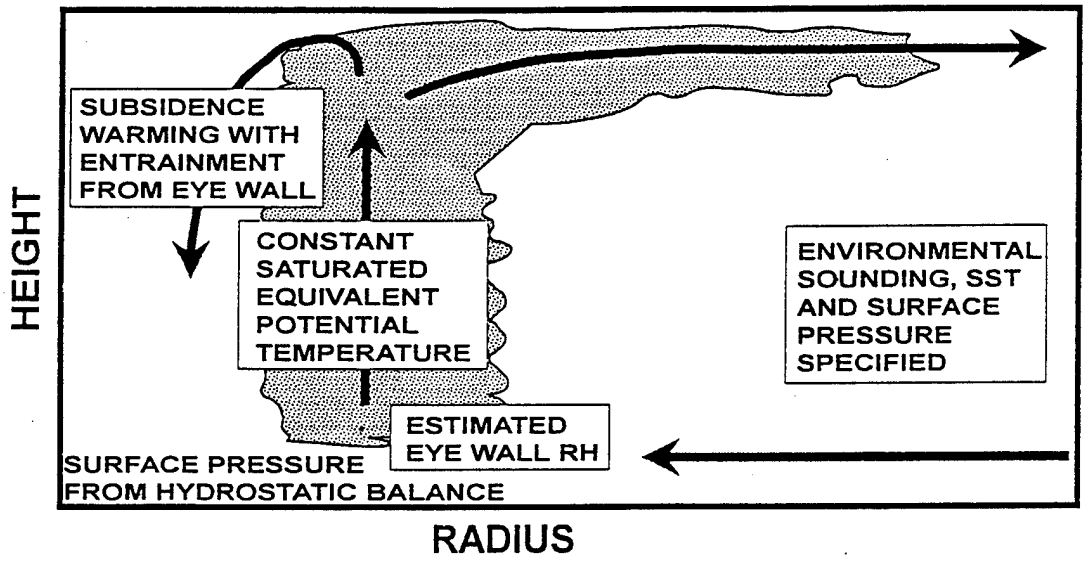

Figure 1.7: Schematic of the process used to determine MPI thermodynamically from the environmental sounding (Holland, 1995).

Due to the simplicity of this model, there are of course some problems with it. One of the most significant of these problems is the lack of detailed storm dynamics since no consideration is given to the complex eyewall structure or slope. These are important considerations to include in an MPI scheme and will be discussed in the following section which considers a buoyant energy approach MPI.

1.4 Modified Buoyant Energy Approach to MPI

The "modified buoyant energy" approach to MPI is very similar to the pure thermodynamic approach as discussed above, but assumes instead that internal TC dynamics and environmental effects do impact the intensity that a TC can achieve. Gray (1995b)

states that "The amount of mass flux that can be processed by the eye-wall clouds of a tropical cyclone is the primary factor specifying how intense it can become." Buoyancy in the eye-wall cloud plus its slope and size of the eye itself, determine how much mass can be processed by a TC. Thus, intensification depends upon the eye-wall cloud pumping through enough mass to exceed surface frictional dissipation and resistance to upper level mass export. The key to these processes happening is significant upward vertical motion within the eye-wall cloud.

An important aspect of this approach is that it attempts to deal with some of the fundamental problems which the approaches already discussed have ignored. Recent surface buoy measurements indicate that the temperature difference between the ocean surface and the overlying air near the surface within a TC is in the 3°-4°C range (Pudov, 1992; Pudov and Holland, 1994; Black and Holland, 1994), previously this difference had been thought to be on the order of one degree Centigrade. The associated equivalent potential temperature decrease due to this difference is on the order of 5-6°K (Gray, 1995), drastically reducing the intensity values that would be predicted by such schemes as the Carnot model and the pure thermodynamic approach.

There are four hypothesized processes which can contribute to this reduced temperature of the surface air beneath the eyewall. These include oceanic turbulent mixing due to strong surface winds; surface wind induced oceanic upwelling; evaporative cooling; and adiabatic expansion cooling due to airflow down gradient towards lower pressure near the eye. All of these processes likely contribute to the observed 4°C temperature difference between the near-surface air and sea surface.

Two of these mechanisms are associated with oceanic processes. Turbulent mixing of the ocean due to the strong TC surface winds can bring cooler water to the sea surface; this effect is very pronounced when the thermocline is fairly shallow. Also, the cyclonic nature of the TC wind circulation leads to upwelling of cooler water due to Ekman pumping. As shown in Fig. 1.8, when surface winds blow in one direction, surface water is forced to the right of this path (in the Northern Hemisphere); when surface winds form a continuous

closed loop in a cyclonic direction surface water is forced away from the center of the eye. Cooler water from below then flows upwards (upwells) to replace this loss. In both of these cases cooler surface water results, which in turn lowers the air temperature. The magnitude of these processes is highly dependent on the wind velocity and the TC's translational velocity.

The other two surface air cooling mechanisms are due to atmospheric effects. As water from the ocean's surface and sea spray evaporate into the near surface air, 2400 Joules are removed from the air for every gram of water that evaporates. This translates into a cooling of 2.4°C for every 1 g kg^{-1} change in the atmospheric mixing ratio. Additionally, as air flows into the TC from the environment towards the eye, it experiences a pressure drop of 30-40 millibars. The temperature fall associated with adiabatic expansion for this pressure drop can be very significant. For example, starting at an environmental temperature of 28°C and pressure of 1000 mb, dry adiabatic expansion to 960 mb will result in a temperature of 24.5°C, a 3.5°C decrease; moist adiabatic expansion results in about 1°C cooling. As the central pressure of a TC falls beyond the 40 mb in this example, the cooling associated with air parcel expansion increases.

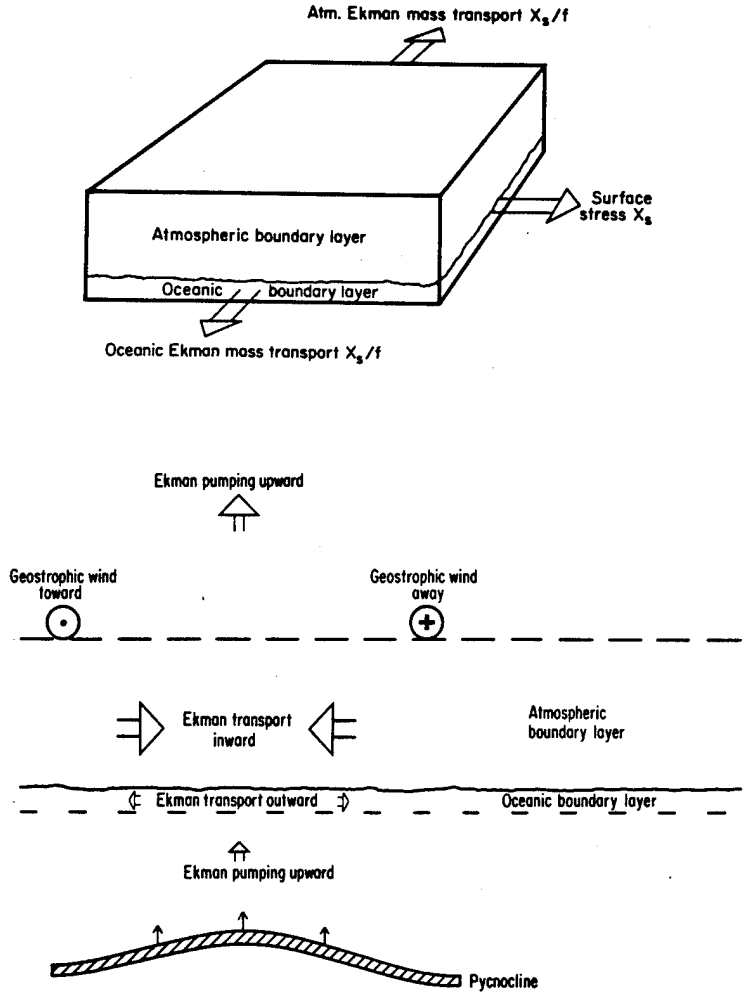

Figure 1.8: Ekman pumping in the ocean brings cooler water to the surface. a) Vectors of steady Ekman mass transport in the Northern Hemisphere (directions reverse in Southern Hemisphere) resulting from surface wind stress at the atmosphere-ocean boundary. b) In a tropical cyclone (depicted here for the Northern Hemisphere), cyclonic surface winds induce inward atmospheric mass transport within the atmospheric boundary layer and outward oceanic mass transport within the oceanic boundary layer. The outward transport of water results in deeper (i.e, cooler) water being pumped towards the surface. Although this water may never reach the surface through Ekman pumping as the cyclone moves, turbulent mixing due to strong winds can significantly cool the surface water, especially to the rear of the tropical cyclone motion (figures from Gill, 1982).

Chapter 2

DATA AND METHODS OF ANALYSIS

The data used in this research are a combination of climatological data sets and actual tropical cyclone (TC) measurements. Best track data for tropical cyclones observed in the Northwest Pacific and North Atlantic basins were used and supplemented with climatological ocean and upper air temperatures. Fully independent data obtained by direct aircraft measurement were used to verify relationships found in the best track data. Details of the data sets and how the data was analyzed are as follows.

2.1 North Atlantic Best Track Data

Tropical cyclone data for the Atlantic ocean basin come from the North Atlantic best track data supplied by the National Hurricane Center (NHC) in Miami, Florida. The database contains information from 1886 until 1993. Aircraft reconnaissance began in 1944, all data prior to 1994 have been neglected in this study. As reported by Landsea (1993), there is a bias in wind strength reports for the years prior to 1971; an approximate 5 knot systematic overestimation of wind strength for TCs of 100 kt has been found. To ensure wind analyses in this research are representative of true wind strength, no wind data prior to 1971 have been used.

Further details of the Atlantic best track data set can be found in Jarvinen, et al (1984). The complete data set is available on the internet via anonymous ftp from typhoon.atmos.colostate.edu under filename 'tra86to93.atl.Z'; additional documentation for this data file is located in the 'README.atl' file at the same site.

2.2 Northwest Pacific Best Track Data

Tropical cyclone data for the Northwest Pacific ocean basin come from the U.S. Navy's Typhoon Analysis (TYAN) best track data set, provided to the Gray research group by Buck Sampson at the Naval Environmental Prediction and Research Facility (NEPRF), Monterey, California.

The data used run from 1945 until 1989 and contain the same information as that in the North Atlantic best track data described above. The other primary TC data set for the Northwest Pacific comes from the Joint Typhoon Warning Center (JTWC) in Guam whereas the JTWC data set may contain more TCs overall, it doesn't contain information on MSLP; thus the decision to use the TYAN data set. As with the Atlantic data, only the years 1971 and later have been used for wind analysis due to possible bias in reported wind strength prior to 1971.

2.3 Global Upper-Air Climate Data

The "Chellia's CAC Global Tropospheric Climate Diagnostics, 1979-1988" data base has been used for climatological upper-air data. This data base is prepared and maintained by the Data Support Section, Scientific Computing Division, National Center for Atmospheric Research which is operated by the University Corporation for Atmospheric Research (UCAR) under sponsorship from the National Science Foundation. The database contains long term monthly global climate statistics in a 144X73 array of 2.5 degree by 2.5 degree gridded data at nine standard pressure levels (1000 mb, 850 mb, 700 mb, 500 mb, 300 mb, 250 mb, 200 mb and 100 mb). Data parameters include geopotential height (Z; in meters), temperature (T; in Kelvin), and zonal and meridional winds (U and V, respectively; in meters per second).

2.4 Ocean Mixed Layer Temperatures Climatology

This data set is as a subset of the Climatological Atlas of the World Ocean created by Sydney Levitus of GFDL. The data represents the result of objective analyses performed

on a 1 degree latitude-longitude grid at a number of constant depth surfaces (used here are the surface, 10m, 20m, 30m and 50m levels). In excess of one million observations were used in creating the original climatological data set. For further details refer to NODC (1984).

2.5 Shea and Gray (1976) Flight Data Summary

Additional data used in this study come from the Shea and Gray (1976) Data Summary of NOAA Research Flight Facility (RFF) aircraft measurements. This data set contains flight information from NOAA/RFF flights during 1957-1967 and 1969. The aircraft used to gather this data included B-47's and B-50's in 1957-1958, and B-57's and DC-6's thereafter. Approximately 100 flights were flown into 22 Atlantic hurricanes and direct independent measurements of wind and pressure were made along numerous radial flight legs during the twelve year period contained in the summary. The data in the Summary are at 2.5 n mi intervals from 5 to 50 n mi radius. Each TC was typically sampled by 4-6 radial legs flown at one level within a 4-8 hour time frame. Further information about this data, such as instruments used, data collection procedures, and data accuracy can be found in Shea and Gray (1976).

2.6 Data Analysis

Best track data for the two ocean basins (Northwest Pacific and North Atlantic) were put into two very large columnar data files. These files included storm name, date, time and location. Minimum mean sea level central pressures (MSLP) and maximum winds (V_{Tmax}) for each TC as determined by post-analysis of each system by the responsible forecast office were also included. Climatological ocean mixed layer temperatures (OMLTs) at five levels were added based upon TC location.

Analyses based upon location, season and ocean temperature were then performed using various FORTRAN routines and plotting programs. Correlation and regression calculations were performed using IMSL (1987) FORTRAN subroutines. Other statistics

such as means, standard deviations, and Student's t-number were coded using standard equations available in any introductory statistics text.

Curves of absolute maximum intensity were subjectively estimated (i.e., "eye-balled") to determine best fit. The decision to use hand analysis rather than computer plotting was based upon a pronounced lack of data at the extreme values. While plotting data using the 95th or 99th percentiles produces curves very near the edge of the data, these curves miss the absolute edge of the data. Thus, it is important to remember when viewing the curves of maximum achieved intensity in this research that the methodology used differs from procedures which others [such as Merrill (1987) or DeMaria and Kaplan (1994)] have used to determined MPI curves. The curves for MPI presented here are indeed the absolute maximum intensities achieved, and not a best fit curve to the center of the top 1 or 5 percent of available data points. The choice of using best fit curves to the top percentiles essentially reduces any MPI curve on the assumption that the absolute highest intensity values are, in reality, overestimates of what was actually occurring. It may be possible, however, that less than even a tenth of one percent of the data points used lie at the true SST-based MPI value of any TC. When viewing the comparisons between MPI curves derived by others and those presented here, keep in mind the difference in methodology which in itself imparts a displacement between the curves.

Chapter 3

TROPICAL CYCLONE INTENSITY VERSUS SSTS IN NORTHWEST PACIFIC AND ATLANTIC OCEAN BASINS: GENERAL RELATIONSHIPS

The data described previously in Chapter 2 will be used in this chapter for assessing the SST-TC intensity associations which were summarized in the introduction. The analysis begins with comparative studies of the relationships between the two primary indices of TC intensity – sea level pressure and tangential wind speeds. These associations are examined for both the Atlantic and Pacific basins, followed by an analyses and interpretation of the causes of the main differences tied to season and latitude. The associations between SST and each of these TC intensity indices are then examined individually, followed by a more general discussion of the relationships in the West Atlantic region. A more detailed discussion of the TC intensity-SST relationship follows in Chapter 4.

3.1 Minimum MSLP Versus Maximum Best Track Tangential Wind Velocity

Graphs comparing minimum central mean sea level pressure (MSLP) versus maximum tangential wind velocity (V_{Tmax}) have been created for the Atlantic and Northwestern Pacific basins. Subsets based on month and latitude stratifications for each basin have also been developed. It is readily apparent in such data that strong variability occurs in the pressure-wind relationship (see Weatherford, 1985). For example the pressure-wind relationship for the Atlantic basin during the months of August, September and October (Fig. 3.1) indicates significant variability. Wind velocity for hurricanes with 980 mb central pressure range from 40 to 100 kt. Similarly, those hurricanes with winds of 90 kt display central pressure values ranging from 942 mb to 995 mb. Similar comparisons can

be made in the Pacific (Fig. 3.2). Obviously, using best fit curves to infer one value from the other in an operational setting yields values which may differ significantly from reality.

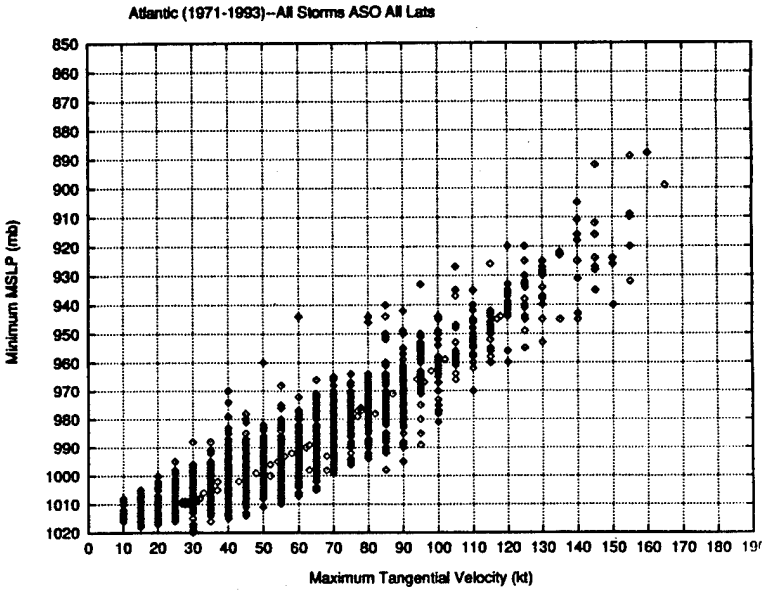

Figure 3.1: Minimum MSLP versus maximum tangential velocity (V_{Tmax}) for the Atlantic basin during August, September and October for the period 1971-1993.

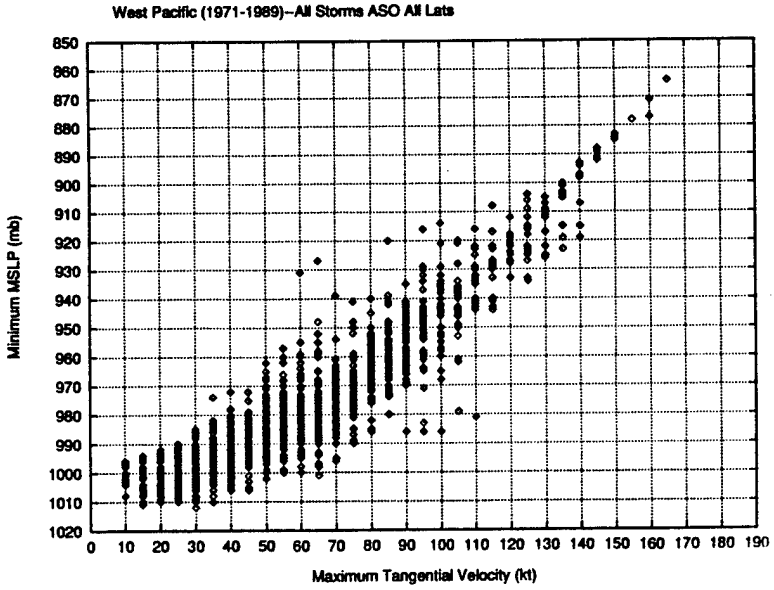

Figure 3.2: Minimum MSLP versus maximum tangential velocity (V_{Tmax}) for the Northwest Pacific basin 1971-1989 during August, September and October.

It is important to note that the data used to make these plots are not fully independent. Part of the relationship in Figures 3.1 and 3.2 is the result of wind observations being used operationally to estimate pressure, and vice versa. An analysis of 22 hurricanes in the Atlantic basin shows the effect to be minimal. The measurements used were made by NOAA Research Flight Facility aircraft during 1957-1967 and 1969, and are fully independent (i.e., MSLP and V_T were each measured). Plotting low-level (below 500 mb) flight data contained in the Shea and Gray (1976) data set fives a very similar pressure-wind distribution (Fig. 3.3) to the TYAN best track data (Figs. 3.1 and 3.2). Thus, the best fit center line curves seem minimally affected by operational use of pressure-wind curves in some of the cases included in the more extensive TYAN data set.

Graphs of minimum MSLP versus average tangential winds at 50 n mi radius were also generated (Figs. 3.4 and 3.5) from the Shea and Gray (1976) data set. Figure 3.4 is of average actual tangential velocity, which contains TC motion in the velocity measurements. The averaging process tends to smooth out the TC motion effect, but radial legs flown into the TCs were not completely symmetric and thus motion does impact the average. If the translational velocity of the hurricane's eye is first removed from the data before the averaging process, another graph (Fig. 3.5) can be produced for TC-relative tangential winds. Interestingly, neither of these plots show any relationship between V_T at 50 n mi radius and MSLP, while V_{Tmax} versus MSLP shows a high degree of correlation. The average radius of maximum wind in this data is approximately 25 n mi from the center of the eye, ranging from 5 n mi to 50 n mi radius.

The pressure-wind relationship shown in Figures 3.1, 3.2 and 3.3 is relatively constant with time within each particular basin. Note that an analysis of the center line of each month's MSLP versus V_T curve plotted for each basin shows very little monthly variation (Figs. 3.6 and 3.7). This is surprising as it would be expected that some degree of seasonal variation of the pressure-wind relationship within each basin would occur.

There is a slight latitudinal variation of intensity within each basin (Figs. 3.8 and 3.9). Higher latitudes have slightly deeper systems given the same tangential velocity. In

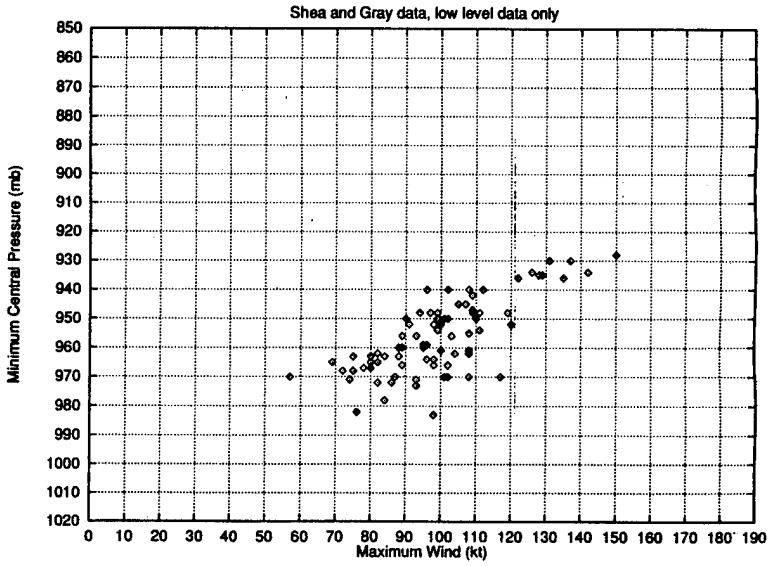

Figure 3.3: Minimum MSLP versus maximum tangential velocity (V_{Tmax}) for 22 Atlantic hurricanes over a twelve year period. Data came from in-situ measurements made by aircraft from the NOAA Research Flight facility during 1957-1967, and 1969 (data from Shea and Gray, 1976).

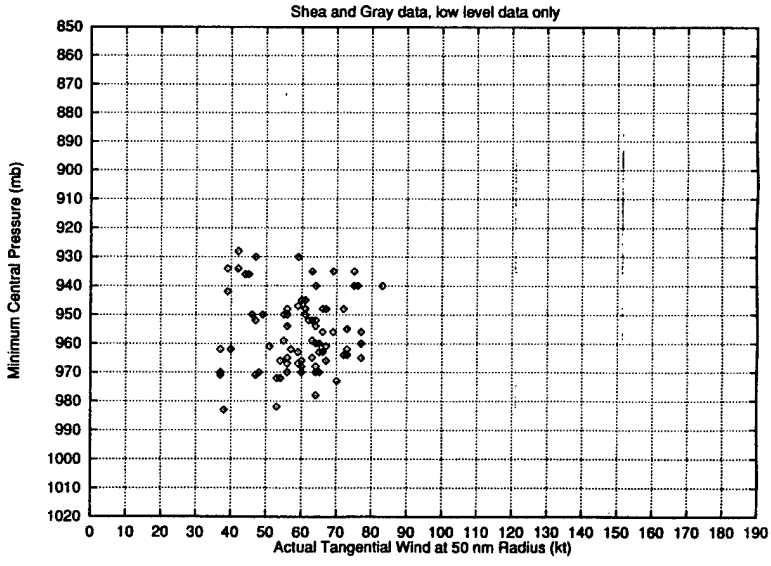

Figure 3.4: Minimum MSLP versus average actual tangential velocity for 22 Atlantic hurricanes (data from Shea and Gray, 1976).

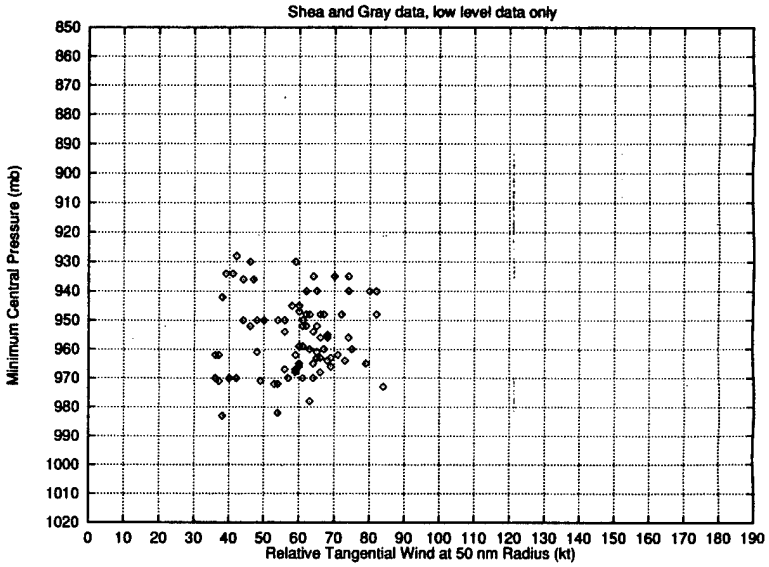

Figure 3.5: Minimum MSLP versus average relative tangential velocity (i.e., TC motion removed from data before averaging) for 22 Atlantic hurricanes (data from Shea and Gray, 1976.

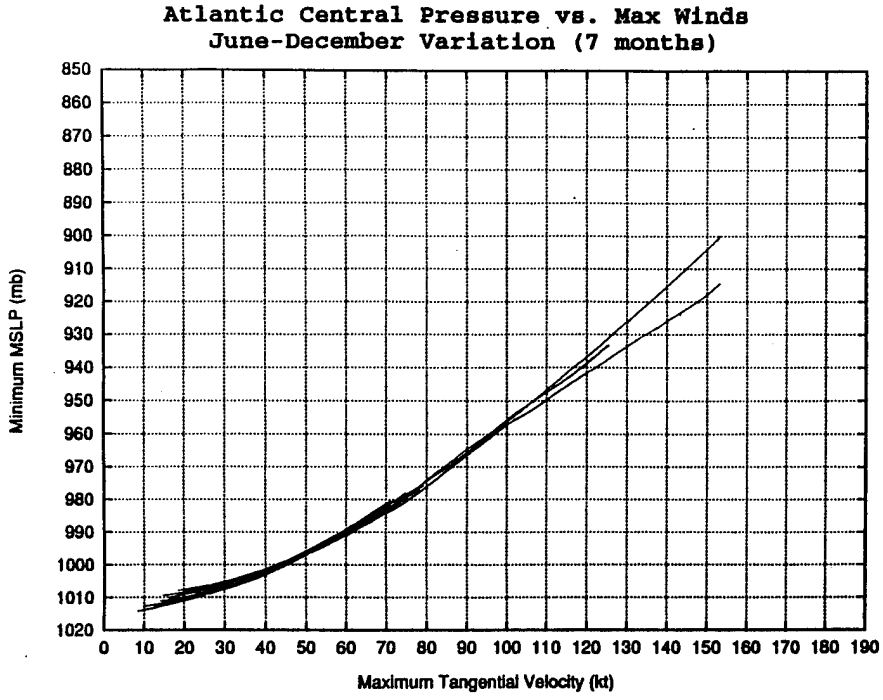

Figure 3.6: Seasonal variation of MSLP versus (V_{Tmax}) for the Atlantic basin June-December.

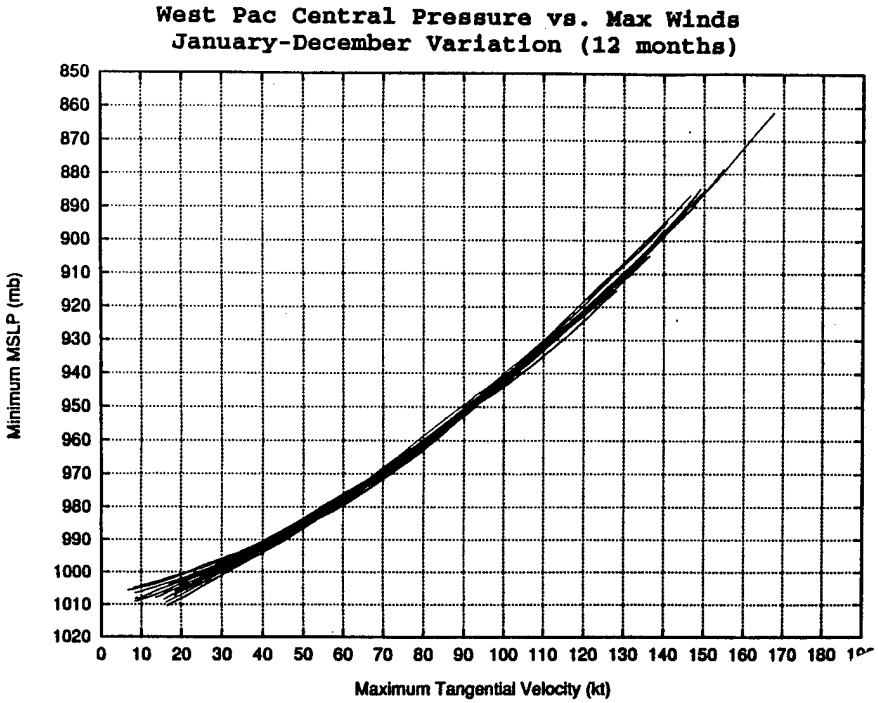

Figure 3.7: Seasonal variation of MSLP versus(V_{Tmax}) for the Northwest Pacific basin January-December.

the Northwest Pacific TCs centered on 40°N are roughly 8 mb deeper than those centered at 10°N for winds less than 50 kt. As wind strength increases, the curves tend to merge. In the Atlantic, the same pattern holds true but the difference is smaller; approximately 5 mb or less. One reason for this change with latitude is that as TCs progress poleward they become lager, and thus to maintain gradient wind balance a deeper eye is needed.

Another likely cause for the tendencies observed in Figs. 3.1 to 3.9 is the life cycle of the TC itself. Weatherford (1989) showed that, as storms mature, they go through a three phase life cycle (Fig. 3.10). Phase 1 is described as simultaneous inner core deepening with outer core intensification. Phase 2 is inner core filling with outer core strengthening. Phase 3 is simultaneous filling of the inner core and outer core weakening. Phase 2 is the portion of the life cycle wherein recurvature predominantly occurs, and this causes trouble with any simplistic theory of TC inner and outer core relationships. During phase 2 the pressure gradient field changes significantly; the central pressure rises, and the storm expands radially outward, decreasing the pressure gradient very rapidly near the eye or

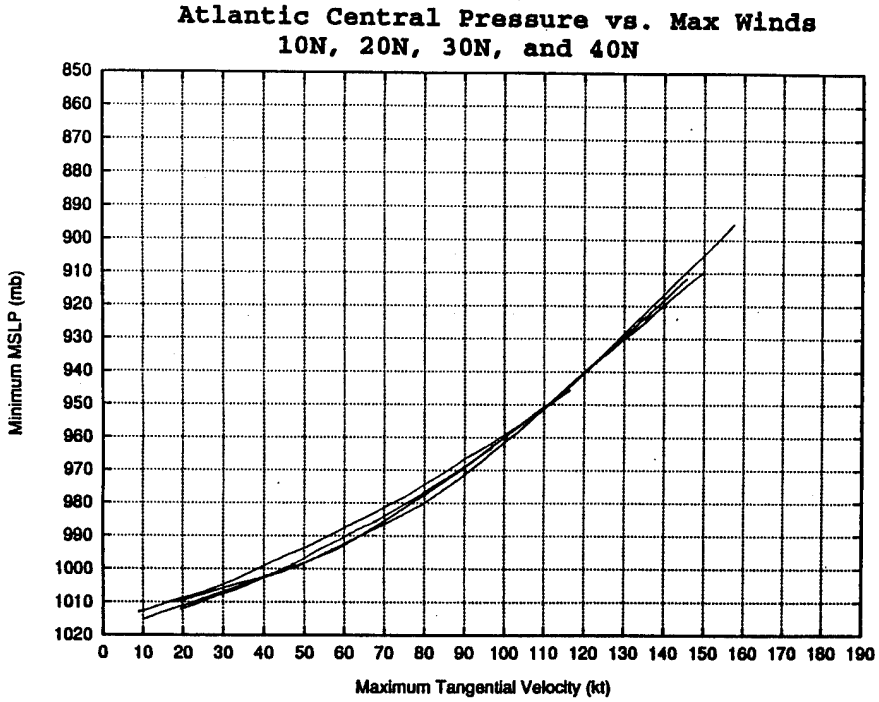

Figure 3.8: Latitudinal variation of MSLP versus maximum tangential velocity (V_{Tmax}) for the Atlantic Basin for 10 degree wide bands centered at 10, 20, 30, and 40 degrees north.

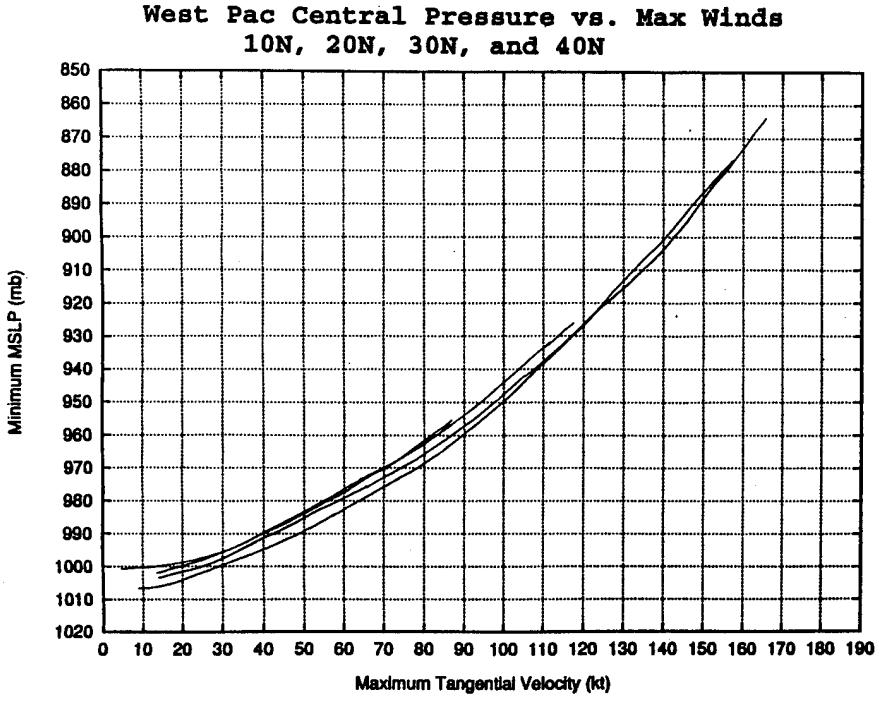

Figure 3.9: Latitudinal variation of MSLP versus maximum tangential velocity (V_{Tmax}) for the Northwest Pacific Basin for 10 degree wide bands centered at 10, 20, 30, and 40 degrees north.

recently filled eye. Thus, as storms move north and recurve while also going through phase 2 of the life cycle, stronger outer winds occur for similar central pressure values (Fig. 3.11), even while the maximum wind speed may diminish and the eye fills.

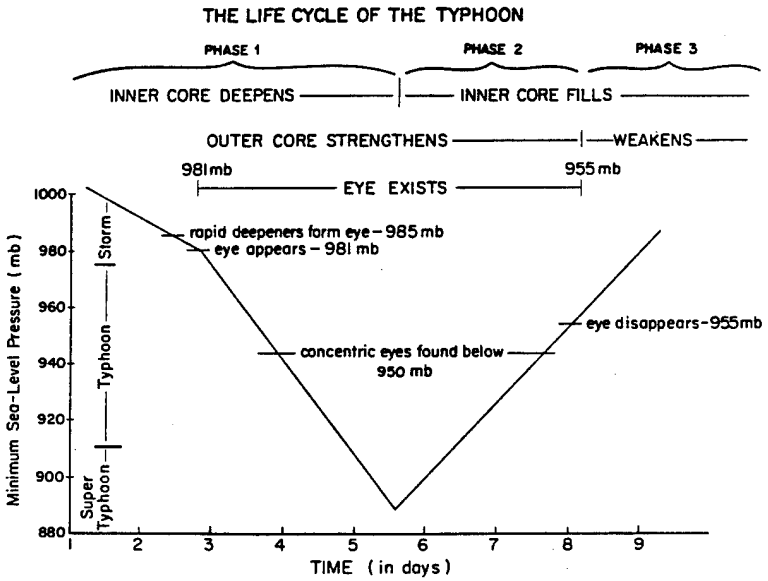

Figure 3.10: The three-phase life cycle of tropical cyclones (from Weatherford, 1989).

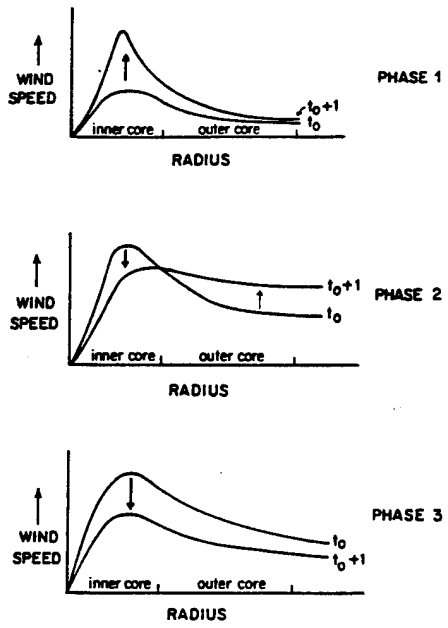

Figure 3.11: Variation of the low level tangential wind profile during the three phases of the life cycle (Weatherford, 1989).

A possible explanation for this latitudinal variation of the pressure-wind relationship is that of the opposing effects of the Coriolis parameter and the changing pressure gradient in the gradient wind balance. The equation describing this three way balance between pressure gradient, Coriolis and centrifugal forces is:

$$\nabla P = \frac{V^2}{R_T} + fV \tag{3.1}$$

where:

$\nabla P = \frac{-1}{\rho}\frac{\partial P}{\partial R}$

V = Wind velocity

R_T = Radius of the trajectory

f = Coriolis parameter ($2\Omega \sin \phi$)

With all else held constant, weakening the pressure gradient term (by filling the eye or by having the TC expand) decreases the wind velocity. Likewise, enlarging the cyclonic circulation results in weakening of the pressure gradient force, thus reducing the wind velocity. Increasing the last term by increasing f as a storm moves poleward results in a slightly stronger pressure gradient and slightly stronger winds. As TCs move poleward during phase 2 the Coriolis parameter increases. This alters the gradient wind balance, forcing the pressure gradient and radius of maximum winds to compensate to maintain gradient wind balance, thus causing the eye to partially fill and the storm to expand radially. As these effects are driven by changes in f, they play a perpetual game of catch up; thus when f increases as a TC moves poleward, it may fill and expand, but it also maintains or even increases its wind circulation. The central pressure and radius of maximum winds are able to compensate quickly enough, however, to prevent the storm from developing winds in excess of what we see observationally.

The pressure-wind relationship also displays a significant difference between the Pacific and Atlantic basins (see Fig. 3.12). For weaker velocities (below $\sim$ 60 kt) the Pacific central pressures are about 10 mb deeper than in the Atlantic. At higher velocities (above

$\sim$ 100 kt) this difference increases to 30 mb. Two things feed into this difference: climatological surface pressure differences, and TC size variation (Fig. 3.13). The climatological surface pressures of the Pacific are about 10 mb less than in the Atlantic (Sadler, 1987a,b) which accounts for all 10 mb difference for weak systems and 10 of the 30 mb difference in the strong systems. The second part of the difference lies in the size of the TCs involved. Pacific TCs often develop much larger outer circulations than do Atlantic TCs (Merrill, 1982, 1984). The mean Pacific TC has a radius of closed isobar that is about 1.5 times larger than that of the mean Atlantic TC's and covers roughly twice the surface area. This tendency leads to weaker pressure gradients in Pacific TCs for equivalent central pressure values and thus to lower wind velocities owing to the gradient wind balance process. The gradient wind equation (Eq. 3.1) shows this association clearly: as TCs increase in radial extent, the pressure gradient must decrease (∂P remains constant while ∂R increases), leading to a required decrease in velocity. Examining this process intuitively using a conservation of momentum argument works well too; as an ice skater spins, any increase in radial extent leads to a decrease in how fast the skater is spinning.

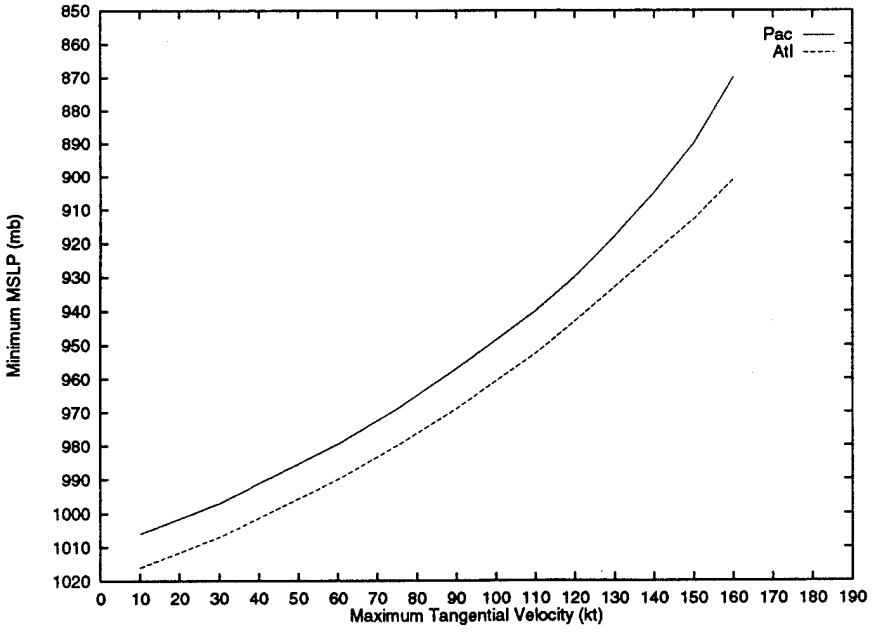

Figure 3.12: Minimum MSLP versus maximum tangential velocity(V_{Tmax}) for Atlantic and Northwest Pacific ocean basins. Note that the pressure-wind relationship for the Pacific is significantly different from that of the Atlantic.

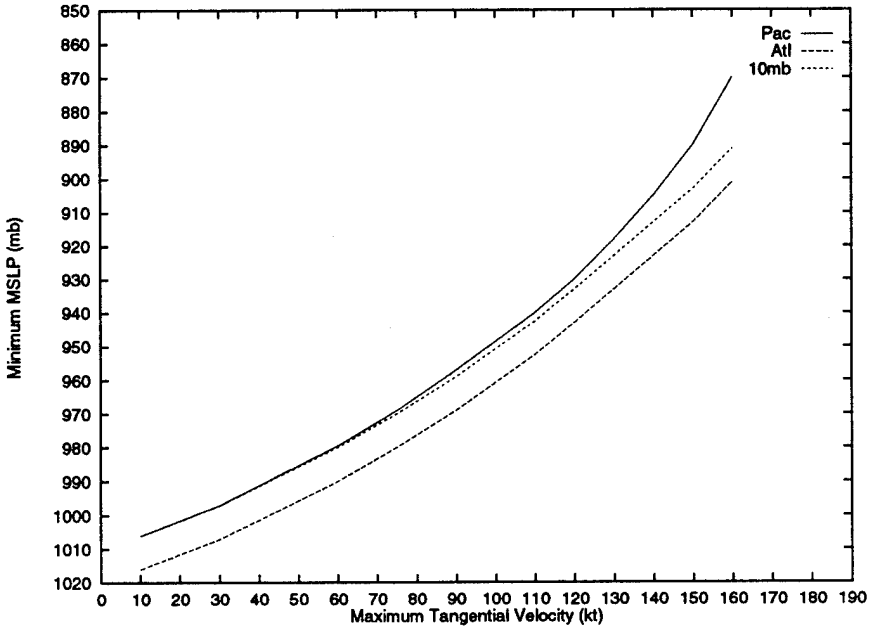

Figure 3.13: Minimum MSLP versus maximum tangential velocity(V_{Tmax}) for Atlantic and Northwest Pacific ocean basins overlaid with 10 mb climatological basin surface pressure difference correction. Note that the correction for ambient surface pressure differences between the basins accounts for all the differences for weak TCs, but only one-third of the difference for strong TCs.

3.2 The 30-30 Concept.

It becomes evident, when looking at graphs of MSLP versus V_{Tmax}, that the pressure-wind relationships follow an exponential shape (eg., Fig. 3.1, 3.2, etc.). At lower intensity levels, the pressure-wind curves display a fair amount of turning. However, at wind speeds beyond roughly 50 kt or central pressure lower than 990 mb, the curves can be approximated by straight lines. Error bounds can also be applied which are linear and parallel to the centerline of the data, as shown in Figures 3.14 and 3.15.

Statistically, the first standard deviation of the spread, comprising roughly two-thirds of the data, lies within approximately 10 mb or 10 kt from the centerline of the data. The second standard deviation, containing approximately 95 percent of the data, lies near 30 mb or 30 kt from the centerline. Although very simplistic, these numbers (i.e., 10 mb–10 kt and 30 mb–30 kt) appear to offer a useful association for tropical meteorologists to

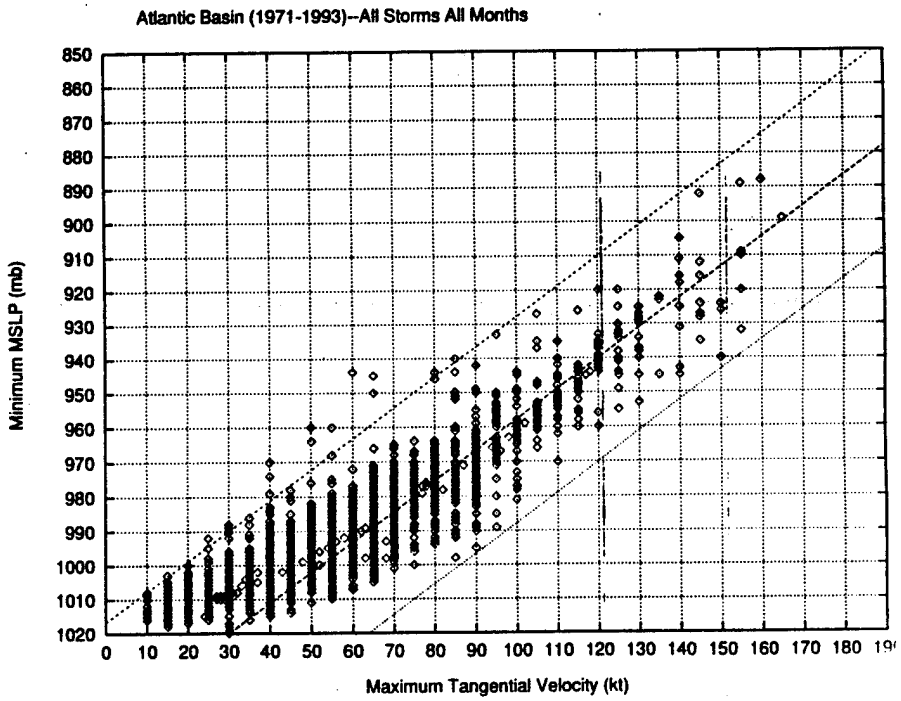

Figure 3.14: MSLP versus V_{Tmax} curve for Atlantic basin with centerline and 30 mb/30 kt error bound lines superimposed.

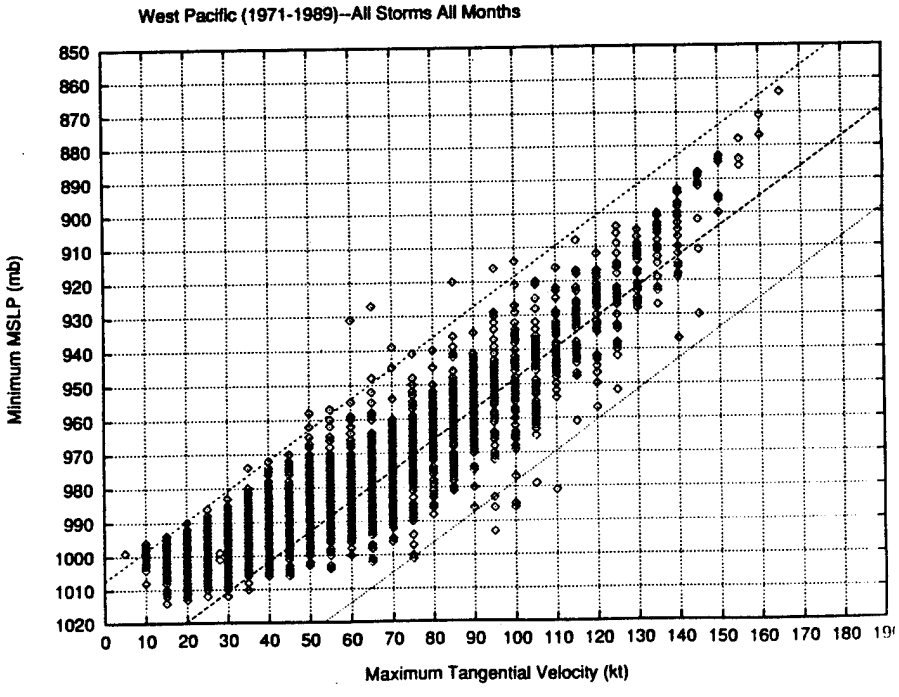

Figure 3.15: MSLP versus V_{Tmax} curve for Northwest Pacific basin with centerline and 30 mb/30 kt error bound lines superimposed.

remember. Bear in mind that these numbers reflect the results of best track averaging; raw data prior to best track results will show slightly higher deviations.

3.3 Minimum MSLP Versus SST

There is significant latitudinal variation of the MSLP-SST relationship, as would be expected since SSTs tend to vary with latitude (Figures 3.16 and 3.17). Interestingly, the peak of extreme minimum MSLP values occurs at about 20°N latitude. Also, for SSTs which are on the cool side of the spectrum, the associated most intense TCs will occur at higher latitudes. When that SST is on the warm side of the spectrum, the more intense storms occur at lower latitudes. Another way of looking at this is to note that as latitude increases, the intensity peak for each latitude goes toward cooler and cooler waters, even though warm waters may exist at that latitude. This effect is likely due to the climatological values of SST corresponding to areas of the high pressure belts wherein subsidence drying and high surface pressure tend to increase insolation, creating the warmest waters at that latitude. These regions have atmospheric environments which are hostile to TCs including high shear, negative vorticity and dry mid-level conditions. Thus, existing TCs typically do not move into those warm water regions without significant loss of intensity; TC formation in those regions is virtually impossible.

This also explains the drop off of the intensity curve at warmer SSTs. Some have speculated that this indicates a fundamental decrease in intensity for higher values of SST, and that TCs do not continue to intensify for SSTs above the 30°C point; I disagree. The likely reason for this apparent drop in intensity for high values of SST is that the warmest tropical waters exist under regions of the atmosphere which are inhospitable to convection, and TCs which reach those warm waters lose their intensity due predominantly to atmospheric affects. If this warmer water were under a region of the atmosphere favorable to convection more intense TCs could form.

The exponential nature of the relationship between the intensity curve versus SST should remain valid even for temperatures warmer than the planet presently sustains. The limiting factors on how close TCs come to this curve are atmospheric effects such as wind

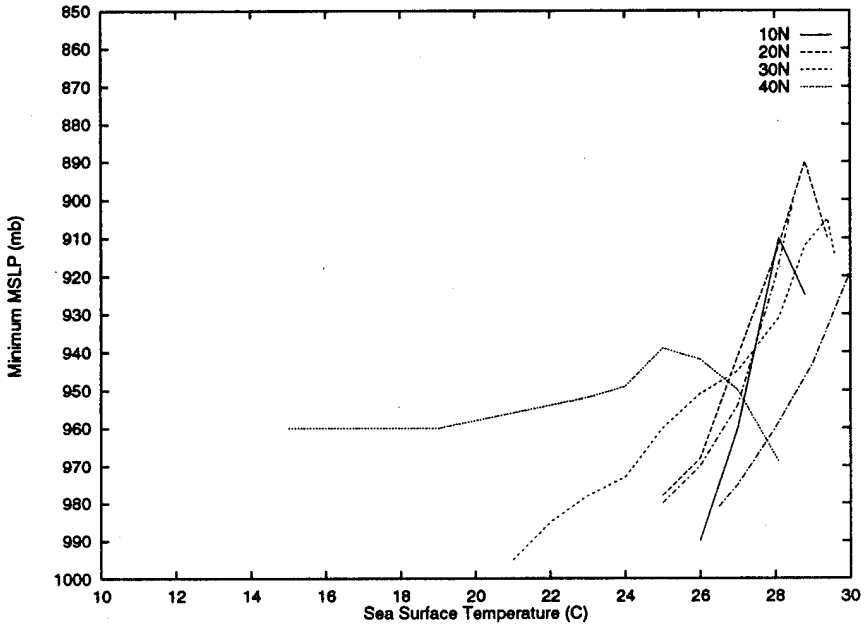

Figure 3.16: Latitudinal variation of minimum MSLP versus SST for the Atlantic basin. The 10 degree wide bands are centered at 10, 20, 30, and 40 degrees north.

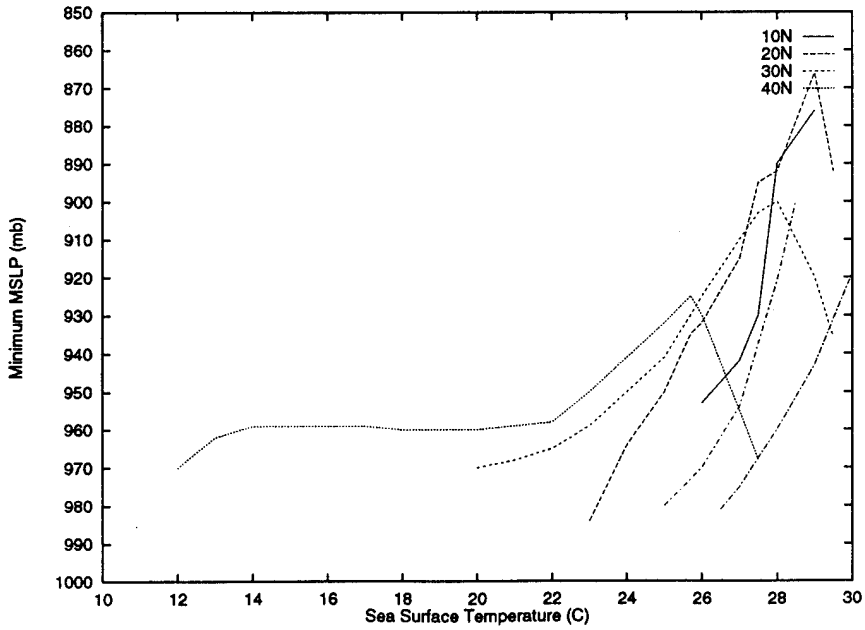

Figure 3.17: Latitudinal variation of minimum MSLP versus SST for the Northwest Pacific ocean basin. The 10 degree wide bands are centered at 10, 20, 30, and 40 degrees north.

shear and mid level moisture, and they ultimately determine how close a TC can come to the theoretical SST-intensity relationship (Gray, 1975). If global warming does indeed occur and warmer waters become present in regions favorable to TCs, there is potential for more intense storms to exist. However, until we know for certain what will happen to upper tropospheric temperatures (most models indicate a general warming of $\sim 5°C$), regional wind shear environments and SSTs (most GCMs just contain a mixed layer ocean), we should reserve judgement on how TC intensity values will change. The amount of buoyancy available and whether that available buoyancy can become physically organized determine the intensity any given TC will reach, and there is still much uncertainty as to how this buoyancy factor may change (Holland, 1995; Gray, 1995).

The MSLP-SST relationship also varies by month as shown in Figures 3.18 and 3.19. Peaks of minimum central pressure are highest (ie., lowest pressures) during September in the Atlantic and October in the Pacific. The other months in each basin show lower values (ie., the TCs don't get as deep) even for similar values of SST. The location of the intensity peaks (in terms of SST) for each month within each basin do remain fairly constant, however.

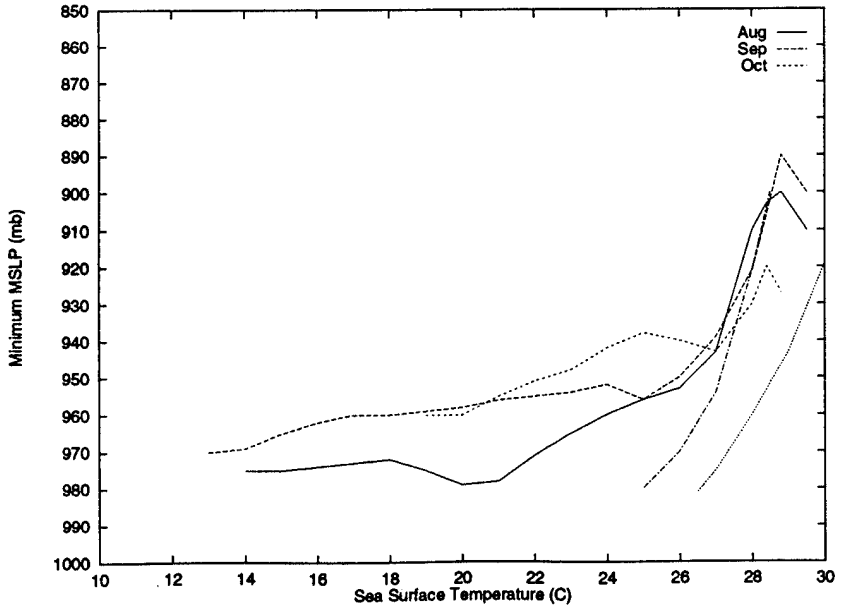

Figure 3.18: Monthly variation of minimum MSLP versus SST for the Atlantic basin, August-October.

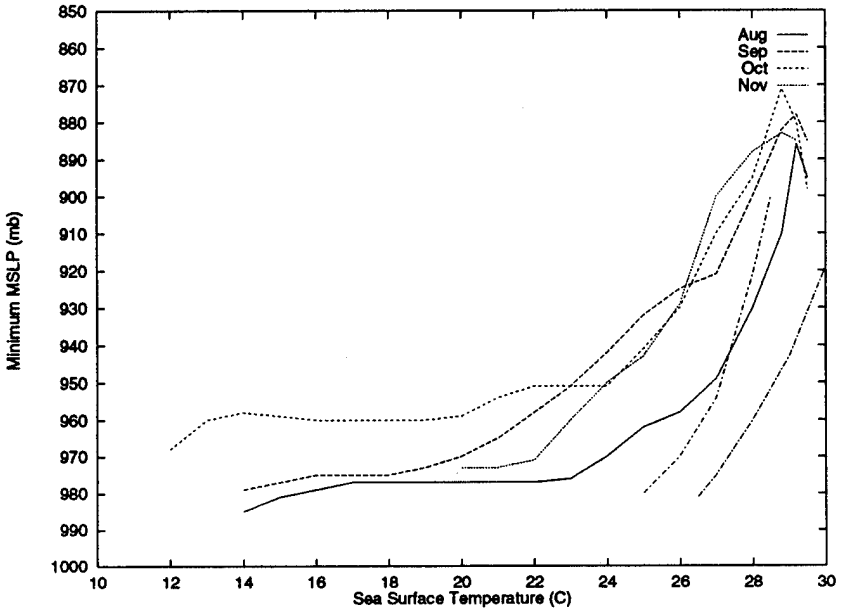

Figure 3.19: Monthly variation of minimum MSLP versus SST for the Northwest Pacific basin, August-November.

Inter-basin variations also exist (Fig. 3.20). For SSTs above 24°C, the Pacific has deeper systems than the Atlantic by as much as 20 mb at the peak SST values. Interestingly, the annual peak values in each basin occur at about the same SST (28.8°C). For SSTs below 24°C, the Atlantic seems to have deeper systems. Some of this may be an artifact of fully developed TCs recurving out from the warm gulf stream into colder water faster than they can fill, expand and lose internal momentum, or possibly that there isn't enough data in these temperatures to show what is really occurring.

It is also worth noting that there are significantly lower pressures in both Atlantic and Pacific when compared to Banner Miller's 1958 curve (Fig. 3.20). Robert Merrill's (1987) Empirical Potential Intensity (EPI) curve (also in Figure 3.20) fits well in the Atlantic between 27°C and 29°C, where it was developed for, but it falls short in the Pacific, and in the Atlantic for SSTs below 27°C. Thus, it is worth stressing the importance of geographic location when applying any MPI curve; researchers and forecasters should be careful to only use empirically derived relationship where they were developed.

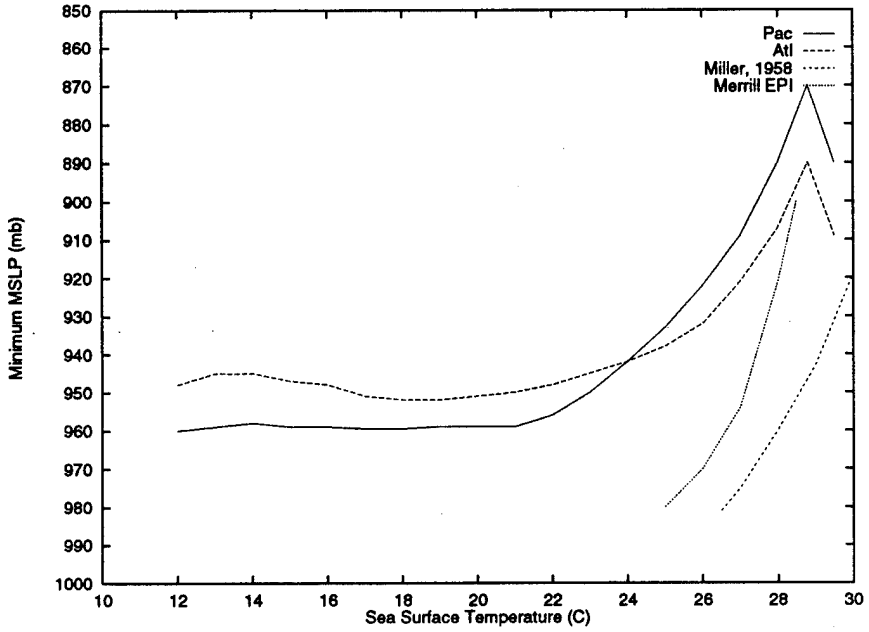

Figure 3.20: Inter-basin variation of minimum MSLP versus SST. Atlantic intensities are higher for SSTs below 24°C while Pacific intensities are higher above 24°C. The curves drawn are for extreme intensity values; Banner Miller's 1958 curve and Merrill's EPI curve are also shown.

3.4 Tangential Velocity Versus SST

The best track reported maximum tangential wind velocity versus SST curves are very similar in nature to the curves discussed for central pressure versus SST. Since the actual winds of a TC are what cause physical damage (the central pressure of a TC is not in itself dangerous) , examining the wind-SST relationship is very important. The wind data used are best track winds, which have in some cases been estimated using a pressure-wind relationship from known surface pressure conditions. The curves behave in a fashion similar to those for the pressure-SST relationship as expected.

As shown in Figures 3.21 and 3.22 there is significant latitudinal variation in intensity as measured by wind velocity when compared to SST. In both the Atlantic and Northwest Pacific basins, increasing latitude from 10°N to 30°N results in more intense TCs for what are traditionally considered cold SSTs (below $\sim$ 26°C). For those TCs up to 40°N the general nature of the curve changes, becoming much less peaked and smoother for any SST change.

Unlike the pressure-SST relationship which maintained its intensity peak near 28.8°C for most latitudes, the peak of the wind-SST curves shift to cooler waters for TCs at higher and higher latitudes. Life cycle changes of the TC are probably the cause for this variation, as outer-core wind strength often increases during recurvature (or during phase 2 in general) even while the eye fills and central pressure increases (Weatherford, 1989).

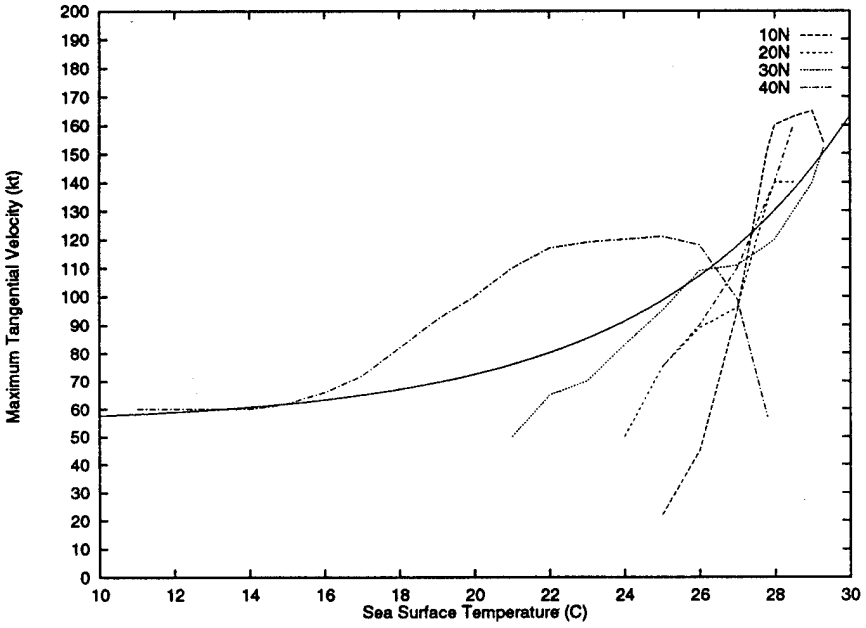

Figure 3.21: Latitudinal variation of tangential velocity (V_{Tmax}) versus SST for the Atlantic basin. (Miller EPI and DeMaria and Kaplan (1994) curves included for reference).

There are also very distinct monthly changes in TC intensity as related to SST (Figs. 3.23 and 3.24). In the Atlantic (Fig. 3.23) during August, the most intense TCs occur in the warmest waters furthest equatorward. During September and October, however, TCs with intensities in excess of 100 kt are able to sustain themselves over very cool water as they recurve along the Atlantic seaboard, maintaining 100 kt winds even over 22-24°C water. This is due to the ability of the TCs to maintain their in-up-and-out buoyancy driven circulation because of cooler upper level temperatures overlying relatively 'warm' SSTs of the gulf stream.

The Northwest Pacific basin (Fig. 3.24) also displays a monthly variation of intensity, but overall it is a basin more favorable to TCs due to environmental features (such as the

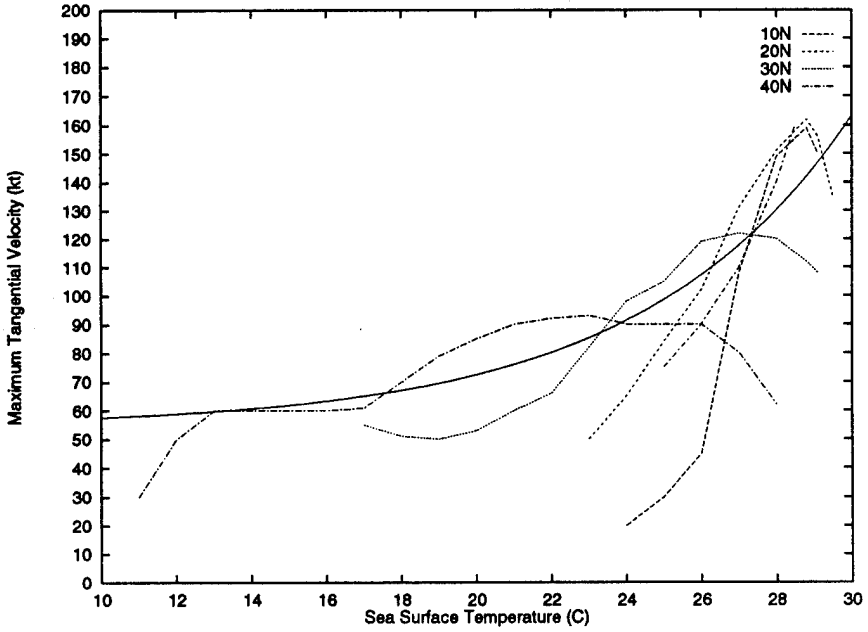

Figure 3.22: Latitudinal variation of tangential velocity (V_{Tmax}) versus SST for the Northwest Pacific basin. (Miller EPI and DeMaria and Kaplan (1994) curves included for reference).

monsoon trough) so monthly effects are less apparent than in the Atlantic basin, which is unfavorable to TCs for most of the year. For the Pacific the month which can sustain the most intense TCs furthest north and into the coolest waters is October.

A significant amount of inter-basin variation is also present in the wind-SST relationship. In the SST range typically associated with TC genesis (above 26.5°C) the basins are very similar. Below this temperature though, the Atlantic develops TCs that have stronger winds given the same SST than Pacific TCs. The explanation for this difference lies in the gradient wind balance equation. Atlantic storms tend to be smaller in overall size than Pacific storms (Merrill, 1982 and 1984), resulting in a stronger pressure gradient, and hence stronger gradient winds for similar SST and central pressure conditions.

An interesting feature of the Atlantic basin TCs is the drastic rise in intensity above 27°C. This feature has been noted before (eg. Evans, 1993; Merrill, 1987) but it has not been explained very well. Evans (1993) developed a "half top-hat" function and overlaid it on Merrill's (1987) scatter plot, but no scientific explanation as to why this feature exists has been offered. The most plausible rationale for this drastic change in character of the

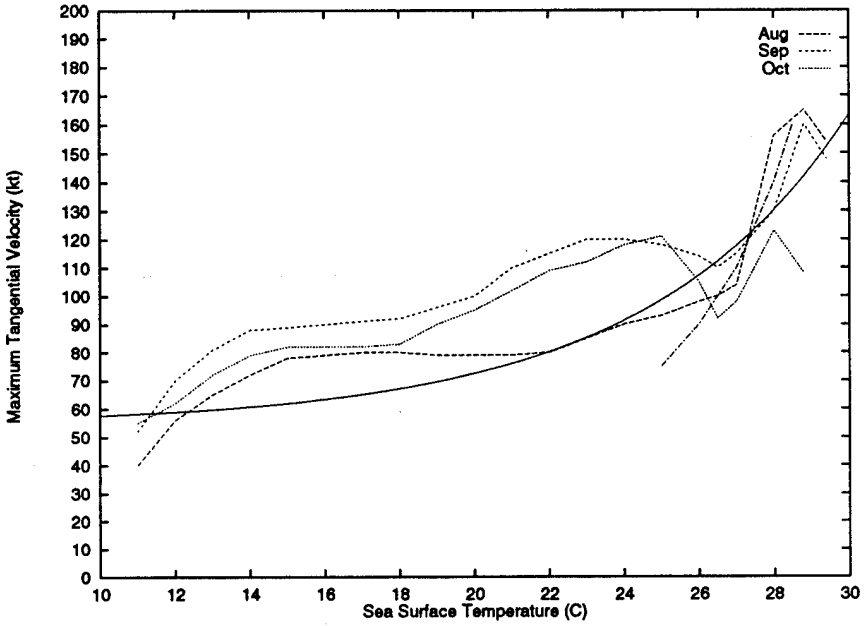

Figure 3.23: Monthly variation of tangential velocity (V_{Tmax}) versus SST for the Atlantic basin. (Miller EPI and DeMaria and Kaplan (1994) curves included for reference).

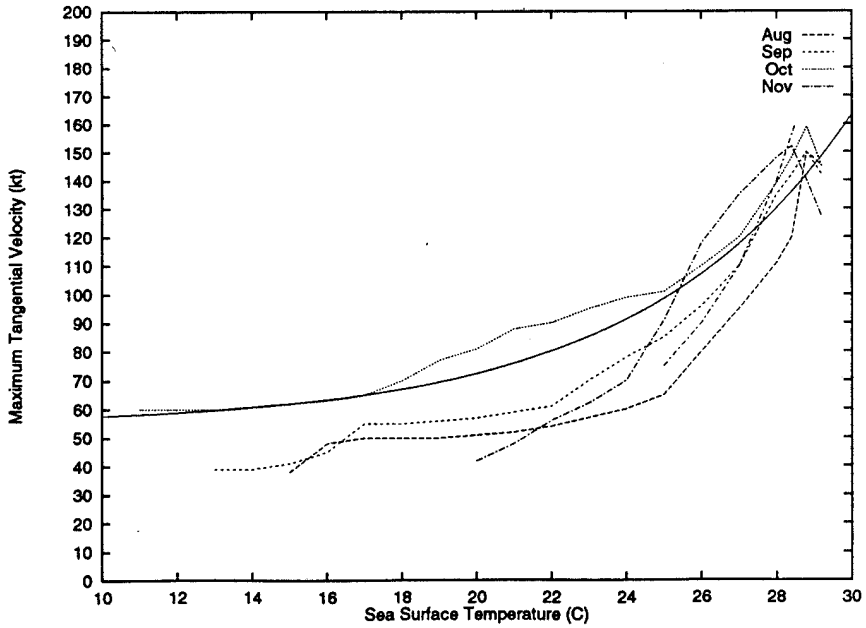

Figure 3.24: Monthly variation of tangential velocity (V_{Tmax}) versus SST for the Northwest Pacific basin. (Miller EPI and DeMaria and Kaplan (1994) curves included for reference).

curve is the presence of an eye. It is likely that eye formation or sudden filling of the eye for weakening TCs occurs within the Atlantic basin very near the 26.5-27.0°C SST point in the majority of cases (Fig. 3.25). The presence of an eye above this threshold allows for additional forced subsidence warming within the eye leading to more pronounced pressure falls, a stronger pressure gradient, and thus stronger winds. Accepting that roughly 20 percent of a TC's central pressure fall is due to the presence of an eye, decreasing the intensity values above the 27°C threshold by 20 percent would smooth the curve out significantly.

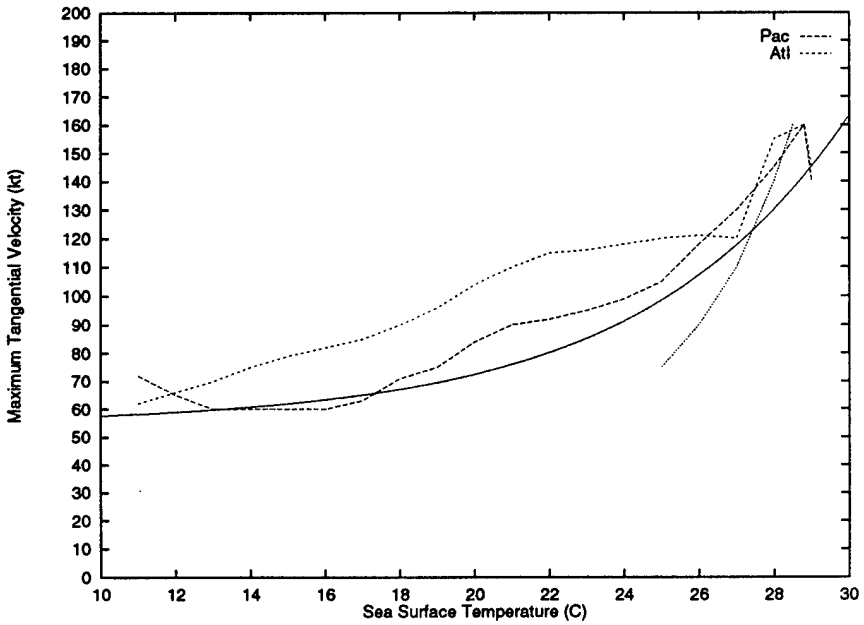

Figure 3.25: Inter-basin variation of maximum tangential velocity (V_{Tmax}) versus SST. Note that Atlantic intensities are higher than those of the Pacific for SSTs below 26.5°C. Also note the different character of the curves: while the Pacific has a very smooth curve, the Atlantic shows a very dramatic increase in intensity above 27°C. Merrill's EPI curve and DeMaria and Kaplan's curve are added for reference.

The dramatic rise in intensity values exhibited by the Atlantic for TCs in warm water is not shown by TCs in the Northwest Pacific basin. It is likely that eye formation or filling is significantly less related to the temperature of the underlying water in the Pacific than in the Atlantic, so the sudden change in the nature of the wind-SST curve visible in the Atlantic near 27°C is masked for Pacific TCs.

3.5 Additional Statistics on Hurricane Variability.

An analysis of the frequency of various strength wind reports in the Atlantic basin sheds some light on TC variability. There are about 14,000 surface wind observations within the Atlantic basin for the month of September during the time frame of 1945-1993 contained in the best track data set. This data set represents a climatology of Atlantic hurricane intensity, frequency, and location. By counting the number of reports exceeding various wind thresholds (eg., 35, 60, and 100kt) in each grid box, a depiction of the storm tracks emerges (Figs. 3.26, 3.27 and 3.28). Climatologies for three equal areas within the basin have been calculated, and the results are shown in Table 3.1. The slight wind bias (5 kt over-reporting for 100 kt TCs prior to 1971) discussed by Landsea (1993) has not been removed. The bias was systematic over the whole basin and should not affect these results.

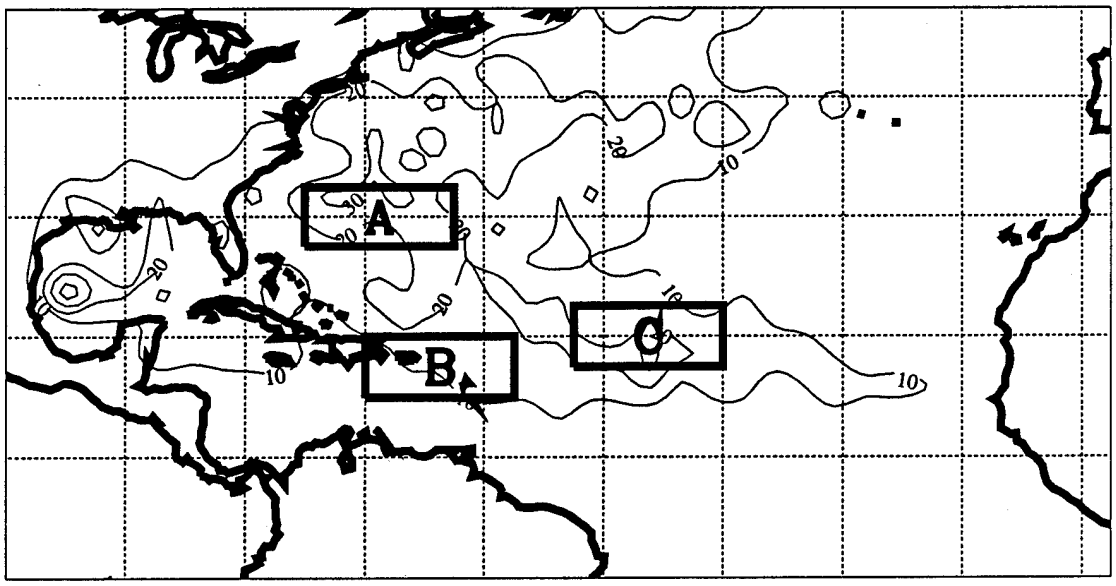

Figure 3.26: Number of wind reports in excess of 35 kt in the Atlantic basin during the years 1945-1993 per 2.5° grid. Areas A, B and C that are discussed in the text are overlaid for reference.

Area A, off the east coast of Florida, has by far the greatest activity at all thresholds, Area B had the least while Area C displays an intermediate level of activity. The climatological mean SST's are 27.5 centigrade in Area A, 28.4 in B and 27.1 in C. Using only

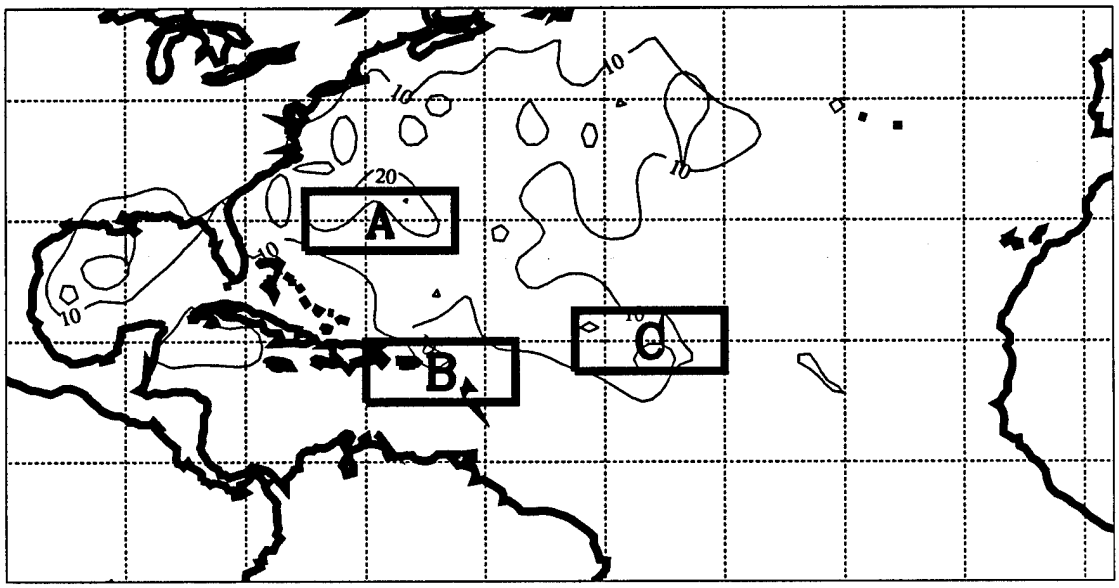

Figure 3.27: Number of wind reports in excess of 60 kt in the Atlantic basin during the years 1945-1993 per 2.5° grid. Areas A, B and C that are discussed in the text are overlaid for reference.

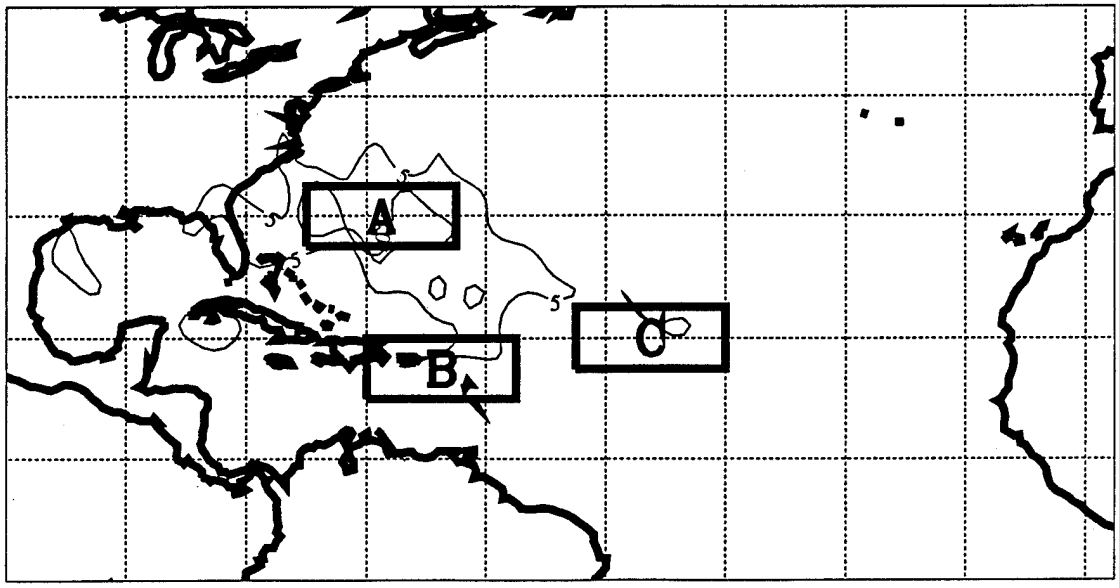

Figure 3.28: Number of wind reports in excess of 100 kt in the Atlantic basin during the years 1945-1993 per 2.5° grid. Areas A, B and C that are discussed in the text are overlaid for reference.

Table 3.1: Wind-Threshold Report Count Summary

	35 kt			60 kt			100 kt		
Area	A	B	C	A	B	C	A	B	C
Sum of reports in Area	253	106	176	201	65	104	101	29	29
Average number reports per $(2.5°)^2$ box	25.3	10.6	17.6	20.1	6.5	10.4	10.1	2.9	2.9
Standard Deviation per $(2.5°)^2$ box	5.8	4.8	4.8	5.7	3.0	3.1	4.1	2.0	1.7
Total reports in basin	4298	4298	4298	2555	2555	2555	636	636	636
% of basin reports in Area	6	2.5	4	8	2.5	4	16	5	5
% of reports in Area A+B+C	47	20	33	53	17	30	64	18	18

SST as a means of forecasting, we would expect Area B to have the most intense hurricane reports. However, while the SST of Area A is nearly one degree colder than Area B, Area A has about three times as much activity. This signal gets stronger with increasing wind strength and, at 100kt, nearly two-thirds of all reports contained in the three areas lie within Area A; the other one-third being equally distributed between Areas B and C. This is not an artifact of storm track concentration either; results for data normalized by number of tropical storms or minimal hurricanes show area A as having the most intense systems. The primary reason for this large difference must surely be something other than SSTs. Sub-surface ocean temperatures at 10, 20, 30 and 50 m were also examined and displayed similar results. Thus the environmental wind features were examined.

Statistical analysis of the data shows the significance of wind shear between the 200 mb and 850 mb levels and meridional and zonal winds in general. The analysis was performed by first removing all grids with SST below 27°C. This SST screening is logical since 26.5°C is roughly the break point between genesis and non-genesis as shown by Gray (1968), and thus including only areas with SST of 27°C or greater will restrict the analysis to tropical systems. The intent of this analysis is to show that while warm water is a requirement for TCs, the presence of warm water does not mean that intense TCs will occur.

The data were divided into separate groups based on number of reports meeting the wind thresholds used (35, 60 and 100 kt). For example, within the 35 kt threshold data were separated into those grids with 9 or more reports of 35 kt, and those with 5 reports or less. This gave 111 reports within the high number of reports category and 149 in the low report number category; roughly the same order of magnitude in each bin, with the portion of data in-between thrown out. The same process was used for number of reports of winds in excess of 60 kt and 100 kt. Student's t-number was then calculated for the following parameters: 850 mb and 200 mb zonal and meridional winds, divergence and vorticity, and zonal, meridional and total wind shear between 850 mb and 200 mb. By calculating Student's t-number, the probability that a sample distribution (such as the high or low number of reports bins) is representative of the whole population can be determined.

Using climatological upper air data from the Climate Analysis Center (CAC) and the best track reported surface winds over the Atlantic from 1945 through 1993, climatological wind fields as they pertain to tropical cyclone frequency were studied. After placing all the data fields into 2.5 by 2.5 degree grids, the information contained was quantitatively compared using standard statistical methods. Analysis of the climatological environment was performed removing any grid area with less than one report (this procedure yields a rough land mask) and all grids with SST colder than 27°C since this is the point at which available thermodynamic energy is sufficient for hurricane development (Gray, 1979; Holland, 1995). Binning the data and performing two-tailed Student's t-tests yields valuable insight into upper level wind, wind shear, and vorticity and divergence effects.

By calculating t-numbers, the probability of sample distributions representing the population was determined, and to ensure validity of the t-statistics, the skewness of each distribution was also calculated. The Student's t-test assumes a Gaussian distribution and t-numbers from strongly skewed distributions are suspect. Distributions used in this analysis were not significantly skewed.

Considering the number of reports involved, a Student's t-number greater than 2.7 would indicate the results are significant to 1 percent (that is, there is a 1 percent chance that the two sample distributions are both representative of the total population and are related to each other). In simple terms, a high t-number indicates that the two samples are very distinct distributions, and unrelated.

The t-number values calculated range from 0.0 to 10.4; results are shown in Table 3.2. The t-number results for upper level zonal wind, low level meridional wind, zonal and meridional shear consistently lie above 2.7 at each of the three wind thresholds. This means that sample distributions of 200 mb U, 850 mb V, U-shear and V-shear over active regions are distinct from corresponding distributions over inactive regions.

Table 3.2: Student's t-number calculations in the Atlantic basin for the month of September for the region where SST is in excess of 27°C.

	Bin (kt)	High Thresh No. Obs.	Low Thresh No. Obs.	High Mean	Low Mean	Skew	t
850 mb u	35	9/111	5/149	–3.9	–4.2	0.03	0.57
(m s^{-1})	60	6/99	4/168	–3.7	–4.4	0.03	0.91
	100	2/102	0/165	–4.1	–4.1	0.03	0.02
850 mb v	35	9/111	5/149	1.6	0.7	–0.28	6.30*
(m s^{-1})	60	6/99	4/168	1.6	0.7	–0.28	6.00*
	100	2/102	0/165	1.7	0.7	–0.28	6.90*
200 mb u	35	9/111	5/149	3.4	–2.30	0.55	10.40*
(m s^{-1})	60	6/99	4/168	3.5	–1.80	0.55	9.70*
	100	2/102	0/165	3.3	–1.80	0.55	9.40*
200 mb v	35	9/111	5/149	–1.6	–0.90	0.02	2.70
(m s^{-1})	60	6/99	4/168	–1.6	–1.00	0.02	2.00
	100	2/102	0/165	–1.6	–1.00	0.02	2.10
U shear	35	9/111	5/149	7.20	2.00	–0.33	6.00*
(m s^{-1}/650 mb)	60	6/99	4/168	7.30	2.60	–0.33	5.30*
	100	2/102	0/165	7.40	2.30	–0.33	5.80*
V shear	35	9/111	5/149	–3.20	–1.50	0.02	3.90*
(m s^{-1}/650 mb)	60	6/99	4/168	–3.20	–1.70	0.02	3.40*
	100	2/102	0/165	–3.30	–1.70	0.02	3.70*
Total shear	35	9/111	5/149	8.30	6.30	0.02	2.20
(m s^{-1}/650 mb)	60	6/99	4/168	8.30	6.60	0.02	1.90
	100	2/102	0/165	8.50	6.40	0.02	2.20

* indicates significance likely.

The region of low vertical wind shear corresponds to locations where, in a climatological context, mid-latitude westerlies tend to enter the flow around the TUTT from the northeast (i.e., Region A). Figure 3.29 and 3.30, portions of Sadler's 200 mb September streamline analyses are provided for reference (Sadler, 1975). The surface and low level trade winds are generally consistent in intensity and direction: at 850 mb, the zonal winds are westerly north of and easterly south of 32.5°N with a uniform intensity gradient. The 200 mb winds do not display this uniformity, being westerly north of 15°N but with a distinct TUTT associated area of northeasterlies. This configuration yields a pocket of minimal zonal shear.

Returning to the areas noted earlier, it is apparent that Area A lies in this region of minimal shear (less than 5 ms^{-1}) and Area B is within the tongue of higher shear (greater than 10 ms^{-1}). This result supports the theory that regions of climatologically frequent hurricanes lie in areas of climatologically low shear. This concept has been applied before on daily time scales for intensity forecasts but not on climatological ones.

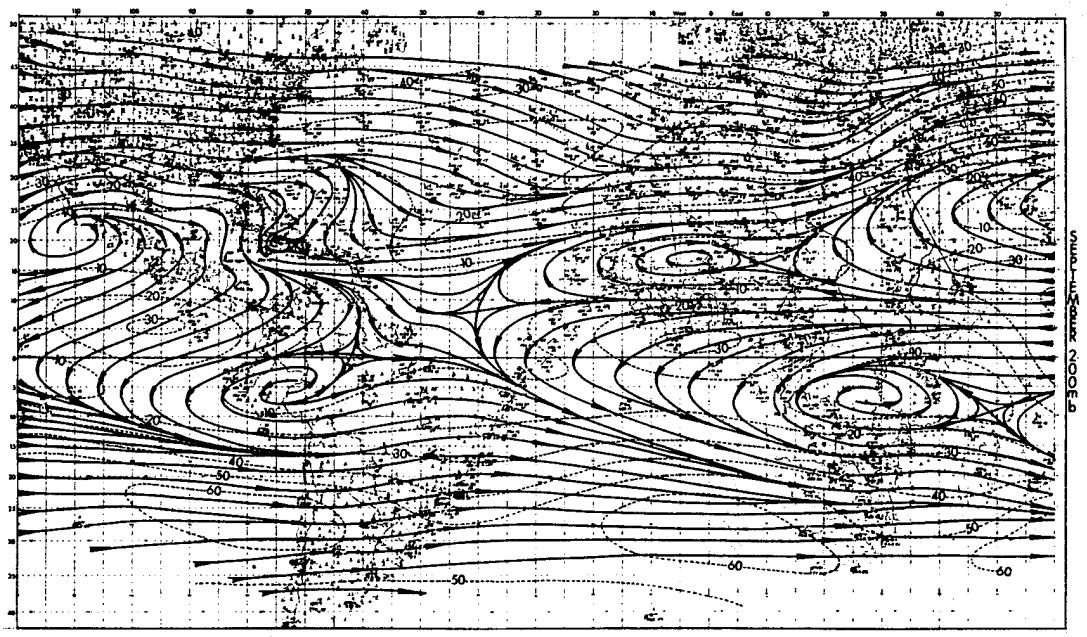

Figure 3.29: 200 mb September streamlines for the Atlantic region (Sadler, 1975).

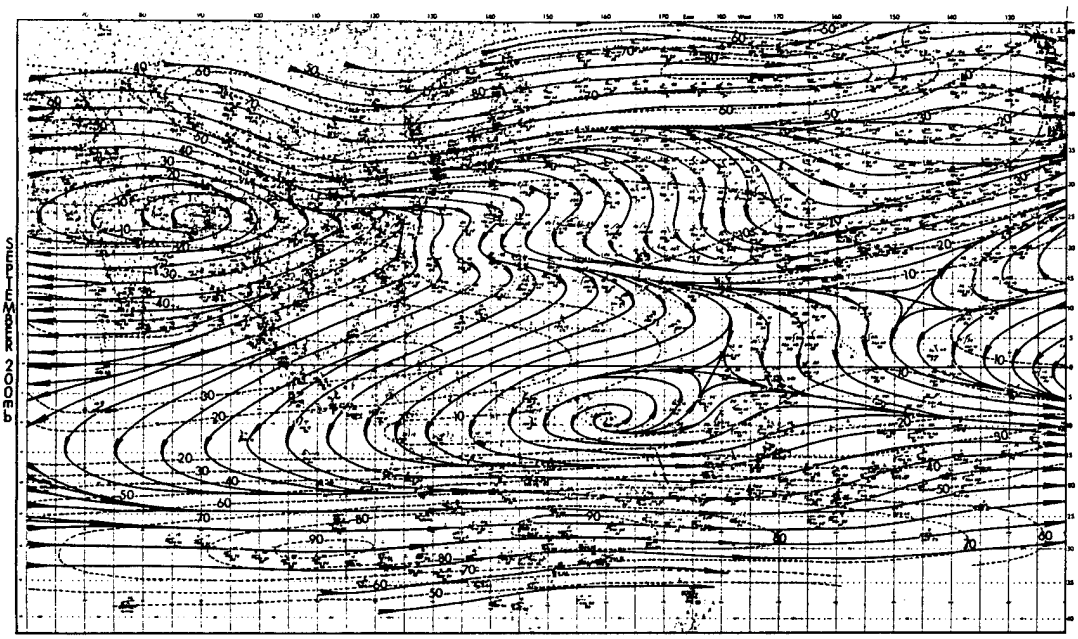

Figure 3.30: 200 mb September streamlines for the Pacific region (Sadler, 1975).

Chapter 4

CAUSES OF VARIATION IN INTENSITY VERSUS SST RELATIONSHIP

The relationships between SST and MSLP and between SST and V_{Tmax} identified in the analyses in Chapter 3 can be further interpreted in terms of the details of TC dynamics and climatology. In this chapter, the specific effects of buoyancy in and around the eye wall as well as eye wall physics, seasonality and latitude effects on the SST-intensity relationship are examined in more detail.

4.1 Buoyancy Control of TC Intensity

Obvious statistical relationships between SST and TC intensity were shown in the previous chapter. Those relationships exist because SST impacts air parcel buoyancy and buoyancy is the ultimate determinant of TC intensity. In general the tropical upper tropospheric temperature gradients are fairly uniform. SST gradients, however, are not nearly so uniform, and thus near-surface air temperature gradients of a greater magnitude than those of upper levels are formed. Additionally, due to the air-sea interaction, surface moisture contents vary significantly with varying surface temperatures. The net result of these combined features is a variation of the buoyancy available for convection. Ultimately, warmer SSTs provide more available buoyancy for parcel ascent, and more intense TCs are the result. Figure 4.1 depicts the buoyant control of intensity process. The dashed line indicates the amount of buoyancy required to sustain a TC at the levels shown. The solid line, potential buoyancy, is determined by the near-surface temperatures (highly dependent upon SST) and upper-level temperatures. The higher the SST value relative to upper-level temperature, the higher the potential (or available) buoyancy. The point

at which the potential and required buoyancy curves intersect is effective SST limitation on intensity.

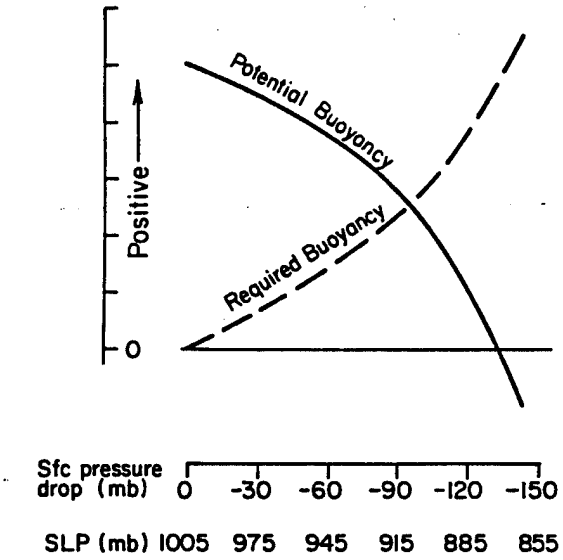

Figure 4.1: Relationship between the buoyancy required for various TC intensities and buoyancy potential based upon near-surface and upper-level temperatures (from Gray, 1995b).

However, while SSTs set the bounding buoyancy conditions and thus an upper limit to the intensity a TC can reach, many TCs never approach this level of intensity. There are other factors that help explain why TCs seldom reach their MPI, and during those rare occasions when all the conditions are favorable TCs are able to approach their SST-based MPI value.

These intensity limiting factors include: vertical wind shear, TC size, TC life cycle, eye size, eye-wall cycle, latitude, and season. Vertical wind shear is generally accepted to be a limiting factor on TC intensity. Two reasons for this are apparent. The first is that a TC is a warm core low, with a warm anomaly in the mid- and upper-level troposphere (Fig. 4.2) and as the upper levels of the TC are ventilated by vertical shear, the warm core is unable to continue warming (Gray, 1979). Without additional warming, further pressure falls are impossible. The second logical reason that shear inhibits TCs is that strong shear will lead to a decoupling of low- and upper-level circulation (Tuleya and Kurihara, 1981).

TC size and life cycle processes have already been discussed in previous sections. Eye-wall processes, latitude and seasonal effects, however, warrant further discussion.

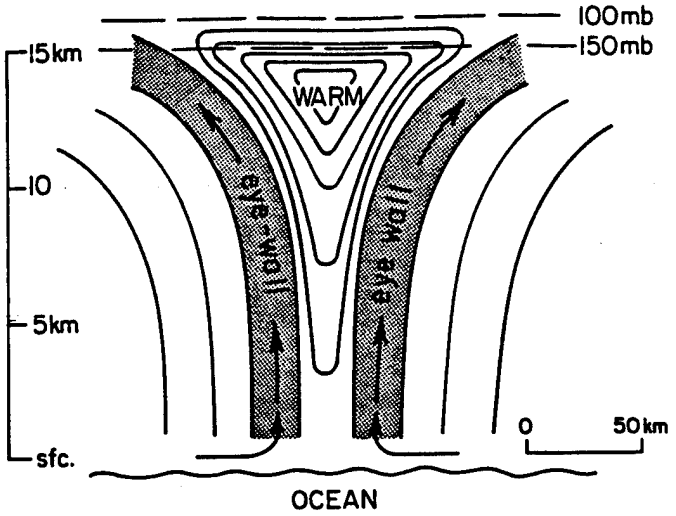

Figure 4.2: General schematic of a tropical cyclone depicting the upper level warm core needed for surface pressure falls (from Gray, 1995b).

4.2 Eye-wall Physics

Figure 4.2 depicts an important eye-wall process in addition to showing the upper level warm core required for surface pressure falls: how the eye-wall slopes, thus enabling updrafts to avoid the extremely stable warm core and continue their upward motion. This assists in maintaining the potential buoyancy discussed above by limiting the effect of stabilization.

In section 3.1 of this paper I discussed the Weatherford (1989) conceptual model of a three phase tropical cyclone life cycle (refer back to Fig. 3.10). Implied in the model are significant variations in eye and eye-wall structure.

As a tropical storm transforms into a tropical cyclone in Phase 1, it develops an eye at around 981 mb. At this point, forced subsidence warming of the eye adds to the existing surface pressure falls and helps fully develop the cyclone. If the warming succeeds in dropping the central pressure below 950 mb, concentric eyes become possible. Figure 4.3, adopted from Gray (1995) depicts the theoretical concentric eyewall cycle proposed by

Willoughby (1990). As radial inflow tends to overshoot the radius at which pressure and wind would balance in the gradient wind equation (Eq. 3.1), incoming radial winds tend to contract the eye-wall region. When the eye becomes too small to vertically evacuate the inflowing air, it forces air to find another escape route, and outer convective rings then form, eventually turning into secondary eye-walls that starve the inner eye of mass to process, leading to a dissipation of the inner eye. The outer ring continues to inward propagating process, and if time allows more secondary eye-walls can form.

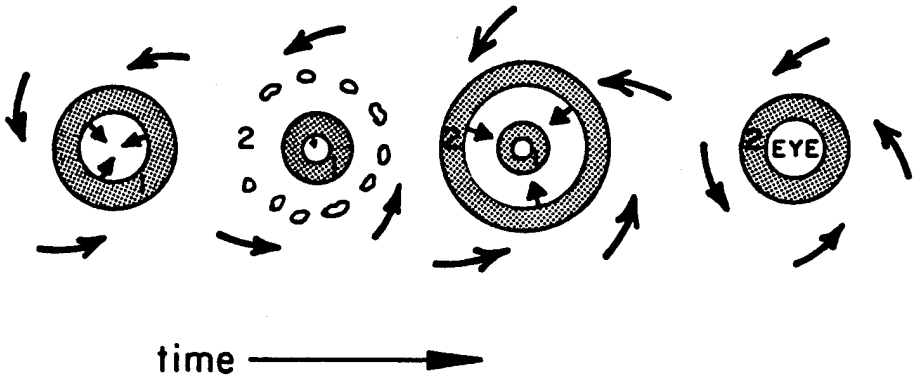

Figure 4.3: Conceptual model of inward propagating eye-wall and concentric eye-wall formation as proposed by Willoughby (1990) (adopted from Gray, 1995b).

There is observational support for the conceptual model of inward propagating eye-walls and concentric rings. Figure 4.4 of the eye radius and central pressure evolution in hurricane Allen from August of 1980 shows the concentric ring formation and inward propagation very well. In this case a 60 mb fluctuation between eye cycles occurred.

Eye diameter has also been found to play a role in limiting the central pressure of TCs. Figure 4.5, a plot of eye diameter versus MSLP for various TCs contained in Weatherford's (1989) data set, shows that eye size is important. The most intense TCs (in terms of central pressure) tend to have eyes of 30 km diameter or less. When eyes were larger than that, central pressure values could were not as low. The plot seems to indicate a nearly linear upper bound.

Similarly, a plot of radius of maximum wind (RMW) versus maximum wind as a measure of intensity shows that the closer to the center the RMW is to the center of the storm, the stronger the winds are (Fig.4.6). There is of course a large amount of scatter to

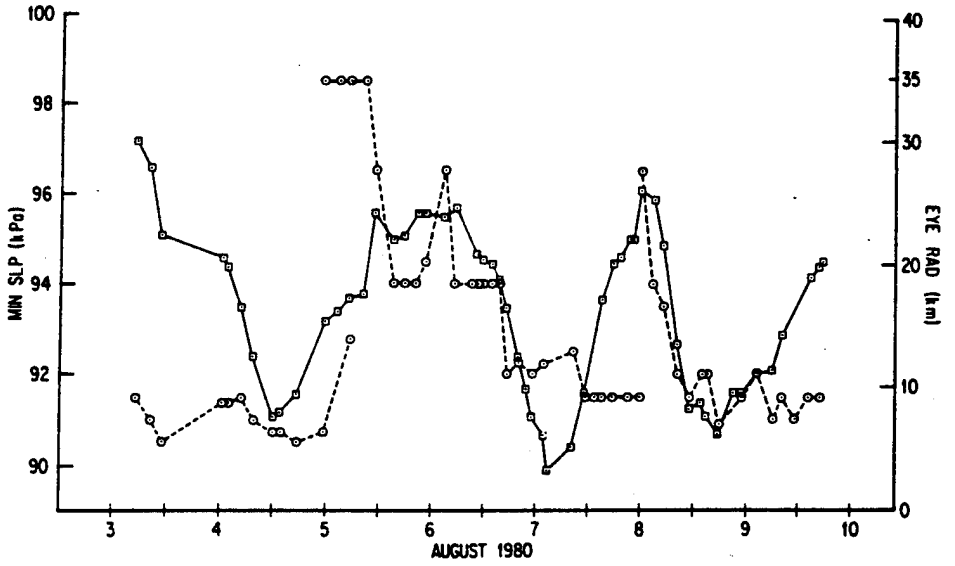

Figure 4.4: Evolution of central pressure and eye radius for hurricane Allen between 3 and 10 August, 1980 (from Willoughby, et al, 1982).

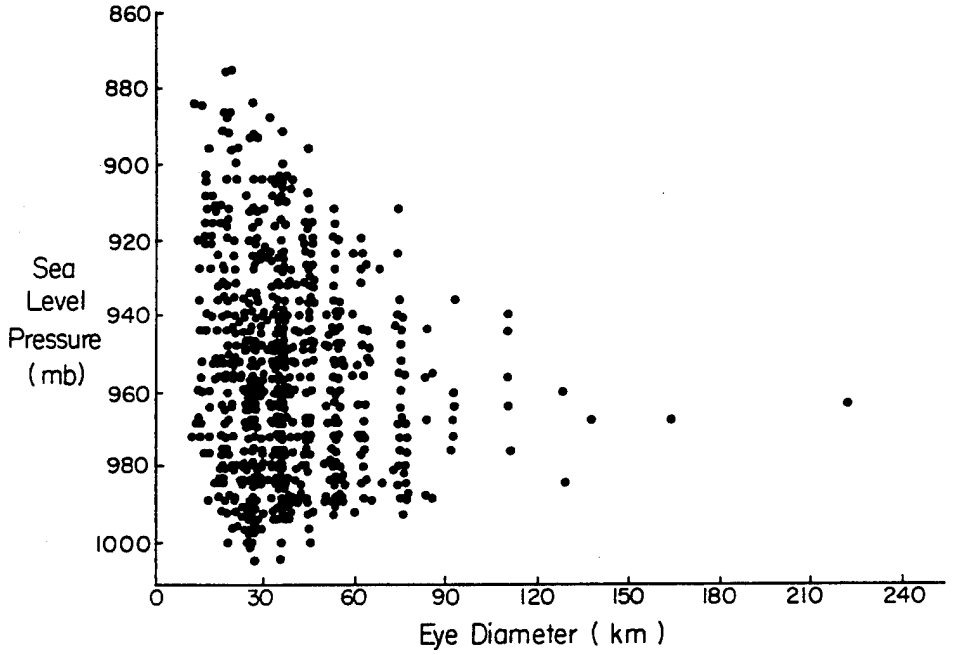

Figure 4.5: Eye diameter versus MSLP for tropical cyclones in the Northwest Pacific basin (Weatherford, 1989).

the diagram, and in individual cases the general idea may not hold true, but statistically there is a relationship and a distinct upper bound.

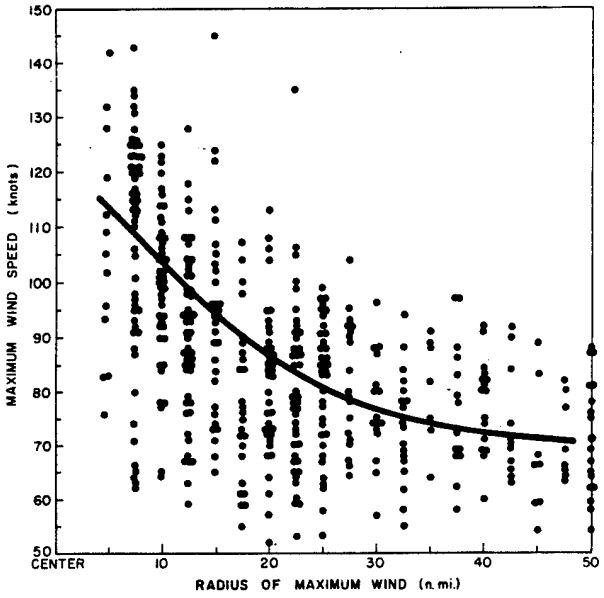

Figure 4.6: Radius of maximum wind versus maximum wind speed. Note the generally larger maximum wind speeds for smaller radii (from Shea and Gray, 1976).

4.3 Impact of Latitude on Intensity

Tropical cyclone intensity quite obviously varies with latitude as shown in the latitude plots of intensity included in chapter 3. Weatherford's (1989) plot of MSLP versus latitude (Fig. 4.7) shows the relationship that exists. TCs are typically most intense in the 15 to 20 N band, and intensity measured as MSLP tends to decrease steadily with increasing latitude. This is due to the stage of the life cycle the TC experiences as it moves poleward of the subtropical ridge and recurves.

To some extent, the only true impact latitude has on intensity is through "f" in the gradient wind balance equation. Latitude can be a good proxy for other real effects, such as shear or ocean thermal energy. Additional latitude effects are covered in the next section on seasonal effects.

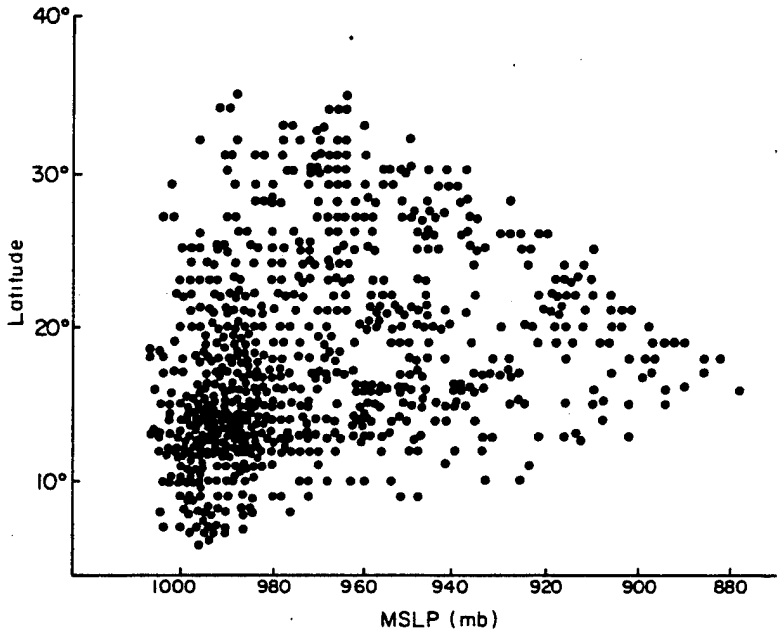

Figure 4.7: Latitude versus central pressure for 750 flight missions flown in the Northwest Pacific basin (Weatherford, 1989). Note the general decrease in intensity with increasing latitude beyond 20 N.

4.4 Seasonal Variation of Intensity

There are also significant seasonal variations of TC intensity. As Earth varies its orbital position relative to the sun through the year, insolation values of the planet change. The average difference in net radiation flux at the top of the atmosphere between January and July is about 25 Wm^{-2} (Piexoto and Oort, 1992). The variation in top of the atmosphere radiation flux is shown in Figure 4.8. This change in net radiation affects the global requirements for rainfall and convective processes leading to that rainfall. During the late spring and early summer time frame there is a minimal requirement for rainfall and a subsequent decrease in overall convection and a decrease in both frequency and intensity of TCs. Observation of the global precipitation pattern as it varies through the year (Fig. 4.9) supports this concept.

Meridional profiles of precipitation (Fig. 4.10) and percentage cloud cover (Fig. 4.11) also display the seasonal variation. Note how the peak precipitation over the oceans remains in the Northern Hemisphere throughout the annual cycle, but reaches a maximum

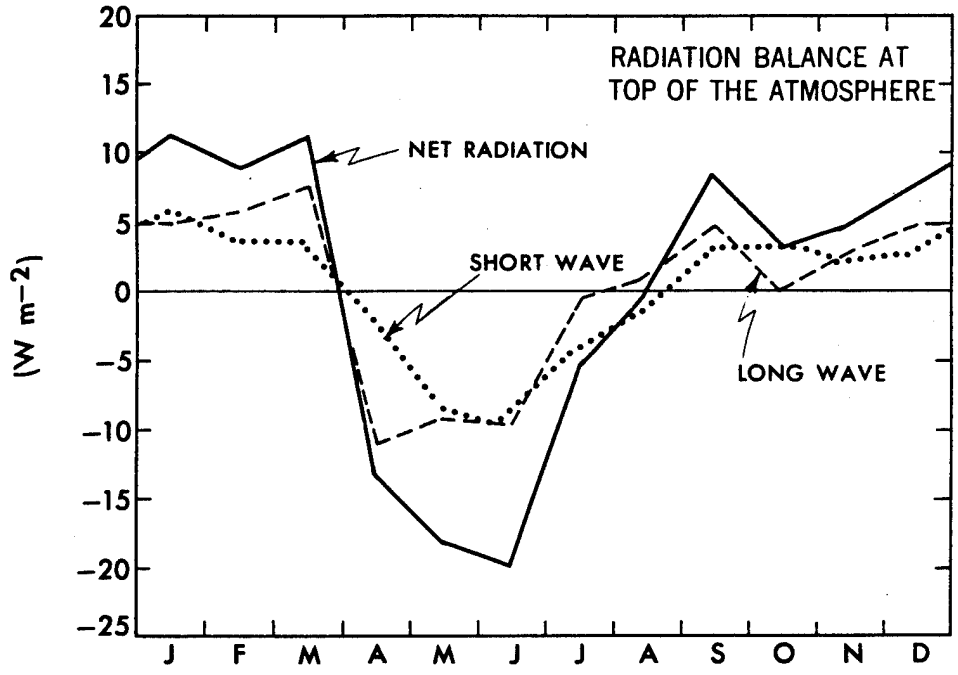

Figure 4.8: Top of the atmosphere radiation balance for short-wave (solar), long-wave (terrestrial) and net balance throughout the annual cycle. Values are departures from the annual mean (from Peixoto and Oort, 1992).

in the Northern Hemisphere summer and a minimum during the winter. This contrasts sharply with the precipitation over land. Over land the precipitation peak switches hemispheres based upon season, and has an annual peak in the southern hemisphere. Cloud cover percentages display a similar trend, and in the northern hemisphere tropics the summer months display a pronounced increase in cloud cover. All of these season and latitude effects feed into the amount of convection the atmosphere either requires or can support (depending upon which side of the chicken-or-the-egg argument is taken) based upon radiative processes. Subsequently, increasing or decreasing this amount of convection over the tropical oceans impacts the frequency and intensity of TCs.

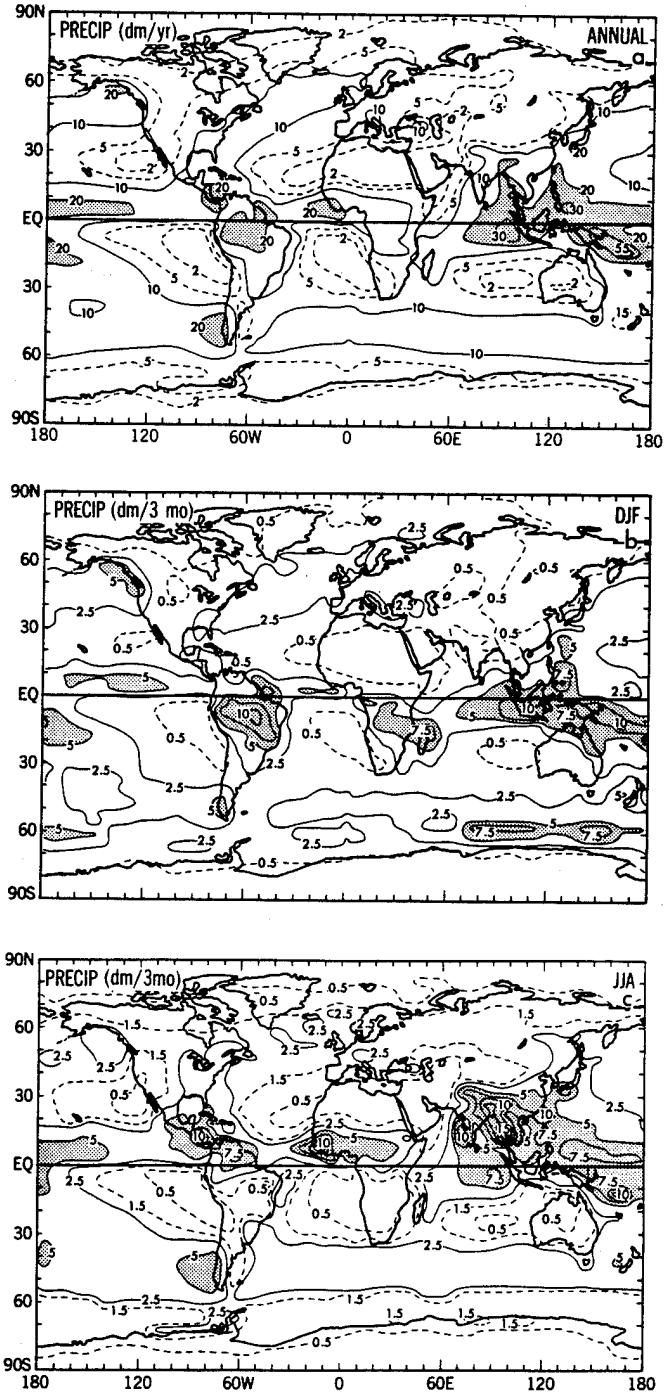

Figure 4.9: Precipitation rate distribution over the globe for a) the yearly average, b) December, January and February, and c) June, July and August (from Peixoto and Oort, 1992).

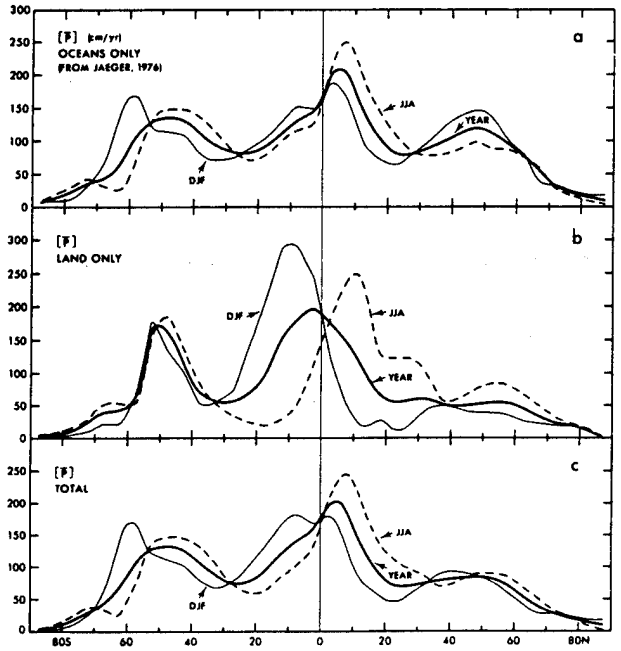

Figure 4.10: Zonal-mean precipitation rate in cm yr^{-1} for a) the ocean areas only, b) the land areas only, and c) combined land and ocean. The annual pattern is the heavy solid line, June, July and August are shown with the dashed line, and December, January and February are shown with the thin solid line (from Peixoto and Oort, 1992).

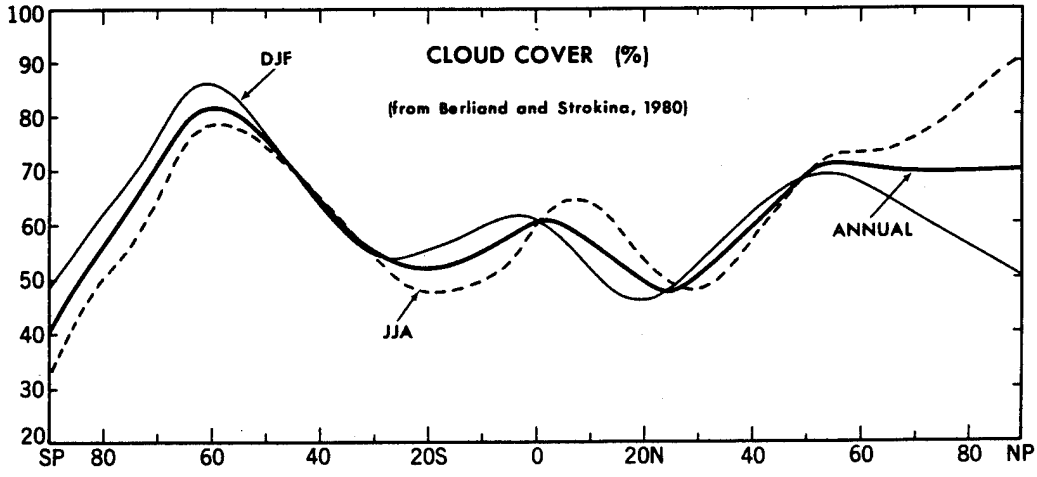

Figure 4.11: Zonal-mean cloud cover percentages for annual (heavy solid line), June, July and August (dashed line), and December, January and February (thin solid line) mean conditions (from Peixoto and Oort, 1992).

Chapter 5

SYNTHESIS OF RESULTS AND SUGGESTIONS FOR FUTURE WORK

5.1 Synthesis of Results

The complexities of the concepts and relationships surveyed in prior chapters can be distilled down to the following conceptual points:

1. In consideration of a definition of intensity, it is important to recognize that inner- and outer-core processes tend to be distinct from one another. The strongest intensity defining relationship is within the inner core between the maximum wind velocity and central pressure (with 55 percent of variance explained and a correlation coefficient of r $\approx$ 0.734). Attempting to relate central pressure to winds in the outer core results in virtually no detectable relationship (correlation coefficient between central pressure and tangential wind velocity at 50 n mi radius is r$\approx$0.004, explaining 0 percent of the variance). Weatherford (1985) showed similar results when comparing central pressure to a measure of wind strength between the 1-2.5°C radii (Fig. 5.1) and commented: "...once a cyclone attained typhoon intensity or forms [sic] an eye, the ability to relate cyclone intensity and strength was nearly lost."

2. Intensity varies by latitude for similar SST values. For equivalent SST, TCs further poleward are slightly more intense (5-10 mb, or 3-5 ms^{-1}) than low latitude storms. Values due to cooler upper level temperatures and greater instability, even after seasonal effects are discounted. Central pressures display this tendency more so than maximum winds because, as eye pressure decreases, the radial extent of the

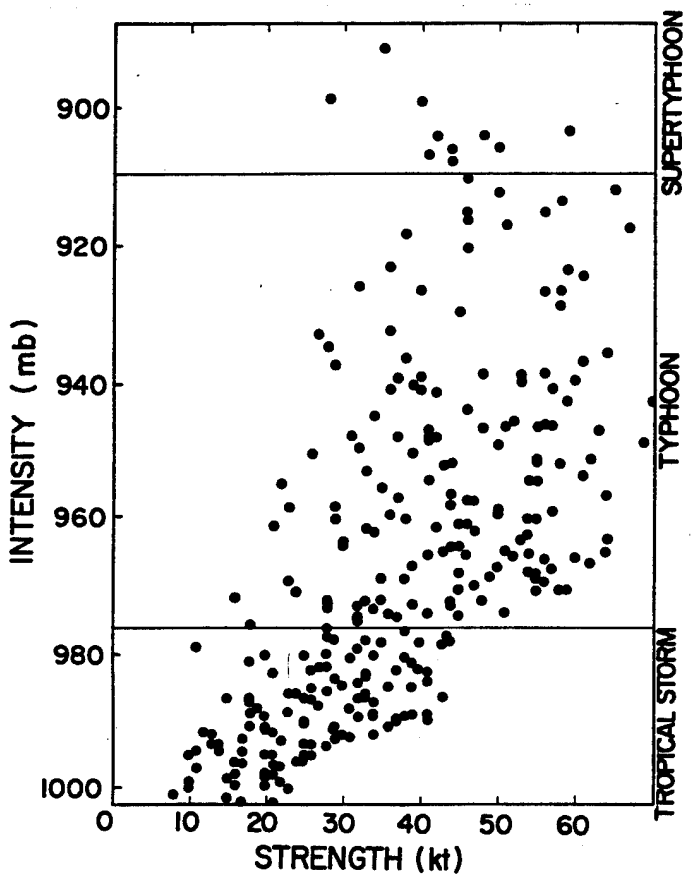

Figure 5.1: Intensity (minimum MSLP) versus outer-core strength ($\bar{V}_T$ for 1-2.5°C radius band) scatttergram (from Weatherford, 1985).

TC can increase, thereby altering the pressure gradient and reducing the net change in wind speed.

3. TCs are most intense during the fall transition months with a September peak of intense TC activity in the Atlantic and a peak during October in the Northwest Pacific. The timing of these maxima is due to SSTs remaining warm at fairly high latitudes while mid- and upper-level temperatures in these areas have begun to cool.

4. The West Pacific monsoon trough environment allows for the development of TCs which are typically larger than Atlantic cyclones. This tendency alters the pressure-wind relationship for the Pacific versus Atlantic TCs. Lower central pressures then occur in the Pacific as a result of the gradient wind balance process.

5. Intensity should not inherently decrease for SST values above 30°C; it likely continues an exponential increase for increasing SST. Atmospheric effects including shear, buoyancy, moisture, et cetera provide limits to the curve for highest SST (i.e., greater than about 30°). The current downward turning point (i.e., maximum) in the intensity SST curve lies at about 28.8°C, regardless of season or basin. The primary factors influencing this downward turn are the presence of wind shear over locations of warm water and deep convection inhibiting stability, subsidence and moisture effects.

6. When developing new methods of forecasting MPI, explicit eyewall physics and environmental features must be included in addition to SSTs. It is unlikely that improvement can be achieved over current MPI schemes without including these features.

5.2 Discussion

This paper has explored variable aspects of tropical cyclone intensity primarily in relation to SSTs but with additional stratifications for variable environment and for structural variability. There exists a wide variety of tropical cyclone intensity and structural

relationships for similar minimum mean sea level pressure (MSLP) best track maximum wind (V_{Tmax}), Sea Surface Temperature (SST) and Outer-Core wind Strength (OCS).

It becomes obvious that no single (say MSLP or V_{Tmax}), double (eg., MSLP and V_{Tmax}) or even triple or quadruple (eg., combinations of MSLP, V_{Tmax}, OCS, SST) measurement is adequate to fully describe the inner- and outer-core structure characteristic of all typhoons and hurricanes. A prevalent misconception regarding tropical cyclones is that the inner- and outer-core circulations of individual tropical cyclones are closely related to each other in some consistent way. There are only weak statistical relationships wherein the strength of the cyclone's inner-core can vary widely from the outer-core circulation.

These variations are a result of eye-wall cloud structural characteristics and the eye cycle (Willoughby, et al., 1982) where the cyclone is in its life cycle (Weatherford, 1988), the variable outer environment (Merrill, 1982) that the tropical cyclone may be embedded in, the latitudinal and seasonal variations of the environmental lapse-rate and the tropical cyclone storm basin of location.

Although statistical relationship between MSLP and maximum wind are well established and highly utilized in the Dvorak (1975, 1984) relationship, it is important to realize that this relationship can be highly skewed in individual cyclone cases. A cyclone with 980 mb MSLP and have maximum winds as high as 100 kt or as low as 50 kt. A cyclone with 100 kt maximum winds can have an MSLP as low as 920 mb or as high as 980 mb. It should also to be noted that there are, depending upon the cyclone's forward movement, large right versus left quadrant wind asymmetries which can greatly influence the cyclone's potential wind and storm surge destruction (Gray, personal communication).

This paper has concentrated on the relationship between SST and tropical cyclone intensity. There is no question that a statistical relationship is present between tropical cyclone intensity and SST. There is an upper intensity limit which a cyclone can obtain that is related to its underlying Sea Surface Temperature. Generally, the higher the SST, the higher the potential intensity. But few TCs are able to reach their highest potential intensity because:

1. they are being sheared by environmentally induced wind flow across their center,

2. the most favorable eye-wall cloud configuration and eye-wall cycle may not be present,
3. they are in a later phase of their life cycles,
4. their outer-core circulation and inertial stability are too strong to allow inner-core vortex spin-up,
5. due to latitude, season or storm basin, their lapse rate stability is not ideal.

All of these factors influence the TC intensity versus SST relationship. Thus, it is to be expected that little direct individual case relationship is found between SST and tropical cyclone intensity. This helps explain some of the previous frustrations of many researchers who have, from theoretical consideration, believed that a more direct relationship would be found.

It had not previously been realized the extent of the potential altering influences of all of the above five parameters and the need for all five to be in the most favorable mode in order for maximum TC intensity to be realized. There can, however, be no denying that a strong statistical influence between SST and intensity exists. This occurs due to enhanced lapse rates which are present in higher SST conditions. As SST rises so too does the surface air's moisture content. For every 1°C SST rise at eye-wall cloud relative humidities of 93 percent, the equivalent potential temperatures of the air goes up 5°K. At middle and upper levels however, moisture contents are much lower than at the surface and moisture changes alter θ_e much less than at the surface. Upper-level horizontal temperature gradients in all the cyclone basins are also less than they are at the surface. The variations of low level θ_e are thus of greater magnitude than middle and upper-level θ_e changes. Thermal buoyancy is therefore largely a product of the low-level sea surface temperatures. The degree to which a tropical cyclone can spin-up is dependent upon the amount of upward mass flux which the eye-wall cloud can process which is dictated to a large extent by buoyancy within the eye-wall cloud.

5.3 Future Work

Some additional work, beyond that included in this thesis, has already been performed. Utilizing the basic moist enthalpy feedback process discussed by Holland (1995),

Malkus and Riehl (1960) and others, climatological SSTs and atmospheric temperature profiles, rudimentary maps of moisture induced pressure fall have been created (see examples in Appendix). These maps represent pressure fall in the region directly below the eye-wall cloud, not the minimum central pressure. The scheme does not yet utilize the features of eye-wall slope, eye size, or highly detailed parcel physics (ice phase and water loading have been discounted for now). Using climatological SSTs and temperature values at nine standard levels produces very interesting maps of pressure fall relative to climatological surface pressures derived from climatological 1000 mb heights. Assumed are a standard Jordan tropical atmospheric profile in the environment, and RH values of 85 to 95 percent directly below the eye-wall cloud. These maps of buoyancy derived "MPI" display a significant amount of geographic variability.

Using these values to normalize historical TC data will establish the climatological probability of TCs reaching their MPI in various regions. It is hoped that real-time data on the TC environment can be integrated into this scheme to enable forecasters to determine both MPI and the likelihood for reaching that MPI in a timely fashion in intensity forecasting. Some track forecasting may need to be included in this method as well, since TC intensity can be affected by gradients of temperature, moisture, etc., present in the environment. Colleagues at Colorado State University have already begun improving the scheme to include more detailed TC physics. It may be possible to integrate these changes during my assignment to JTWC and perform operational testing of the concept while performing the tasks of a Typhoon Duty Officer.

REFERENCES

DeMaria, M. and J. Kaplan, 1994: Sea surface temperature and maximum intensity of Atlantic tropical cyclones. *J. Clim.*, 7, 1324-1334.

Dvorak, V. F., 1975: Tropical cyclone intensity analysis and forecasting from satellite imagery. *Mon. Wea. Rev.*, 103, 420–430.

Dvorak, V. F., 1984: Tropical cyclone intensity analysis using satellite data. NOAA Technical Report NESDIS 11, U. S. Dept. of Commerce, Washington, D. C., 47 pp.

Emanuel, K. A., 1986: An air-sea interaction theory for tropical cyclones. Part I: Steady-state maintenance. *J. Atmos. Sci.*, 43, 585-604.

Emanuel, K. A., 1988: Toward a general theory of hurricanes. *Am. Sci.*, 76, 371-9.

Emanuel, K. A., 1991: The theory of hurricanes. *Annu. Rev. Fluid Mech.*, 23, 179-96.

Evans, J. L., 1993: Sensitivity of tropical cyclone intensity to sea surface temperature. *J. Clim.*, 6, 1133-1140.

Gill, A. E., 1982: *Atmosphere-ocean dynamics.* Academic Press, ISBN 0-12-283520-4, 622 pp.

Gray, W. M., 1975: Tropical cyclone genesis. Dept. of Atmos. Sci. Paper No. 234, Colo. State Univ., Ft. Collins, CO, 121 pp.

Gray, W. M., 1995a: Limiting influences on the maximum intensity of tropical cyclones. Presentation at the 21st AMS Conference on Hurricanes and Tropical Meteorology, Miami, FL.

Gray, W. M., 1995b: Tropical cyclones. Monograph for the Twelfth WMO quadrennial Congress in Geneva, Switzerland, June, 161 pp.

Gray, W. M. and D. J. Shea 1976: Data summary of NOAA's hurricane inner-core radial leg flight penetrations 1957-1967, and 1969. Dept. of Atmos. Sci. Paper No. 257, Colo. State Univ., Fort Collins, CO, 220 pp.

Gray, W. M., 1979: Hurricanes: their formation, structure, and likely role in the tropical circulation. *Supplement to Meteorology Over the Tropical Oceans.* Published by RMS, James Glaisher House, Grenville Place, Bracknell, Berkshire, RG 12 1BX , D. B. Shaw, ed., pp. 155-218.

Gray, W. M., E. Buzzell, G. Burton and Collaborators, 1982: Tropical cyclone and related meteorological data sets available at CSU and their utilization. Dept. Atmos. Sci., Colorado State University, 186 pp.

Holland, G. J., 1995: The maximum potential intensity of tropical cyclones. Submitted to *J. Atmos. Sci.*

Holliday, C. R. and A. H. Thompson, 1979: Climatological characteristics of rapidly intensifying typhoons. *Mon. Wea. Rev.*, 107, 1022-1034.

IMSL (International Mathematics and Statistics Library), 1987: FORTRAN subroutines for statistical analysis, users manual, 1232 pp.

Jarvinen, B. R., C. J. Neumann and M. A. S. Davis, 1984: A tropical cyclone data tape for the North Atlantic basin, 1886-1983: Contents, limitations and uses. Noaa Tech. Memorandum NWS NHC 22.

Landsea, C. W., 1993: A climatology of intense (or major) Atlantic hurricanes. *Mon. Wea. Rev.*, 121, 1703-1713.

Malkus, J. S. and H. Riehl, 1960: On the dynamics and energy transformation in steady-state hurricanes. *Tellus*, 12, 1-20.

Merrill, R. T., 1982: A comparison of large and small tropical cyclones. Dept. of Atmos. Sci. Paper No. 352, Colo. State Univ., Ft. Collins, CO, 80523, 75 pp.

Merrill, R. T., 1984: A comparison of large and small tropical cyclones. *Mon. Wea. Rev.*, 112, 7, 1408-1418.

Merrill, R. T., 1988: Characteristics of the Upper-Tropospheric Environmental Flow around Hurricanes. *J. Atmos. Sci.*, 45, 1665-1677.

Miller, B. I., 1958: On the Maximum Intensity of Hurricanes. *J. Meteor.*, 15, 184-195.

Miller, B. I., 1958: The three dimensional wind structure around a tropical cyclone. National Hurricane Research Report No. 15, Miami, FL, 33146, 41 pp.

NODC, 1984: Climatological Atlas of the World, Monthly Analyses. Environmental Information Summary No. 84-6, National Oceanographic Data Center, Washington D.C., 20235, 5 pp.

Peixoto, J. P. and A. H. Oort, 1992: *Physics of climate.* American Institute of Physics, ISBN 0-88318-712-4.

Riehl, H., 1954: *Tropical Meteorology.* McGraw Hill Book Co., Inc. New York, NY, 392 pp.

Sadler, J. C., 1975: The Upper Tropospheric Circulation Over the Global Tropics. Department of Meteorology, University of Hawaii, Honolulu, Hawaii. UHMET-75-05. 35 pp.

Sadler, J. C., 1976: A Role of the Tropical Upper Tropospheric Trough in Early Season Typhoon Development. *Mon. Wea. Rev.*, 104, 1266-1278.

Sadler, J. C., M. A. Lander, A. M. Hori, and L K. Oda, 1987a: *Tropical marine climate atlas, Volume I: Indian Ocean and Atlantic Ocean..* Report UHMET 87-01), Dept. of Meteor., Univ. of Hawaii, Honolulu, HI.

Sadler, J. C., M. A. Lander, A. M. Hori, and L K. Oda, 1987b: *Tropical marine climate atlas, Volume II: Pacific Ocean..* Report UHMET 87-02), Dept. of Meteor., Univ. of Hawaii, Honolulu, HI.

Tuleya, R. E. and Y. Kurihara, 1981: A numerical study on the effects of environmental flow on tropical storm genesis. *Mon. Wea. Rev.*, 109, 2487-2506.

Wallace, J. M. and P. U. Hobbs, 1977: *Atmospheric science, an introductory survey.* Academic Press, ISBN 0-12-732950-1, 467 pp.

Weatherford, C. L., 1985: Typhoon structural variability. Dept. of Atmos. Sci. Paper No. 391, Colo. State Univ., Ft. Collins, CO, 80523, 75 pp.

Weatherford, C. L., 1989: The structural evolution of typhoons. Dept. of Atmos. Sci. Paper No. 446, Colo. State Univ., Ft. Collins, CO, 185 pp.

Weatherford, C. L., and W. M. Gray, 1988a: Typhoon structure as revealed by aircraft reconnaissance: Part I: Data analysis and climatology. *Mon. Wea. Rev.*, Vol. 116, 5, 1032-1043.

Weatherford, C., and W. M. Gray, 1988b: Typhoon structure as revealed by aircraft reconnaissance: Part II: Structural variability. *Mon. Wea. Rev.*, Vol. 116, 5, 1044-1056.

Willoughby, H. E. , J. A. Clos and M. G. Shoreibah, 1982: Concentric eye walls, secondary wind maxima and the evolution of the hurricane vortex. *J. Atmos. Sci.*, 39, 2, 395–411.

Appendix A

GRAPHS OF ATLANTIC BASIN INTENSITY RELATIONSHIPS

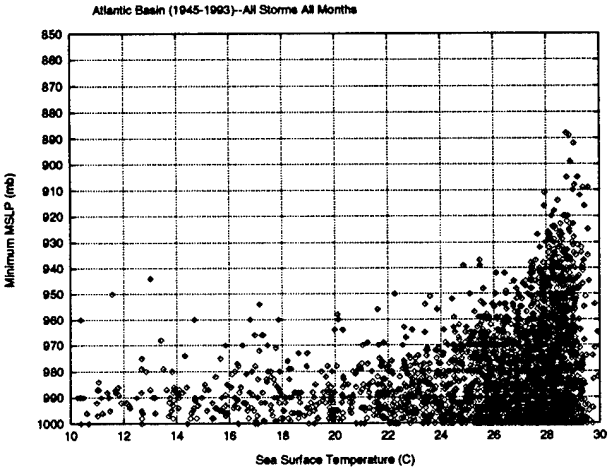
Atlantic Basin (1945-1993)--All Storms All Months
Minimum MSLP (mb)
850
860
870
880
890
900
910
920
930
940
950
960
970
980
990
1000
10
12
14
16
18
20
22
24
26
28
30
Sea Surface Temperature (C)

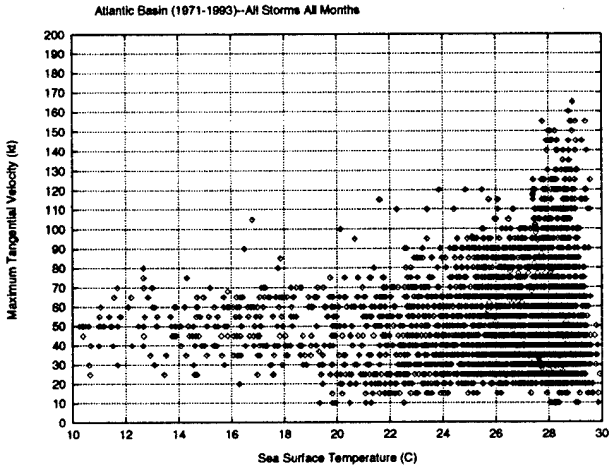
Atlantic Basin (1971-1993)--All Storms All Months
Maximum Tangential Velocity (kt)
200
190
180
170
160
150
140
130
120
110
100
90
80
70
60
50
40
30
20
10
0
10
12
14
16
18
20
22
24
26
28
30
Sea Surface Temperature (C)

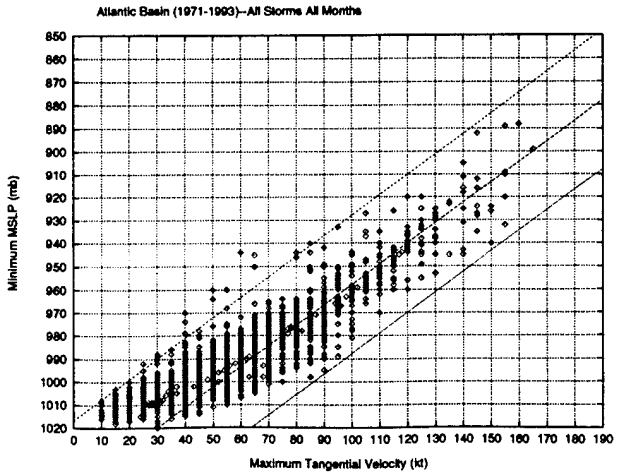
Atlantic Basin (1971-1993)--All Storms All Months
Minimum MSLP (mb)
850
860
870
880
890
900
910
920
930
940
950
960
970
980
990
1000
1010
1020
0
10
20
30
40
50
60
70
80
90
100
110
120
130
140
150
160
170
180
190
Maximum Tangential Velocity (kt)

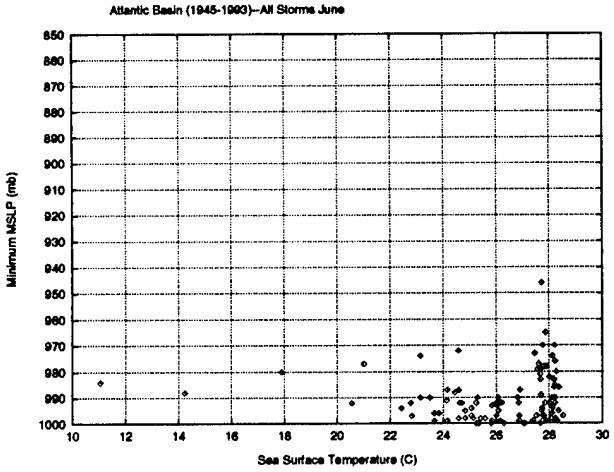
Atlantic Basin (1945-1993)--All Storms June
Minimum MSLP (mb)
850
860
870
880
890
900
910
920
930
940
950
960
970
980
990
1000
10
12
14
16
18
20
22
24
26
28
30
Sea Surface Temperature (C)

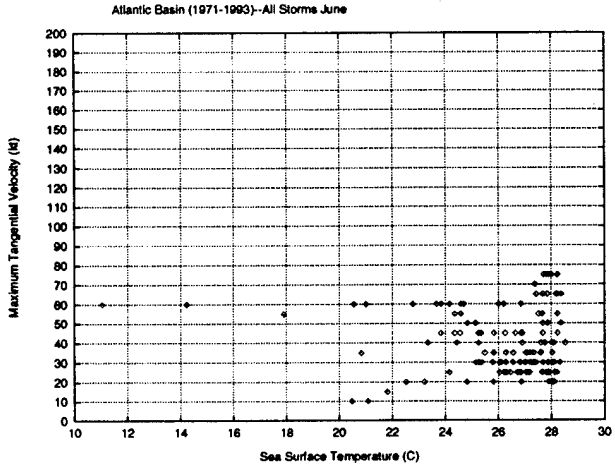
Atlantic Basin (1971-1993)--All Storms June
Maximum Tangential Velocity (kt)
200
190
180
170
160
150
140
130
120
110
100
90
80
70
60
50
40
30
20
10
0
10
12
14
16
18
20
22
24
26
28
30
Sea Surface Temperature (C)

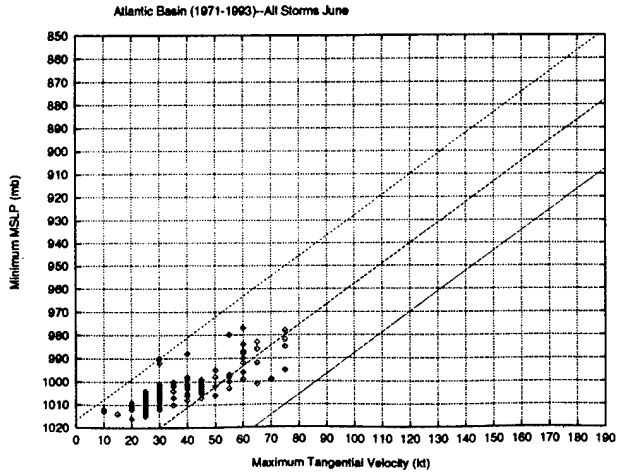
Atlantic Basin (1971-1993)--All Storms June
Minimum MSLP (mb)
850
860
870
880
890
900
910
920
930
940
950
960
970
980
990
1000
1010
1020
0
10
20
30
40
50
60
70
80
90
100
110
120
130
140
150
160
170
180
190
Maximum Tangential Velocity (kt)

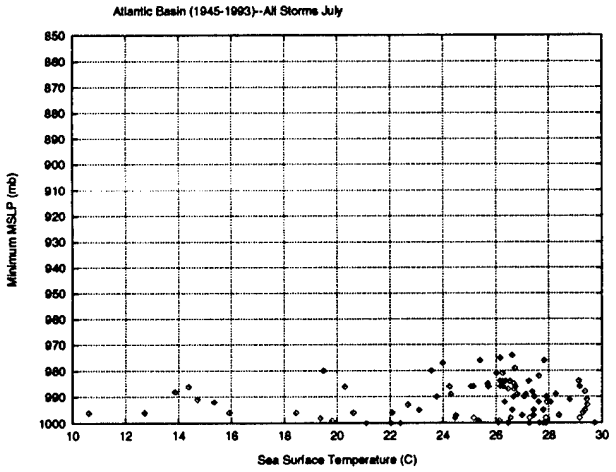
Atlantic Basin (1945-1993)--All Storms July
Minimum MSLP (mb)
850
860
870
880
890
900
910
920
930
940
950
960
970
980
990
1000
10
12
14
16
18
20
22
24
26
28
30
Sea Surface Temperature (C)

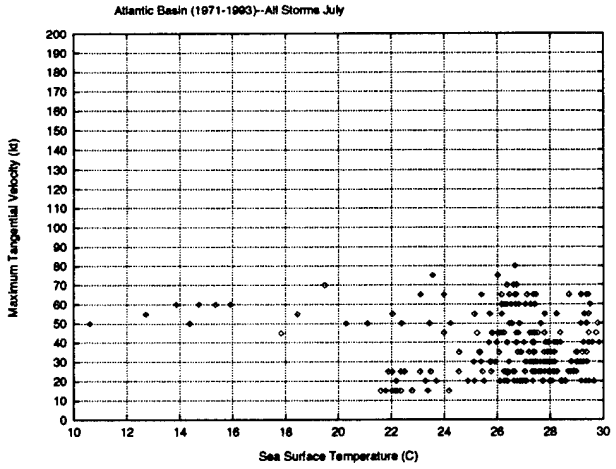
Atlantic Basin (1971-1993)--All Storms July
Maximum Tangential Velocity (kt)
200
190
180
170
160
150
140
130
120
110
100
90
80
70
60
50
40
30
20
10
0
10
12
14
16
18
20
22
24
26
28
30
Sea Surface Temperature (C)

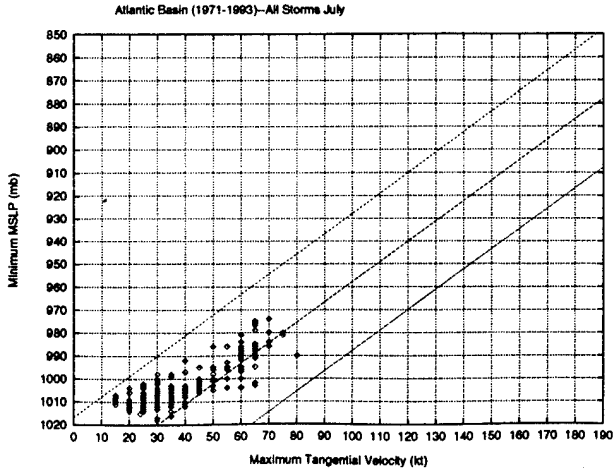
Atlantic Basin (1971-1993)--All Storms July
Minimum MSLP (mb)
850
860
870
880
890
900
910
920
930
940
950
960
970
980
990
1000
1010
1020
0
10
20
30
40
50
60
70
80
90
100
110
120
130
140
150
160
170
180
190
Maximum Tangential Velocity (kt)

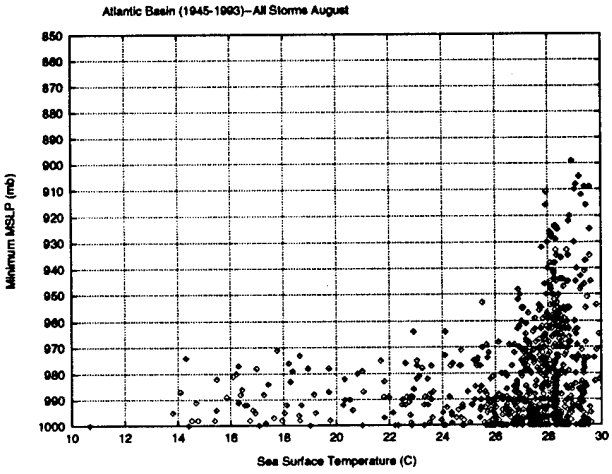
Atlantic Basin (1945-1993)--All Storms August
Minimum MSLP (mb)
850
860
870
880
890
900
910
920
930
940
950
960
970
980
990
1000
10
12
14
16
18
20
22
24
26
28
30
Sea Surface Temperature (C)

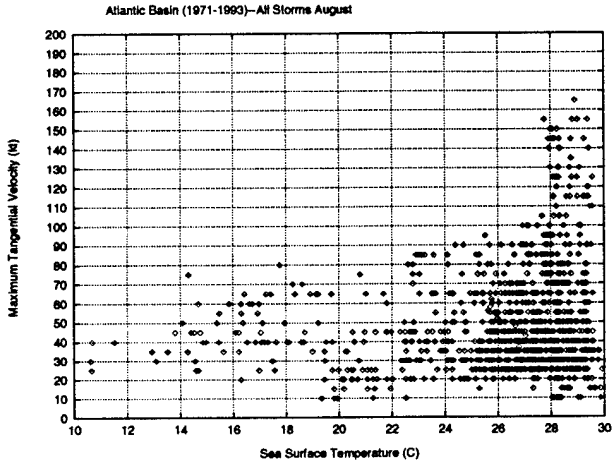
Atlantic Basin (1971-1993)--All Storms August
Maximum Tangential Velocity (kt)
200
190
180
170
160
150
140
130
120
110
100
90
80
70
60
50
40
30
20
10
0
10
12
14
16
18
20
22
24
26
28
30
Sea Surface Temperature (C)

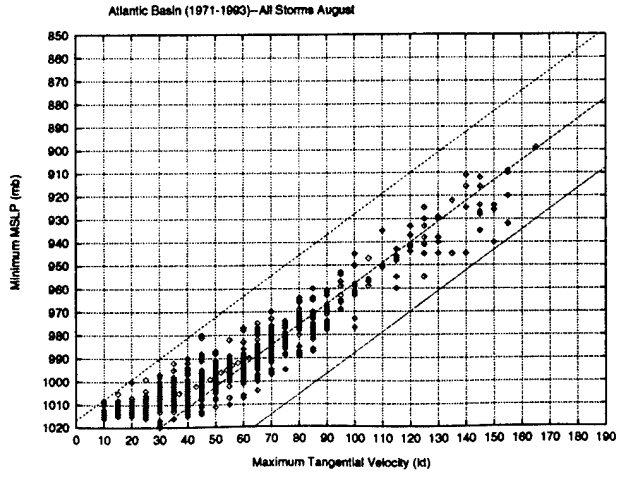
Atlantic Basin (1971-1993)--All Storms August
Minimum MSLP (mb)
850
860
870
880
890
900
910
920
930
940
950
960
970
980
990
1000
1010
1020
0
10
20
30
40
50
60
70
80
90
100
110
120
130
140
150
160
170
180
190
Maximum Tangential Velocity (kt)

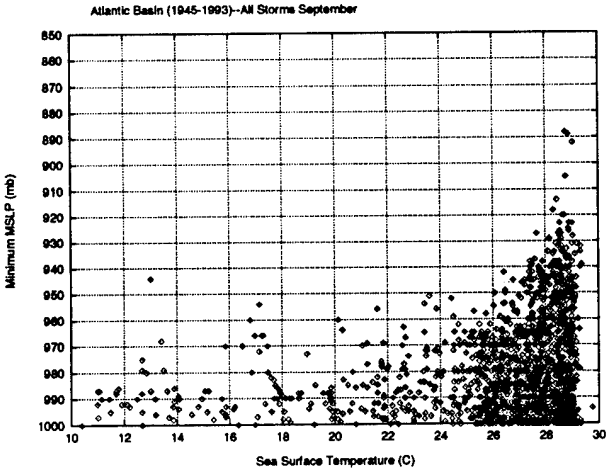
Atlantic Basin (1945-1993)--All Storms September
Minimum MSLP (mb)
850
860
870
880
890
900
910
920
930
940
950
960
970
980
990
1000
10
12
14
16
18
20
22
24
26
28
30
Sea Surface Temperature (C)

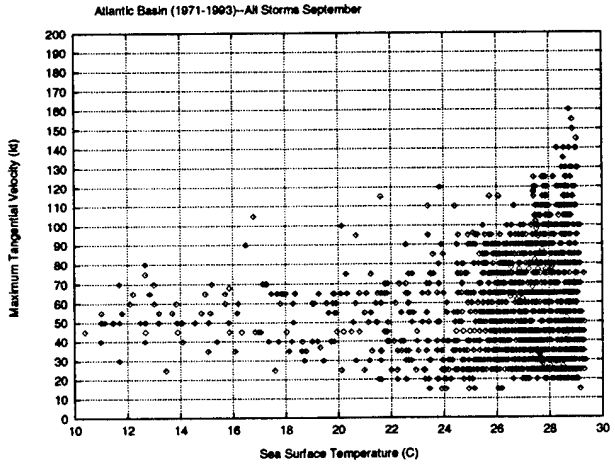
Atlantic Basin (1971-1993)--All Storms September
Maximum Tangential Velocity (kt)
200
190
180
170
160
150
140
130
120
110
100
90
80
70
60
50
40
30
20
10
0
10
12
14
16
18
20
22
24
26
28
30
Sea Surface Temperature (C)

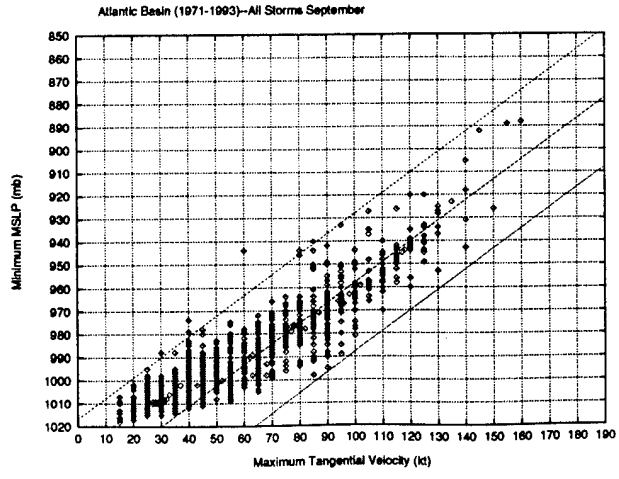
Atlantic Basin (1971-1993)--All Storms September
Minimum MSLP (mb)
850
860
870
880
890
900
910
920
930
940
950
960
970
980
990
1000
1010
1020
0
10
20
30
40
50
60
70
80
90
100
110
120
130
140
150
160
170
180
190
Maximum Tangential Velocity (kt)

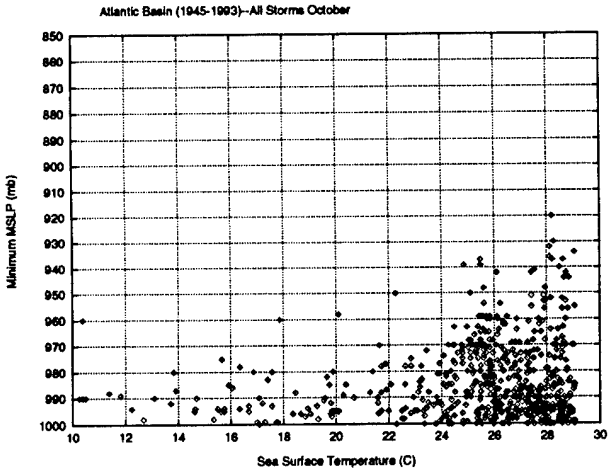
Atlantic Basin (1945-1993)--All Storms October
Minimum MSLP (mb)
Sea Surface Temperature (C)

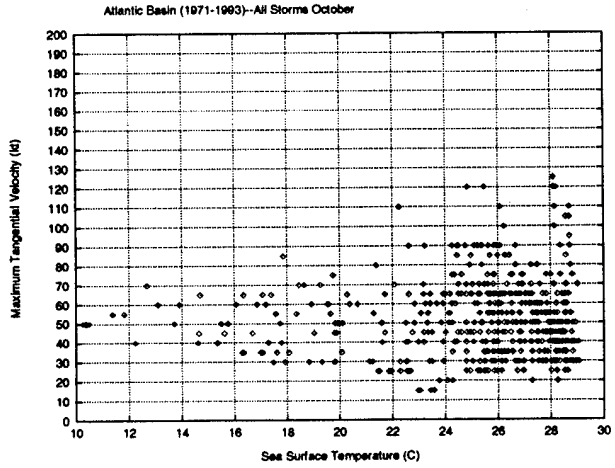
Atlantic Basin (1971-1993)--All Storms October
Maximum Tangential Velocity (kt)
Sea Surface Temperature (C)

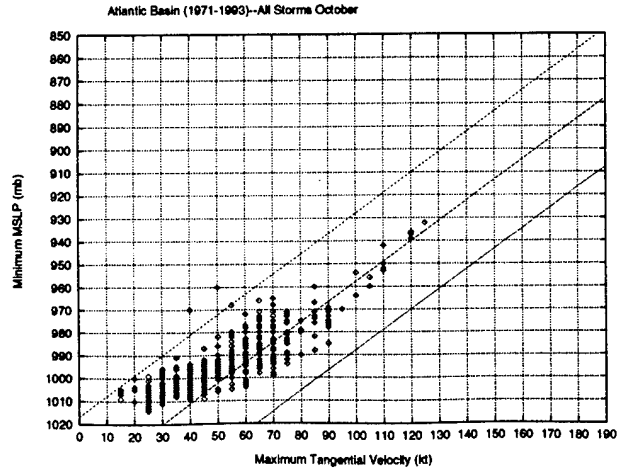
Atlantic Basin (1971-1993)--All Storms October
Minimum MSLP (mb)
Maximum Tangential Velocity (kt)

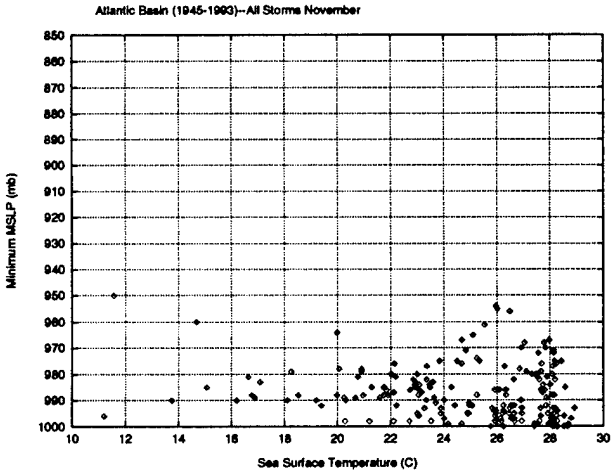
Atlantic Basin (1945-1993)--All Storms November
Minimum MSLP (mb)
850
860
870
880
890
900
910
920
930
940
950
960
970
980
990
1000
10
12
14
16
18
20
22
24
26
28
30
Sea Surface Temperature (C)

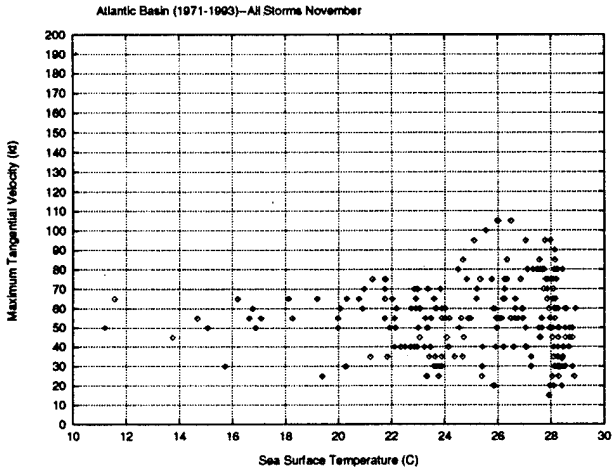
Atlantic Basin (1971-1993)--All Storms November
Maximum Tangential Velocity (kt)
200
190
180
170
160
150
140
130
120
110
100
90
80
70
60
50
40
30
20
10
0
10
12
14
16
18
20
22
24
26
28
30
Sea Surface Temperature (C)

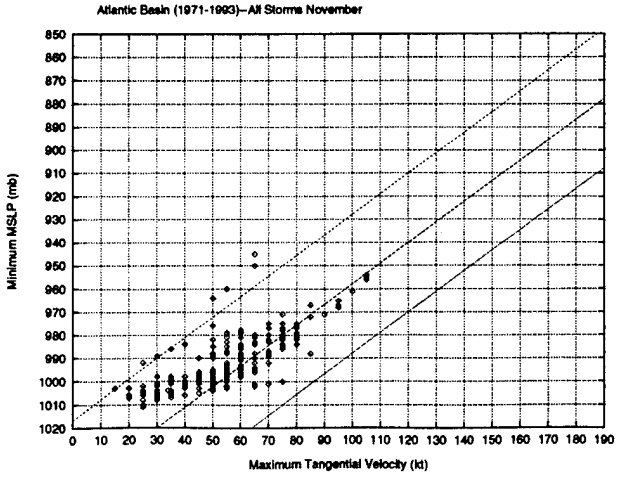
Atlantic Basin (1971-1993)--All Storms November
Minimum MSLP (mb)
850
860
870
880
890
900
910
920
930
940
950
960
970
980
990
1000
1010
1020
0
10
20
30
40
50
60
70
80
90
100
110
120
130
140
150
160
170
180
190
Maximum Tangential Velocity (kt)

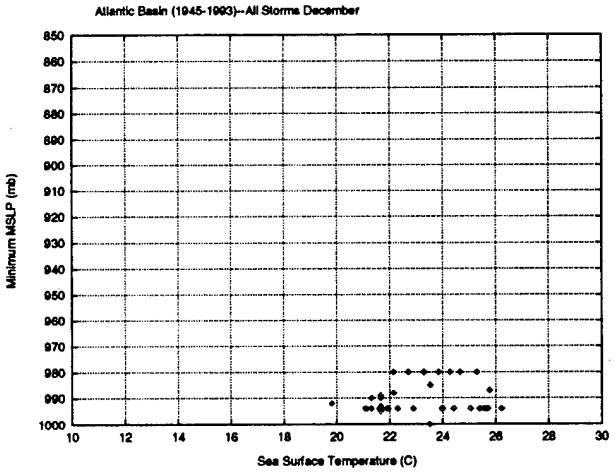
Atlantic Basin (1945-1993)--All Storms December
Minimum MSLP (mb)
850 860 870 880 890 900 910 920 930 940 950 960 970 980 990 1000
10 12 14 16 18 20 22 24 26 28 30
Sea Surface Temperature (C)

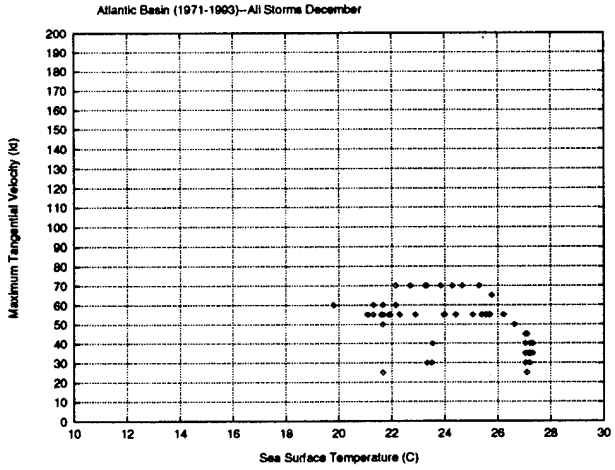
Atlantic Basin (1971-1993)--All Storms December
Maximum Tangential Velocity (kt)
200 190 180 170 160 150 140 130 120 110 100 90 80 70 60 50 40 30 20 10 0
10 12 14 16 18 20 22 24 26 28 30
Sea Surface Temperature (C)

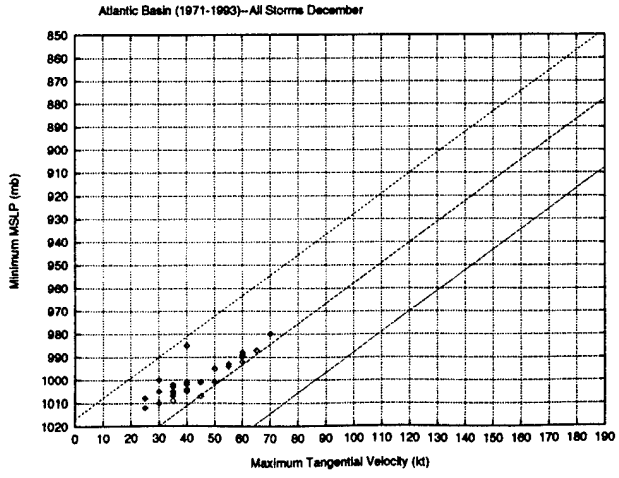
Atlantic Basin (1971-1993)--All Storms December
Minimum MSLP (mb)
850 860 870 880 890 900 910 920 930 940 950 960 970 980 990 1000 1010 1020
0 10 20 30 40 50 60 70 80 90 100 110 120 130 140 150 160 170 180 190
Maximum Tangential Velocity (kt)

Appendix B

GRAPHS OF NORTHWEST PACIFIC BASIN INTENSITY RELATIONSHIPS

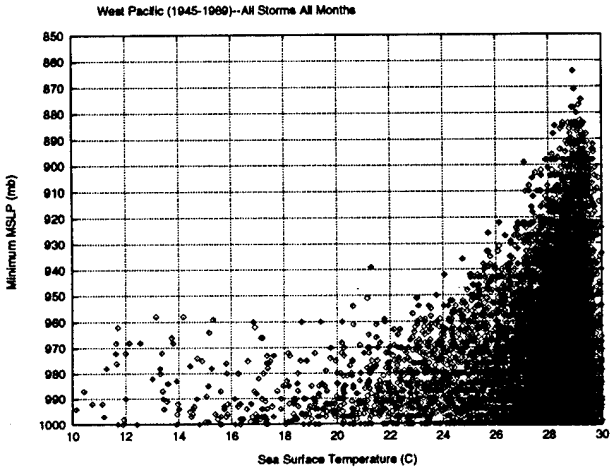
West Pacific (1945-1969)--All Storms All Months
Minimum MSLP (mb)
850
860
870
880
890
900
910
920
930
940
950
960
970
980
990
1000
10
12
14
16
18
20
22
24
26
28
30
Sea Surface Temperature (C)

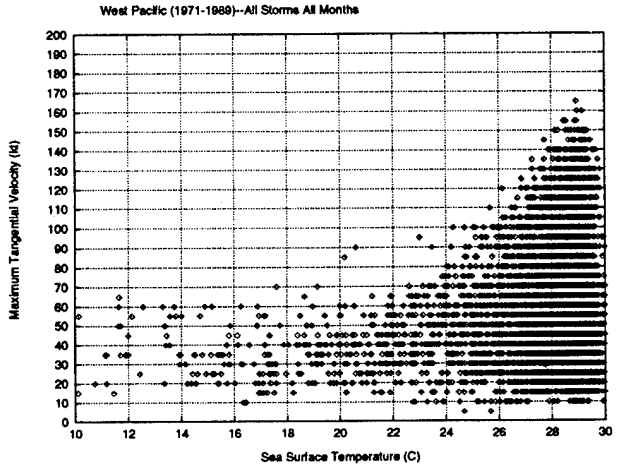
West Pacific (1971-1989)--All Storms All Months
Maximum Tangential Velocity (kt)
200
190
180
170
160
150
140
130
120
110
100
90
80
70
60
50
40
30
20
10
0
10
12
14
16
18
20
22
24
26
28
30
Sea Surface Temperature (C)

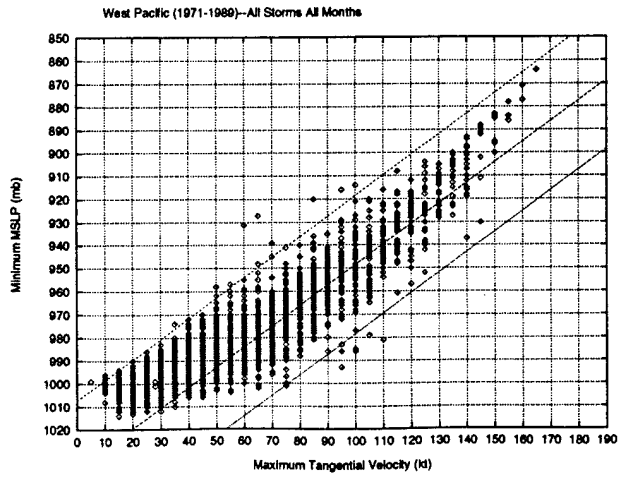
West Pacific (1971-1989)--All Storms All Months
Minimum MSLP (mb)
850
860
870
880
890
900
910
920
930
940
950
960
970
980
990
1000
1010
1020
0
10
20
30
40
50
60
70
80
90
100
110
120
130
140
150
160
170
180
190
Maximum Tangential Velocity (kt)

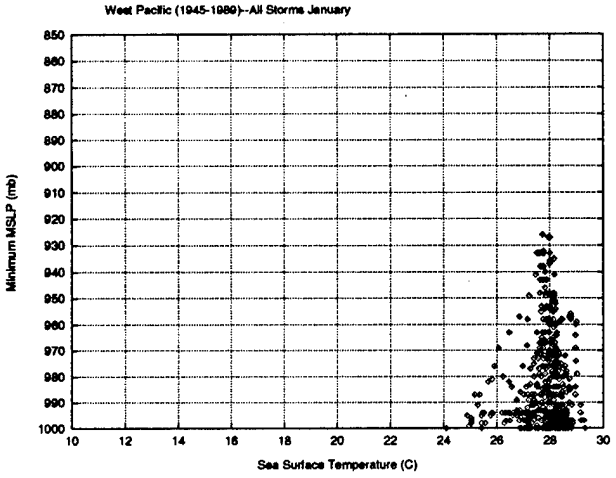
West Pacific (1945-1989)--All Storms January
Minimum MSLP (mb)
850
860
870
880
890
900
910
920
930
940
950
960
970
980
990
1000
10
12
14
16
18
20
22
24
26
28
30
Sea Surface Temperature (C)

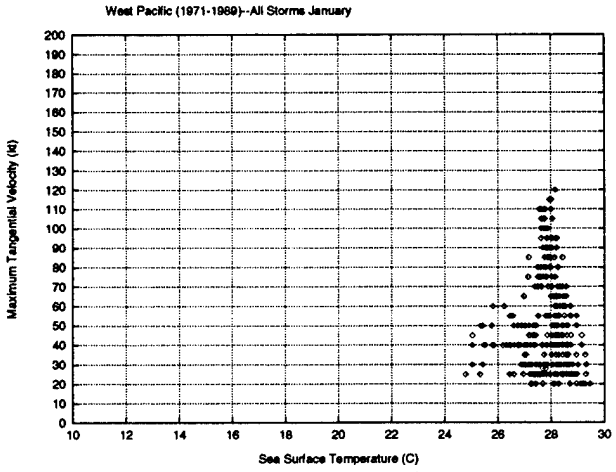
West Pacific (1971-1989)--All Storms January
Maximum Tangential Velocity (kt)
200
190
180
170
160
150
140
130
120
110
100
90
80
70
60
50
40
30
20
10
0
10
12
14
16
18
20
22
24
26
28
30
Sea Surface Temperature (C)

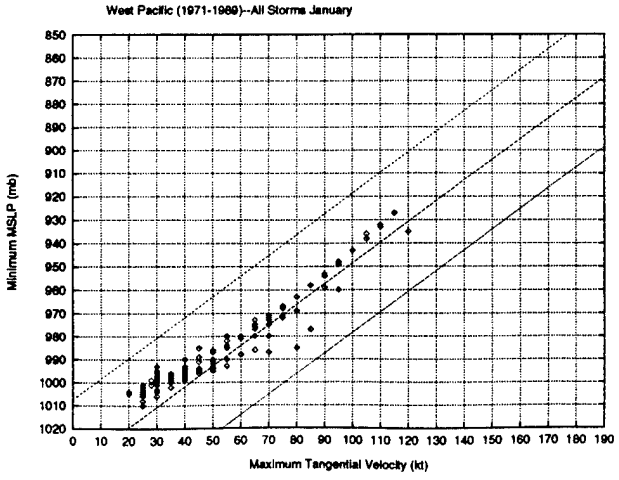
West Pacific (1971-1989)--All Storms January
Minimum MSLP (mb)
850
860
870
880
890
900
910
920
930
940
950
960
970
980
990
1000
1010
1020
0
10
20
30
40
50
60
70
80
90
100
110
120
130
140
150
160
170
180
190
Maximum Tangential Velocity (kt)

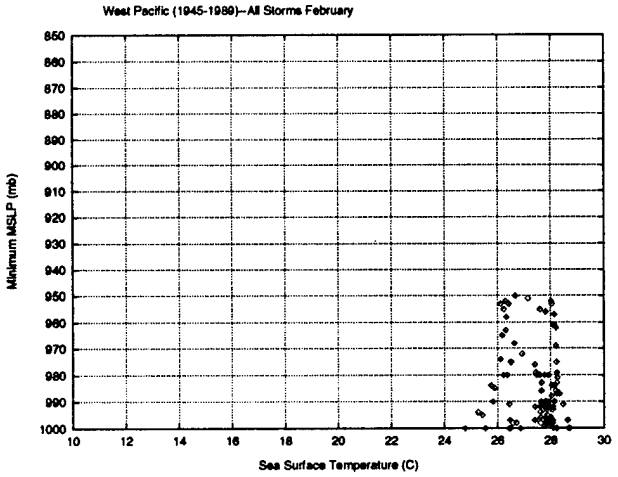
West Pacific (1945-1989)--All Storms February
Minimum MSLP (mb)
850
860
870
880
890
900
910
920
930
940
950
960
970
980
990
1000
10
12
14
16
18
20
22
24
26
28
30
Sea Surface Temperature (C)

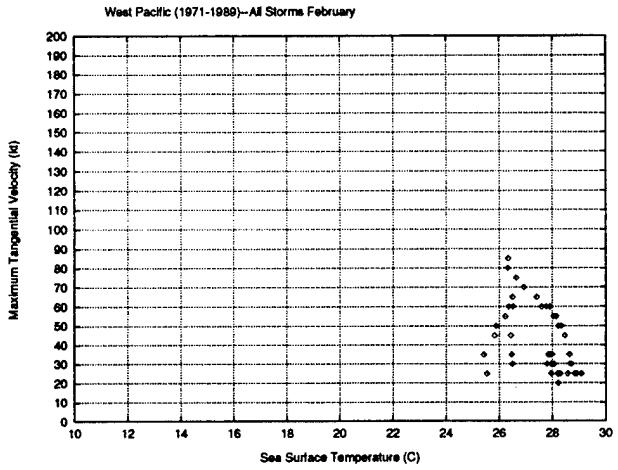
West Pacific (1971-1989)--All Storms February
Maximum Tangential Velocity (kt)
200
190
180
170
160
150
140
130
120
110
100
90
80
70
60
50
40
30
20
10
0
10
12
14
16
18
20
22
24
26
28
30
Sea Surface Temperature (C)

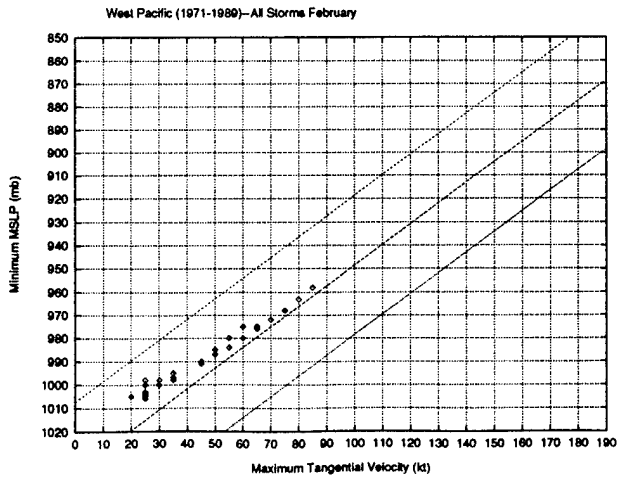
West Pacific (1971-1989)--All Storms February
Minimum MSLP (mb)
850
860
870
880
890
900
910
920
930
940
950
960
970
980
990
1000
1010
1020
0
10
20
30
40
50
60
70
80
90
100
110
120
130
140
150
160
170
180
190
Maximum Tangential Velocity (kt)

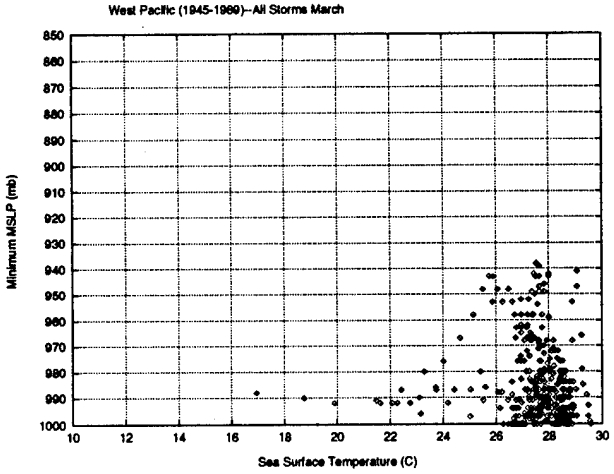
West Pacific (1945-1989)--All Storms March
Minimum MSLP (mb)
850
860
870
880
890
900
910
920
930
940
950
960
970
980
990
1000
10
12
14
16
18
20
22
24
26
28
30
Sea Surface Temperature (C)

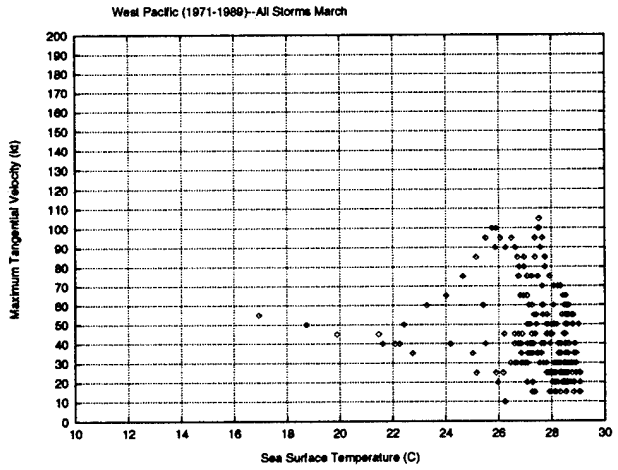
West Pacific (1971-1989)--All Storms March
Maximum Tangential Velocity (kt)
200
190
180
170
160
150
140
130
120
110
100
90
80
70
60
50
40
30
20
10
0
10
12
14
16
18
20
22
24
26
28
30
Sea Surface Temperature (C)

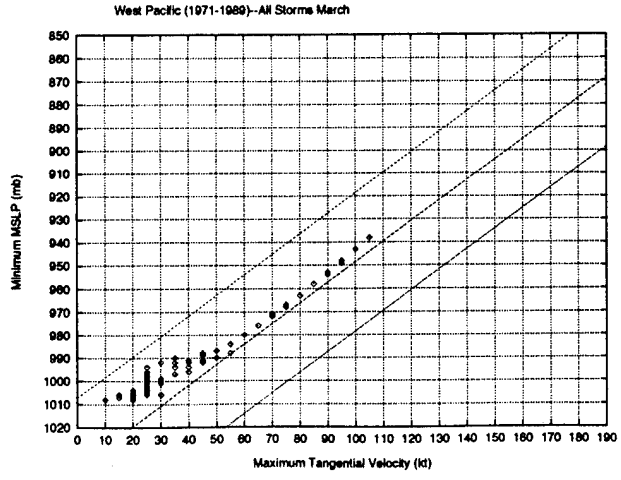
West Pacific (1971-1989)--All Storms March
Minimum MSLP (mb)
850
860
870
880
890
900
910
920
930
940
950
960
970
980
990
1000
1010
1020
0
10
20
30
40
50
60
70
80
90
100
110
120
130
140
150
160
170
180
190
Maximum Tangential Velocity (kt)

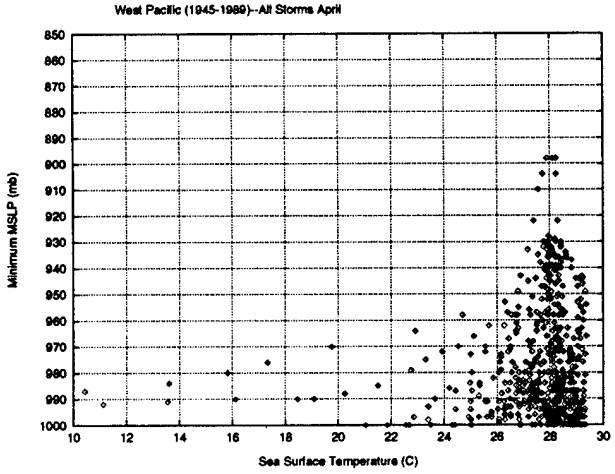
West Pacific (1945-1989)--All Storms April
Minimum MSLP (mb)
850
860
870
880
890
900
910
920
930
940
950
960
970
980
990
1000
10
12
14
16
18
20
22
24
26
28
30
Sea Surface Temperature (C)

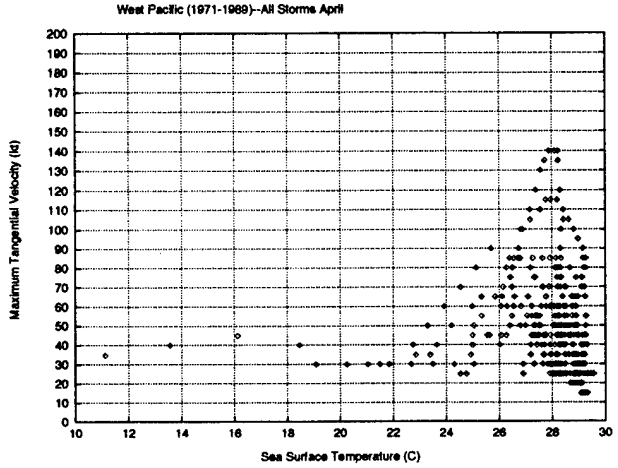
West Pacific (1971-1989)--All Storms April
Maximum Tangential Velocity (kt)
200
190
180
170
160
150
140
130
120
110
100
90
80
70
60
50
40
30
20
10
0
10
12
14
16
18
20
22
24
26
28
30
Sea Surface Temperature (C)

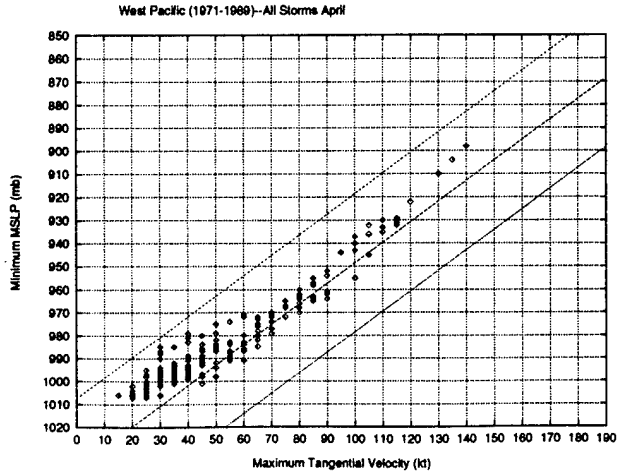
West Pacific (1971-1989)--All Storms April
Minimum MSLP (mb)
850
860
870
880
890
900
910
920
930
940
950
960
970
980
990
1000
1010
1020
0
10
20
30
40
50
60
70
80
90
100
110
120
130
140
150
160
170
180
190
Maximum Tangential Velocity (kt)

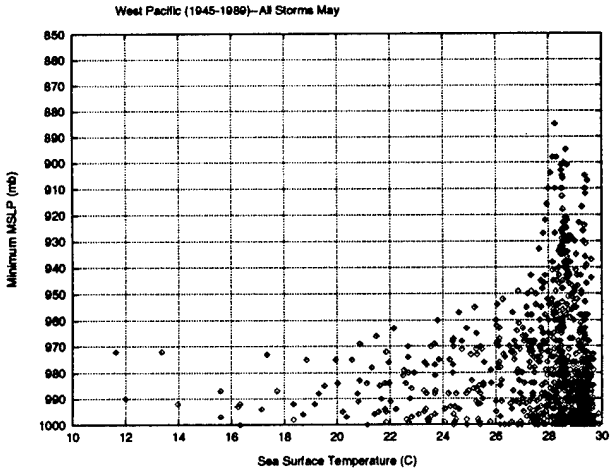
West Pacific (1945-1989)--All Storms May
Minimum MSLP (mb)
850
860
870
880
890
900
910
920
930
940
950
960
970
980
990
1000
10
12
14
16
18
20
22
24
26
28
30
Sea Surface Temperature (C)

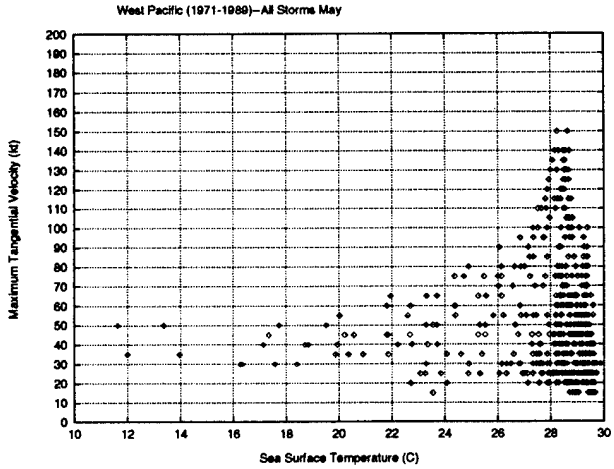
West Pacific (1971-1989)--All Storms May
Maximum Tangential Velocity (kt)
200
190
180
170
160
150
140
130
120
110
100
90
80
70
60
50
40
30
20
10
0
10
12
14
16
18
20
22
24
26
28
30
Sea Surface Temperature (C)

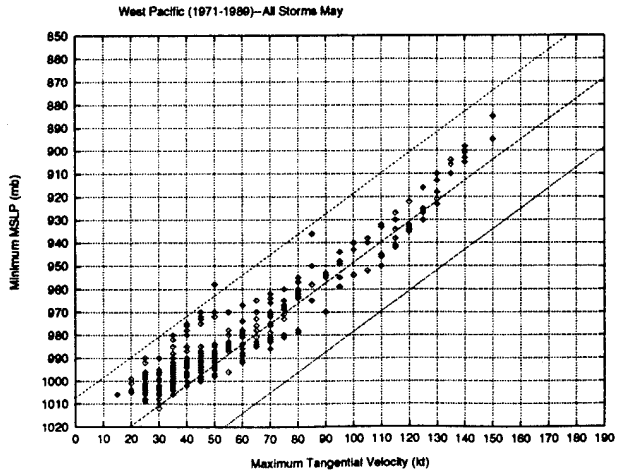
West Pacific (1971-1989)--All Storms May
Minimum MSLP (mb)
850
860
870
880
890
900
910
920
930
940
950
960
970
980
990
1000
1010
1020
0
10
20
30
40
50
60
70
80
90
100
110
120
130
140
150
160
170
180
190
Maximum Tangential Velocity (kt)

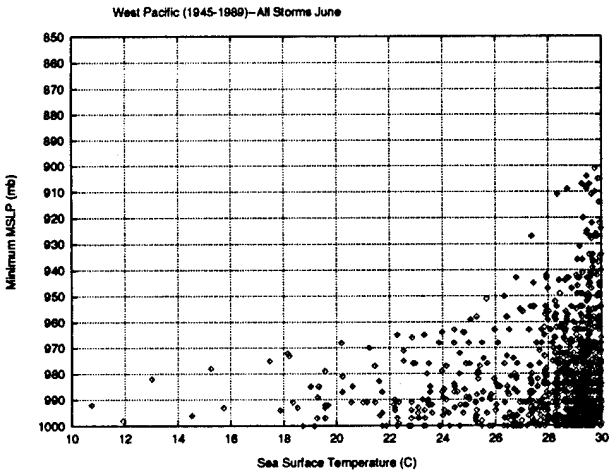
West Pacific (1945-1989)--All Storms June
Minimum MSLP (mb)
850
860
870
880
890
900
910
920
930
940
950
960
970
980
990
1000
10
12
14
16
18
20
22
24
26
28
30
Sea Surface Temperature (C)

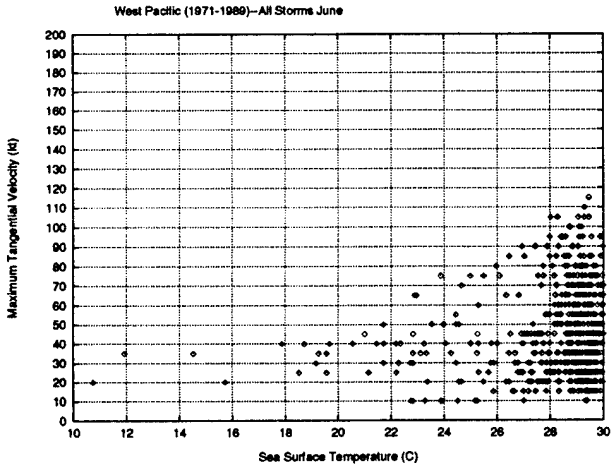
West Pacific (1971-1989)--All Storms June
Maximum Tangential Velocity (kt)
200
190
180
170
160
150
140
130
120
110
100
90
80
70
60
50
40
30
20
10
0
10
12
14
16
18
20
22
24
26
28
30
Sea Surface Temperature (C)

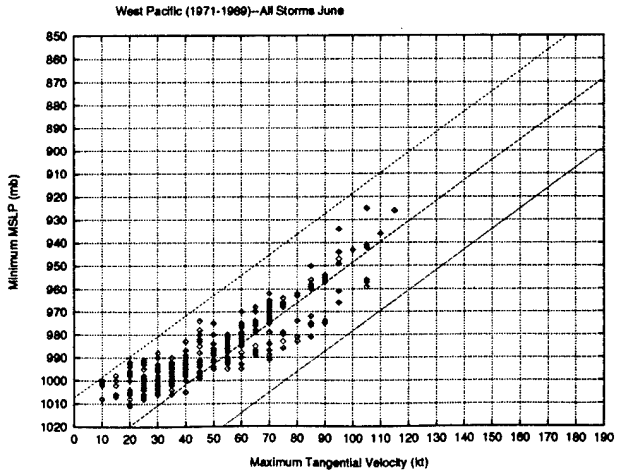
West Pacific (1971-1989)--All Storms June
Minimum MSLP (mb)
850
860
870
880
890
900
910
920
930
940
950
960
970
980
990
1000
1010
1020
0
10
20
30
40
50
60
70
80
90
100
110
120
130
140
150
160
170
180
190
Maximum Tangential Velocity (kt)

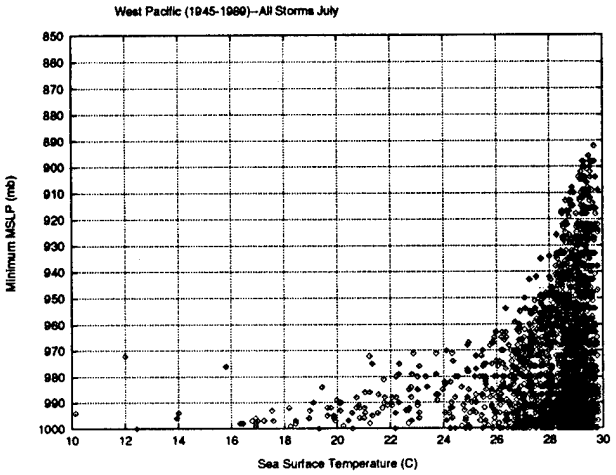
West Pacific (1945-1989)--All Storms July
Minimum MSLP (mb)
Sea Surface Temperature (C)

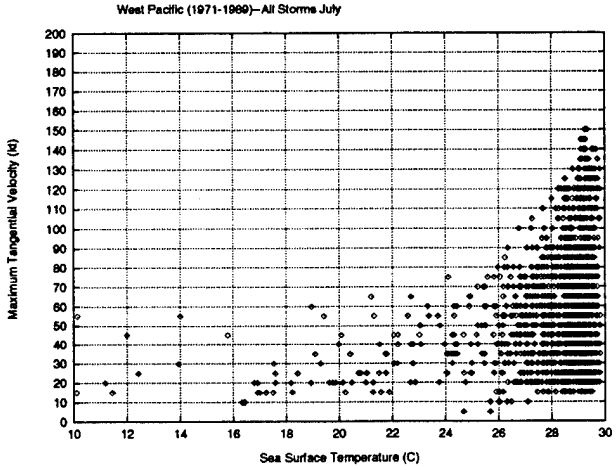
West Pacific (1971-1989)--All Storms July
Maximum Tangential Velocity (kt)
Sea Surface Temperature (C)

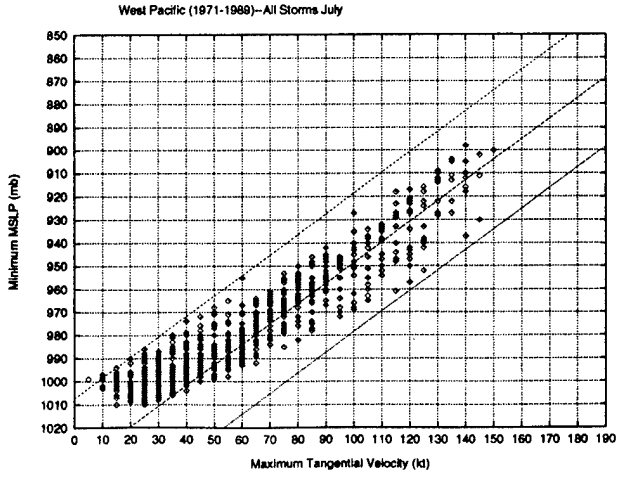
West Pacific (1971-1989)--All Storms July
Minimum MSLP (mb)
Maximum Tangential Velocity (kt)

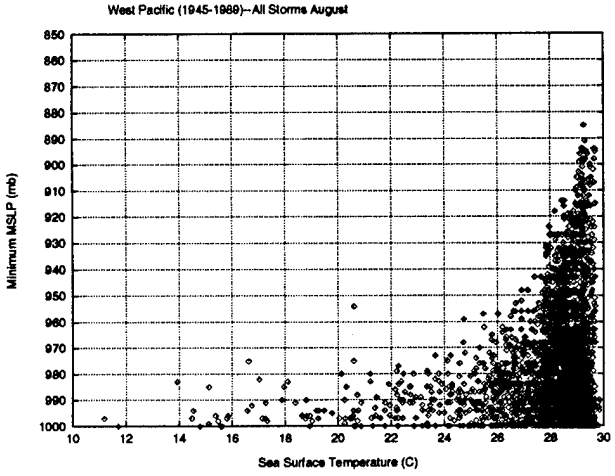
West Pacific (1945-1989)--All Storms August
Minimum MSLP (mb)
850
860
870
880
890
900
910
920
930
940
950
960
970
980
990
1000
10
12
14
16
18
20
22
24
26
28
30
Sea Surface Temperature (C)

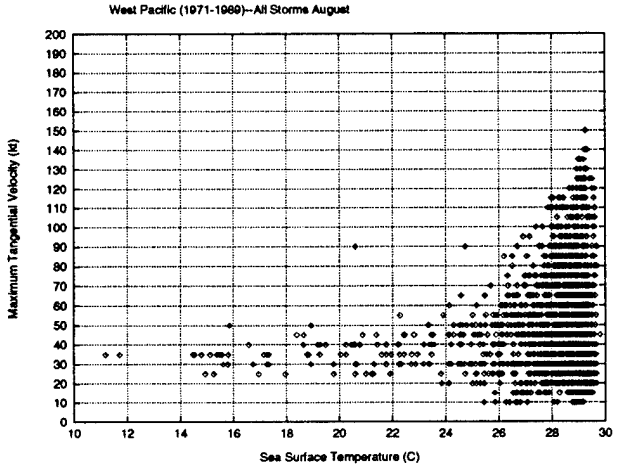
West Pacific (1971-1989)--All Storms August
Maximum Tangential Velocity (kt)
200
190
180
170
160
150
140
130
120
110
100
90
80
70
60
50
40
30
20
10
0
10
12
14
16
18
20
22
24
26
28
30
Sea Surface Temperature (C)

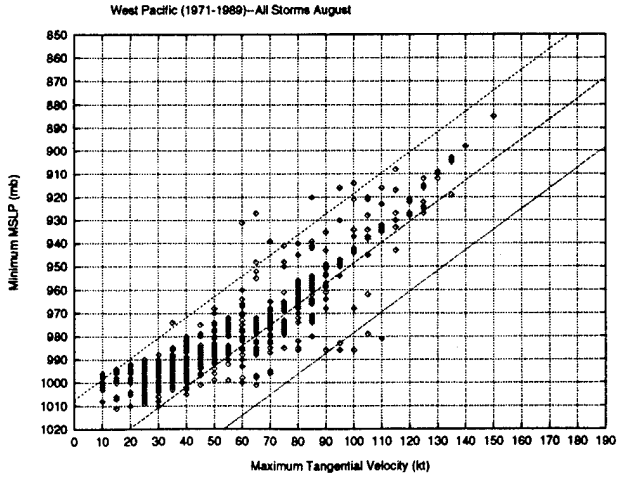
West Pacific (1971-1989)--All Storms August
Minimum MSLP (mb)
850
860
870
880
890
900
910
920
930
940
950
960
970
980
990
1000
1010
1020
0
10
20
30
40
50
60
70
80
90
100
110
120
130
140
150
160
170
180
190
Maximum Tangential Velocity (kt)

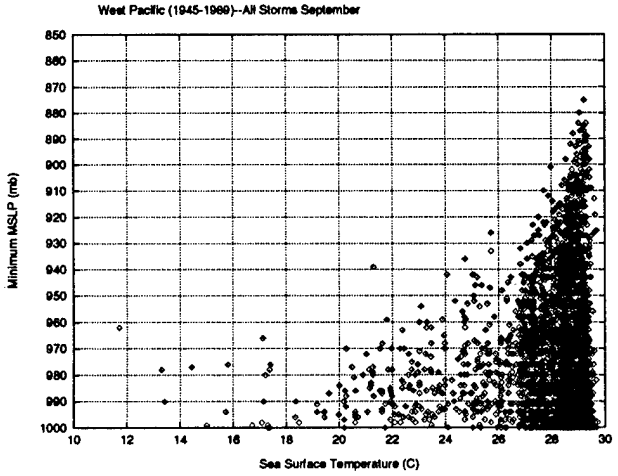
West Pacific (1945-1989)--All Storms September
Minimum MSLP (mb)
850
860
870
880
890
900
910
920
930
940
950
960
970
980
990
1000
10
12
14
16
18
20
22
24
26
28
30
Sea Surface Temperature (C)

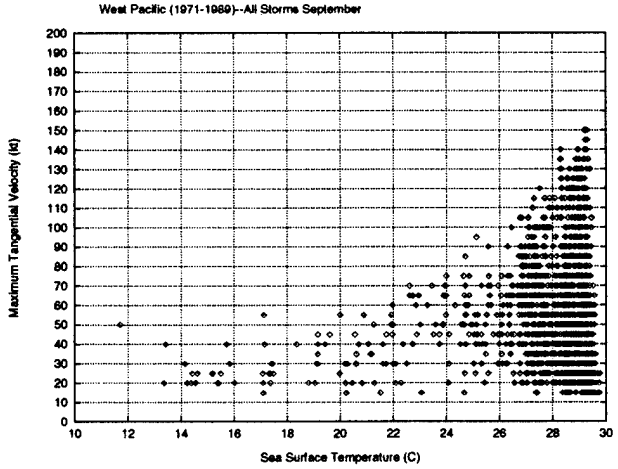
West Pacific (1971-1989)--All Storms September
Maximum Tangential Velocity (kt)
200
190
180
170
160
150
140
130
120
110
100
90
80
70
60
50
40
30
20
10
0
10
12
14
16
18
20
22
24
26
28
30
Sea Surface Temperature (C)

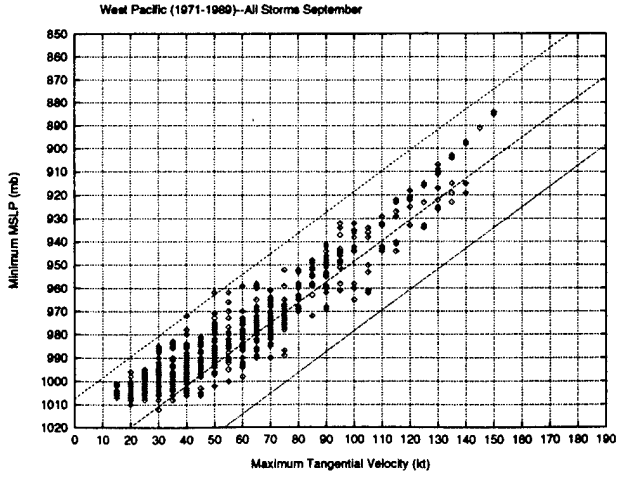
West Pacific (1971-1989)--All Storms September
Minimum MSLP (mb)
850
860
870
880
890
900
910
920
930
940
950
960
970
980
990
1000
1010
1020
0
10
20
30
40
50
60
70
80
90
100
110
120
130
140
150
160
170
180
190
Maximum Tangential Velocity (kt)

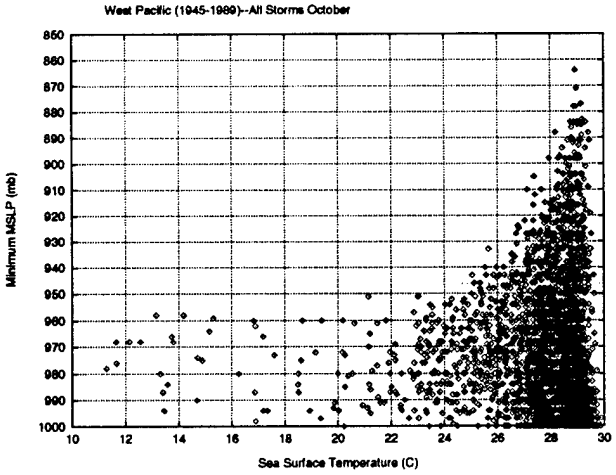
West Pacific (1945-1989)--All Storms October
Minimum MSLP (mb)
Sea Surface Temperature (C)

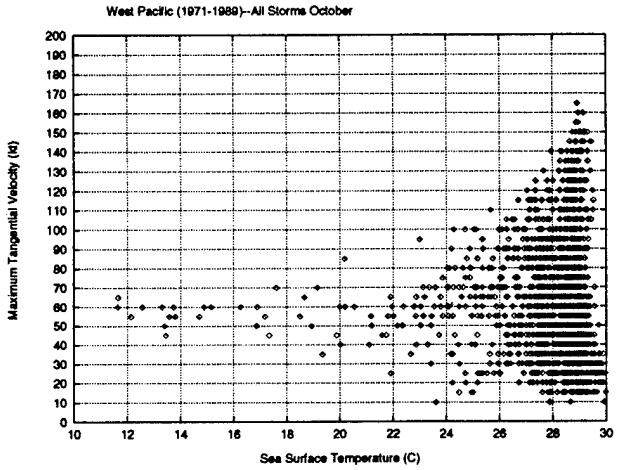
West Pacific (1971-1989)--All Storms October
Maximum Tangential Velocity (kt)
Sea Surface Temperature (C)

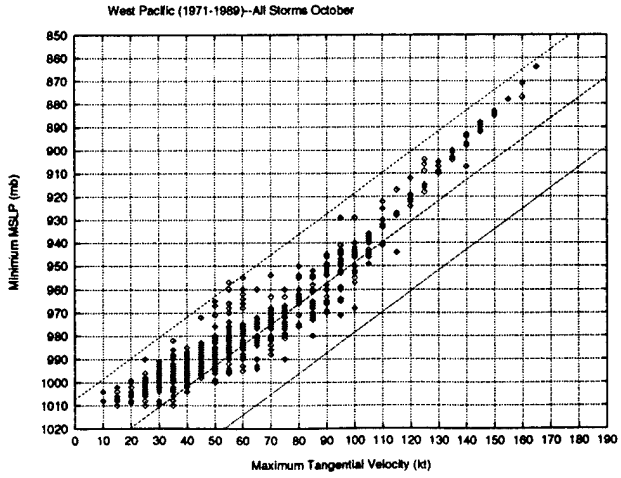
West Pacific (1971-1989)--All Storms October
Minimum MSLP (mb)
Maximum Tangential Velocity (kt)

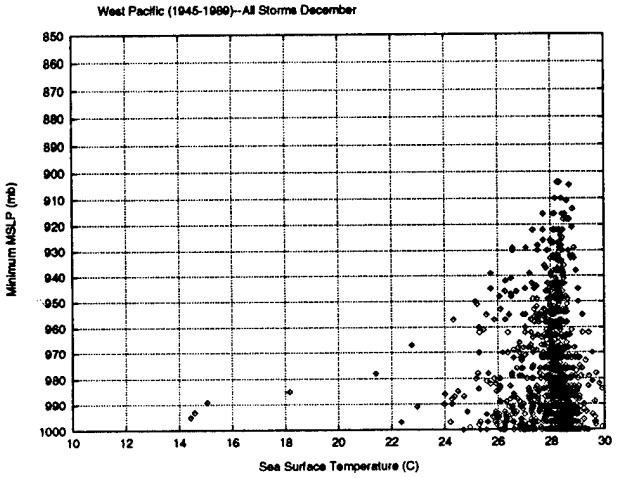
West Pacific (1945-1989)--All Storms December
Minimum MSLP (mb)
850
860
870
880
890
900
910
920
930
940
950
960
970
980
990
1000
10
12
14
16
18
20
22
24
26
28
30
Sea Surface Temperature (C)

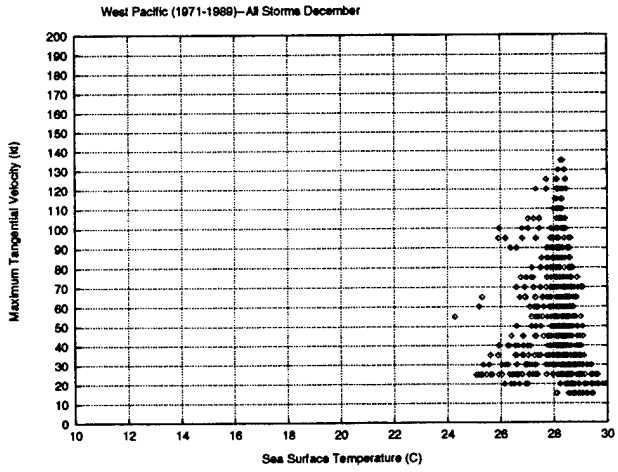
West Pacific (1971-1989)--All Storms December
Maximum Tangential Velocity (kt)
200
190
180
170
160
150
140
130
120
110
100
90
80
70
60
50
40
30
20
10
0
10
12
14
16
18
20
22
24
26
28
30
Sea Surface Temperature (C)

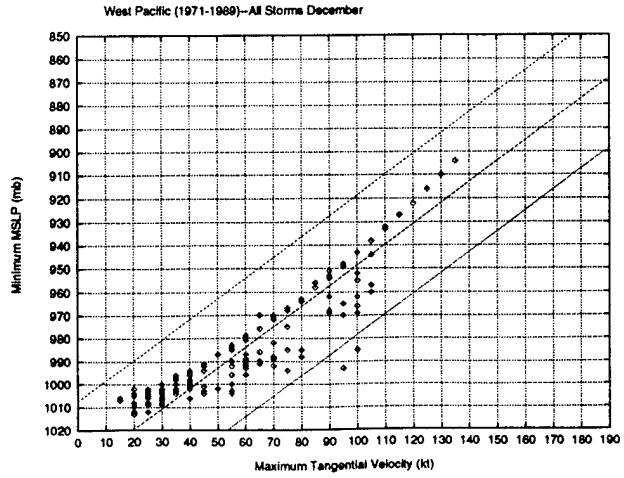
West Pacific (1971-1989)--All Storms December
Minimum MSLP (mb)
850
860
870
880
890
900
910
920
930
940
950
960
970
980
990
1000
1010
1020
0
10
20
30
40
50
60
70
80
90
100
110
120
130
140
150
160
170
180
190
Maximum Tangential Velocity (kt)